AD-A111 005   NAVAL POSTGRADUATE SCHOOL MONTEREY CA   F/G 8/10
RAPID OCEANOGRAPHIC DATA GATHERING: SOME PROBLEMS IN USING REMO--ETC(U)
SEP 81 G W LUNDELL
UNCLASSIFIED NPS68-81-006   NL

1 OF 2
AD
4111005

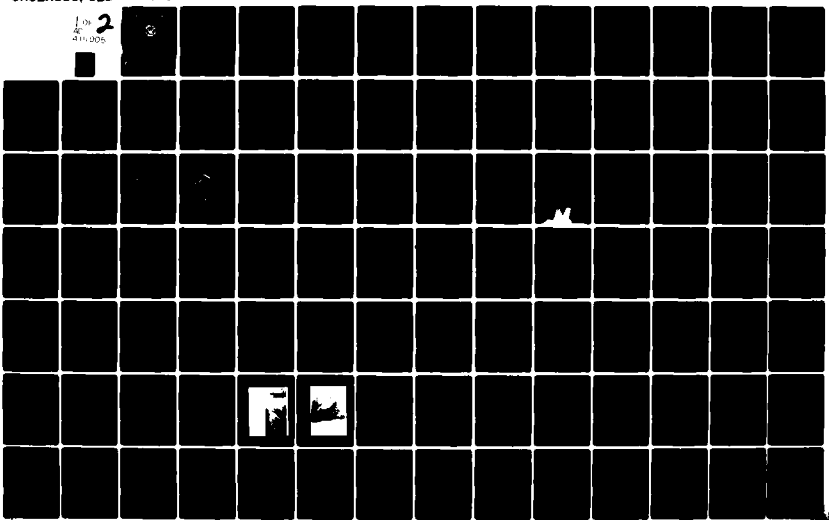

NPS68-81-006

LEVEL II

NAVAL POSTGRADUATE SCHOOL
Monterey, California

THESIS

RAPID OCEANOGRAPHIC DATA GATHERING:
SOME PROBLEMS IN USING REMOTE SENSING TO DETERMINE
THE HORIZONTAL AND VERTICAL THERMAL DISTRIBUTIONS
IN THE NORTHEAST PACIFIC OCEAN

by

Glenn W. Lundell

September 1981

Thesis Advisor: G. H. Jung

Approved for public release; distribution unlimited.

Prepared for:
Naval Ocean Systems Center
Code 531
San Diego, California 92152

SECURITY CLASSIFICATION OF THIS PAGE (When Data Entered)

REPORT DOCUMENTATION PAGE

READ INSTRUCTIONS BEFORE COMPLETING FORM

1. REPORT NUMBER: NPS 68-81-006	2. GOVT ACCESSION NO.: AD-A111 005
3. RECIPIENT'S CATALOG NUMBER	
4. TITLE (and Subtitle): Rapid Oceanographic Data Gathering: Some Problems in Using Remote Sensing to Determine the Horizontal and Vertical Thermal Distributions in the Northeast Pacific Ocean	5. TYPE OF REPORT & PERIOD COVERED: Master's Thesis; September 1981
	6. PERFORMING ORG. REPORT NUMBER
7. AUTHOR(s): Glenn W. Lundell	8. CONTRACT OR GRANT NUMBER(s)
9. PERFORMING ORGANIZATION NAME AND ADDRESS: Naval Postgraduate School, Monterey, California 93940	10. PROGRAM ELEMENT, PROJECT, TASK AREA & WORK UNIT NUMBERS: N6600181 WR00082
11. CONTROLLING OFFICE NAME AND ADDRESS: Naval Postgraduate School, Monterey, California 93940	12. REPORT DATE: September 1981
	13. NUMBER OF PAGES: 188
14. MONITORING AGENCY NAME & ADDRESS (if different from Controlling Office)	15. SECURITY CLASS. (of this report): Unclassified
	15a. DECLASSIFICATION/DOWNGRADING SCHEDULE

16. DISTRIBUTION STATEMENT (of this Report)

Approved for public release; distribution unlimited.

17. DISTRIBUTION STATEMENT (of the abstract entered in Block 20, if different from Report)

18. SUPPLEMENTARY NOTES

19. KEY WORDS (Continue on reverse side if necessary and identify by block number)

Satellite; NOAA-6; Remote Sensing; GOSSTCOMP; Northeast Pacific Ocean; Thermal Structure; Sea Surface Temperature; Subsurface Thermal Structure; Fronts; Eddies; AXBT

20. ABSTRACT (Continue on reverse side if necessary and identify by block number)

NOAA-6 satellite AVHRR data and AXBT data were collected in the Northeast Pacific Ocean in late 1980 as part of the Naval Postgraduate School-sponsored Acoustic Storm Transfer and Response Experiment which was in turn part of the U.S.-Canadian Storm Transfer and Response Experiment (STREX). Some of the problems in transferring AXBT geographical positions to satellite images were solved by designing a computer program with accuracies of less than 2 pixels.

DD FORM 1 JAN 73 1473 EDITION OF 1 NOV 65 IS OBSOLETE
S/N 0102-014-6601

UNCLASSIFIED
SECURITY CLASSIFICATION OF THIS PAGE (When Data Entered)

#20 - ABSTRACT - (CONTINUED)

Thermal comparisons were made between AXBT, NOAA-6, and GOSSTCOMP data with the result that NOAA-6 data was on the average 2.9°C colder than AXBT data and 3.2°C colder than GOSSTCOMP data. Linear regression methods reduced to 0.3°C the difference between NOAA-6 and AXBT data. Use of this method over a period of 15 days produced a mean error of 0.5°C.

Although NOAA-6 cannot sense directly the subsurface thermal structure, it is excellent for observing surface manifestations of horizontal thermal features. Further investigation into using satellite data as the basis of an empirical relationship between the surface temperature and the subsurface vertical thermal structure is warranted.

Approved for public release; distribution unlimited.

Rapid Oceanographic Data Gathering: Some Problems in Using Remote Sensing to Determine the Horizontal and Vertical Thermal Distributions in the Northeast Pacific Ocean

by

Glenn W. Lundell
Lieutenant, United States Navy
B.S., University of Miami, 1973

Submitted in partial fulfillment of the requirements for the degree of

MASTER OF SCIENCE IN SYSTEMS TECHNOLOGY

from the

NAVAL POSTGRADUATE SCHOOL
September 1981

Author: Glenn W Lundell

Approved by: Glenn H Jung, Thesis Advisor

Second Reader

Chairman, ASW Academic Group

Academic Dean

ABSTRACT

NOAA-6 satellite AVHRR data and AXBT data were collected in the Northeast Pacific Ocean in late 1980 as part of the Naval Postgraduate School-sponsored Acoustic Storm Transfer and Response Experiment which was in turn part of the U.S.-Canadian Storm Transfer and Response Experiment (STREX). Some of the problems in transferring AXBT geographical positions to satellite images were solved by designing a computer program with accuracies of less than 2 pixels. Thermal comparisons were made between AXBT, NOAA-6, and GOSSTCOMP data with the result that NOAA-6 data was on the average 2.9°C colder than AXBT data and 3.2°C colder than GOSSTCOMP data. Linear regression methods reduced to 0.3°C the difference between NOAA-6 and AXBT data. Use of this method over a period of 15 days produced a mean error of 0.5°C.

Although NOAA-6 cannot sense directly the subsurface thermal structure, it is excellent for observing surface manifestations of horizontal thermal features. Further investigation into using satellite data as the basis of an empirical relationship between the surface temperature and the subsurface vertical thermal structure is warranted.

TABLE OF CONTENTS

LIST OF TABLES

LIST OF FIGURES

FIGURE

FIGURE

FIGURE

TABLE OF ABBREVIATIONS

ADACS	Attitude Determination and Control Subsystem
ASCII	American National Standard Code for Information Interchange
ASTREX	Acoustic Storm Transfer and Response Experiment
AVHRR	Advanced Very High Resolution Radiometer
AXBT	Air-Dropped Expendable Bathythermograph
C	Celsius
CDA	Command and Data Acquisition
cm	centimeters
DCS	Data Collection System
DTG	Date Time Group; day of month followed by GMT
DTR	Digital Tape Recorder
ESA	Earth Sensor Assembly
ESL	Electromagnetic Systems Laboratory
GMT	Greenwich Mean Time (also known as Zulu time)
GOES	Geostationary Operational Environmental Satellite
GOSSTCOMP	Global Operational Sea Surface Temperature Computation
HEPAD	High Energy Proton and Alpha Detector
HIRS/2	High Resolution Infrared Radiation Sounder
HRPT	High Resolution Picture Transmission
IDIMS	Interactive Digital Image Manipulation System
IFOV	Instantaneous Field-of-View
IMP	Instrument Mounting Platofrm
IR	Infrared

K	Kelvin
km	kilometer
m	meter
MEPED	Medium Energy Proton and Electron Detector
MIRP	Manipulated Information Rate Processor
MSU	Microwave Sounding Unit
NASA	National Aeronautics and Space Administration
NEΔT	Noise Equivalent Differential Temperature
NESS	National Environmental Satellite Service
NL	Scan line number
nm	nautical mile
NOAA	National Oceanic and Atmospheric Administration
NS	Sample number
RSS	Reaction Support Structure
s	sample standard deviation
SEM	Space Environment Monitor
SSU	Stratospheric Sounding Unit
STREX	Storm Transfer and Response Experiment
TEP	Total Energy Detector
TIP	TIROS Information Processor
TOVS	TIROS Operational Vertical Sounder
VHRR	Very High Resolution Radiometer
XSU	Cross-strap Unit
μm	microns

TABLE OF SYMBOLS

ENGLISH SYMBOLS

a	semi-major axis
an	ascending node
b	semi-minor axis
e	eccentricity
f	non-rotating (fixed) earth measurement
H	mean satellite altitude
i	inclination
i_-	retrograde inclination
$L_{1,2,3,4}$	box latitudes
L_b	AXBT (buoy) latitude
$L_{c,d}$	check procedure latitudes
L_o	Landmark latitude
L_p	pixel latitude
L_s	subsatellite point latitude
NL	scan line number
NS	sample number
R	local earth radius
t	time

GREEK SYMBOLS

α	common angle
γ	common angle
$\Delta\lambda$	change in longitude between the landmark and the subsatellite point
$\Delta\lambda_{an}$	change in the ascending node longitude

$\Delta\lambda_{dn}$	change in the descending node longitude
$\Delta\lambda_{p}$	change in longitude between pixel and subsatellite point
$\Delta\lambda_{r}$	change in longitude due to earth's rotation
ϵ	common angle
θ_g	geocentric angle
θ_p	zenith angle
θ_s	scan angle
$\lambda_{1,2,3,4}$	box longitudes
λ_{an}	ascending node longitude
λ_{an}^{f}	fixed-earth ascending node longitude
λ_b	AXBT longitude
λ_{dn}	descending node longitude
λ_{dn}^{f}	fixed-earth descending node longitude
λ_o	landmark longitude
λ_p	pixel longitude
λ_s	subsatellite point longitude
ϕ_g	great circle distance
ϕ_o	great circle distance between node and landmark
ϕ_s	great circle distance between node and the subsatellite point
ϕ_t	great circle distance between node and subsatellite point

ACKNOWLEDGEMENTS

The opportunity to work with experts in fields that had been only an avocation prior to my arrival at the Naval Postgraduate School has been a rewarding and enjoyable experience. The guidance and support of my thesis advisor, Dr. Glenn Jung, Professor, Department of Oceanography, and LCDR Cal Dunlap, Assistant Professor, Department of Oceanography, has been tremendous, especially when the proverbial "light at the end of the tunnel" was pretty dim.

This thesis presented many problems that may have been left unresolved were it not for the expertise and understanding of Dr. James Mueller, Adjunct Professor, Department of Oceanography. His conceptualizations of the overall geometric problems in correcting satellite imagery were extremely helpful. In addition, satellite support came from Mr. Bob Wrigley, Technology Applications Branch at NASA Ames Research Center, who gave unselfishly of his time both to ensure access to the NASA-IDIMS system and to coach me in its use. Mr. Larry Breaker, NOAA-NESS, was kind enough to supply the satellite tapes and the ephemeris data in addition to answering my many questions on NOAA-6 operations.

Finally, a special thanks goes to my colleagues in the Environmental Acoustic Research Group, LCDR Thom Holt and Mr. Gene Brown (NAVOCEANO), who not only arranged the P-3C flights but also provided a sounding board on which to bounce ideas.

I. INTRODUCTION

The collection of oceanographic data has always been time consuming and expensive. With the development of environmental satellites, a method for the rapid gathering of oceanographic data was available to complement that data gathered on research cruises. Unfortunately, there are still some problems in using satellite data, such as the effects of the atmosphere on the radiative transmission path and the effect of the geometric distortion of thermal features found on polar-orbiting satellite images as from NOAA-6.

This thesis is part of a series of on-going studies at the Naval Postgraduate School by the Department of Oceanography Environmental Acoustic Research Group. The overall goal of the Group is to continue the development of those aspects of acoustical oceanography that have a significant effect on naval tactical applications. In pursuit of this goal, the Group was a participant in the joint U.S.-Canadian Storm Transfer and Response Experiment (STREX) held in the fall of 1980 in the Northeast Pacific Ocean. The Group is particularly interested in investigating whether or not satellites can fulfill the role presently played by ships and/or air-dropped expendable bathythermographs (AXBT) in gathering sea surface temperature data for use in forecasting the ocean's thermal structure, using procedures similar to those developed by the U.S. Naval Oceanographic Office Antisubmarine Warfare Environmental

Prediction (ASWEPS) Program in the early 1960's. If direct correlations could be found between satellite-derived sea surface temperatures and the vertical thermal structure, then a rapid method of surveying the world's oceans could result, with numerous naval ramifications.

As a part of the experiment conducted by the Group under the title Acoustic Storm Transfer and Response Experiment (ASTREX), this thesis was directed toward the examination of some of the problems in using satellites to observe the horizontal and vertical thermal distributions in the waters of the Northeast Pacific Ocean. Of particular interest was the problem of locating open-ocean geographic positions (ship, AXBT, etc.) on satellite images with as much accuracy as possible. A major portion of this thesis is devoted to this subject. If comparisons are to be made between satellite-obtained thermal values and ground-truth thermal values, then an elimination of location errors between the two media makes the results that much more significant. The reasons why NOAA-6 satellite imagery is distorted and a method to eliminate any location errors successfully are presented below. In addition, once location accuracy was assured, various meaningful comparisons were made between satellite, bathythermograph, and GOSSTCOMP (Global Operational Sea Surface Temperature Computation) data. The results of these comparisons are also presented.

II. REMOTE SENSING IN OCEANOGRAPHIC RESEARCH

In 1870 and 1879 respectively, the authors Edward Everett Hale and Jules Verne wrote about placing an artificial satellite in orbit, Hale using a huge waterpowered flywheel and Verne a gun of sufficient muzzle velocity (Corliss, 1967). Hale envisioned the satellite as an aid to both navigation and communication. Up until 1935, the idea of launching man into space remained the ideas of small amateur organizations with some notable exceptions, such as the efforts of Robert Goddard in Auburn, Massachusetts, in the 1920's.

With the stirrings of war in Europe in the late 1930's, the now infamous V-2 rockets were developed and launched from Peenemuende by a team of German scientists including Wernher von Braun. Captured en masse in 1945 by the Allies, this group of scientists and their hardware were transferred to the United States. The Army Air Force subsequently commissioned a study by Rand Corporation, who reported in 1946 for the first time that an earth-orbiting artificial satellite could be used scientifically in the fields of meteorology, biology, and communications (Corliss, 1967). This launched a nine-year effort by lobbyists both inside and outside the government culminating in President Eisenhower's announcement on 29 July 1955 that the U.S. would launch an earth-orbiting scientific satellite to investigate the environment. The Soviet Union announced similar plans on the following day. October 4, 1957 saw the

launch of Sputnik-I by Russia followed on 31 January 1958 by the launch of the first U.S. satellite, Explorer-I. Since that time, hundreds of scientific satellites have been launched in order to investigate topics from numerous fields. One of these, NOAA-6, was the satellite whose data were used on this project. NOAA-6 is an earth-orbiting, environment-sensing spacecraft with applications in meteorology and oceanography. This section reviews the use of satellites in oceanographic studies, provides a description of the operation of NOAA-6, and briefly summarizes the normal oceanographic conditions for that region of the Northeast Pacific Ocean where the experiment took place.

A. OCEANOGRAPHIC CHARACTERISTICS OF THE PROJECT AREA

The area chosen for this project encompassed that region of the Northeast Pacific Ocean between latitudes 40 N and 50 N and between longitudes 126 W and 139 W. See Figure 1. The oceanographic conditions of this region have been extensively studied by Tully (1961; 1964), Tabata (1964; 1965; 1978), and Roden (1975) among others. The reader is referred to these works for more detailed information as only a brief summary of their findings is described below.

As seen in Figure 1, the project area is located mainly in an oceanic water mass transitional region between the Subarctic Water Mass, predominantly to the north of 45 N, and the Pacific Equatorial Water Mass, predominantly to the south of 23 N. The Subarctic Current flowing eastward along 45 N

Figure 1. Major surface currents and water masses of the Northeast Pacific Ocean (after Kibblewhite _et al._, 1977)

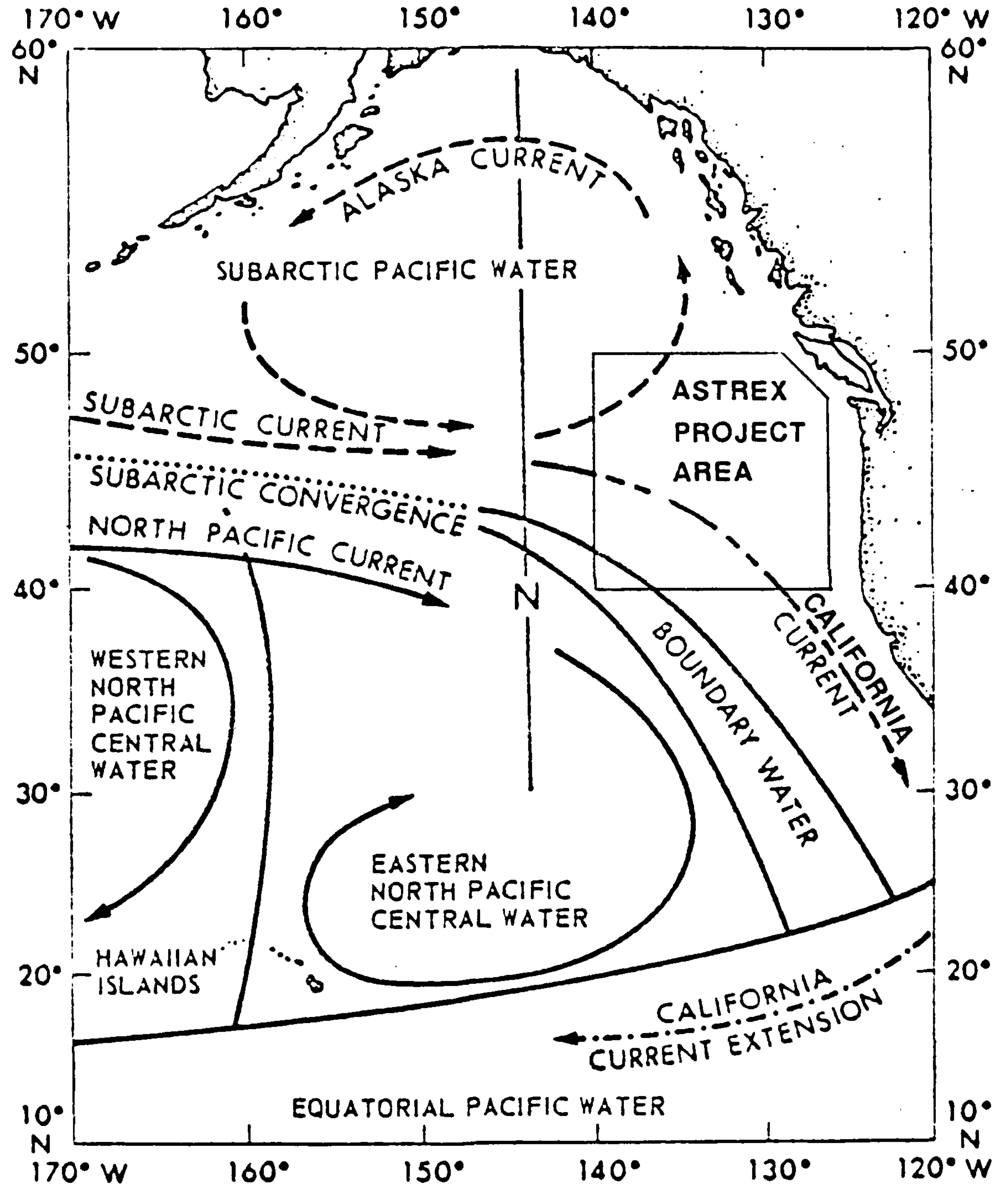

latitude divides on the northwest side of the project area into the Alaska Current, which circles counterclockwise to the north along the Canadian and Alaska coastlines; and into the California Current, which flows southward along the western coast of the United States. Observations from the project area would be expected to show the physical characteristics of the Subarctic Water Mass; however, those observations in the southern portion of the project area may be somewhat tempered by the colder offshore waters of the California Current.

1. Thermal-Salinity Structure

An excess of precipitation over evaporation of approximately 25 cm/year (Tabata and Giovando, 1962) has helped to create a layer of water extending to a depth of 100 meters in the Subarctic Water Mass that is isohaline during the winter months. A permanent halocline extending from 100 to between 200 and 300 meters exists in which the salinity increases by 1 ‰ to approximately 33.8 ‰ and marks the maximum limit of seasonal effects (Tully, 1964).

The top of the permanent halocline at 100 meters also marks the maximum depth of the seasonal thermocline. During the summer, the thermocline forms between 25 and 50 meters, influenced heavily by wind mixing effects alone. With the coming of the fall and winter months with their intensive storms, the surface waters begin to cool considerably and both convection and wind mixing erode the thermocline until isothermal conditions exist to the top of the permanent halocline. This condition usually is reached by February at which point

the waters continue to cool until the end of March, when the heating season begins. See Figure 2 for a general depiction of the seasonal structure. Figures 3 and 4 show the expected mean thermal structure for the project area for the months of November and December. Figure 5 shows the annual surface salinity maxima while Figures 6 and 7 show the expected layer depths also for November and December.

Both the Subarctic Current and the California Current have surface speeds less than one knot with volume transport averaging 10 to 15 million cubic meters per second (Knauss, 1978). As a result, the water in the project area is exposed to constant climatic conditions over many months and has sufficient time to adjust to seasonal variations. During November and December, there is an expected net heat loss in the project area ranging up to 400 g-cal/cm^2/day (Tabata, 1961). This heat loss is directly responsible for the winter convective mixing process mentioned above; therefore, the vertical thermal structure is due more to the area's heat budget, storm cycle, and salinity layers than to any influx of new water.

2. Internal Waves

Internal waves have been shown to cause amplitude fluctuations of 4.5 to 5 meters at the level of the seasonal thermocline in the Northeast Pacific Ocean (Tabata and Giovando, 1962). These oscillations may cause a periodic thickening of the thermocline from 10 to 50 meters due to phase differentials between the top and bottom of the thermocline (Tully, 1964). These periodic fluctuations vary with depth as oscillations of

Figure 2. Seasonal oceanographic structure of the Northeast Pacific Ocean (from Tully, 1964)

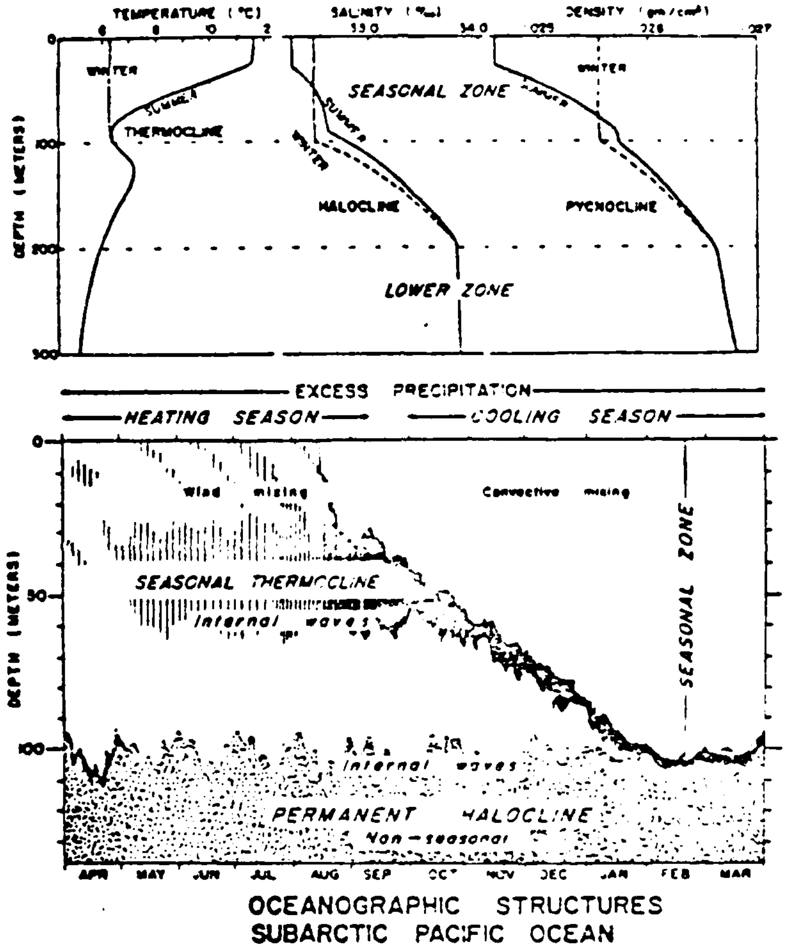

Figure 3. November mean vertical temperature structure in the project area (data from Robinson, 1976)

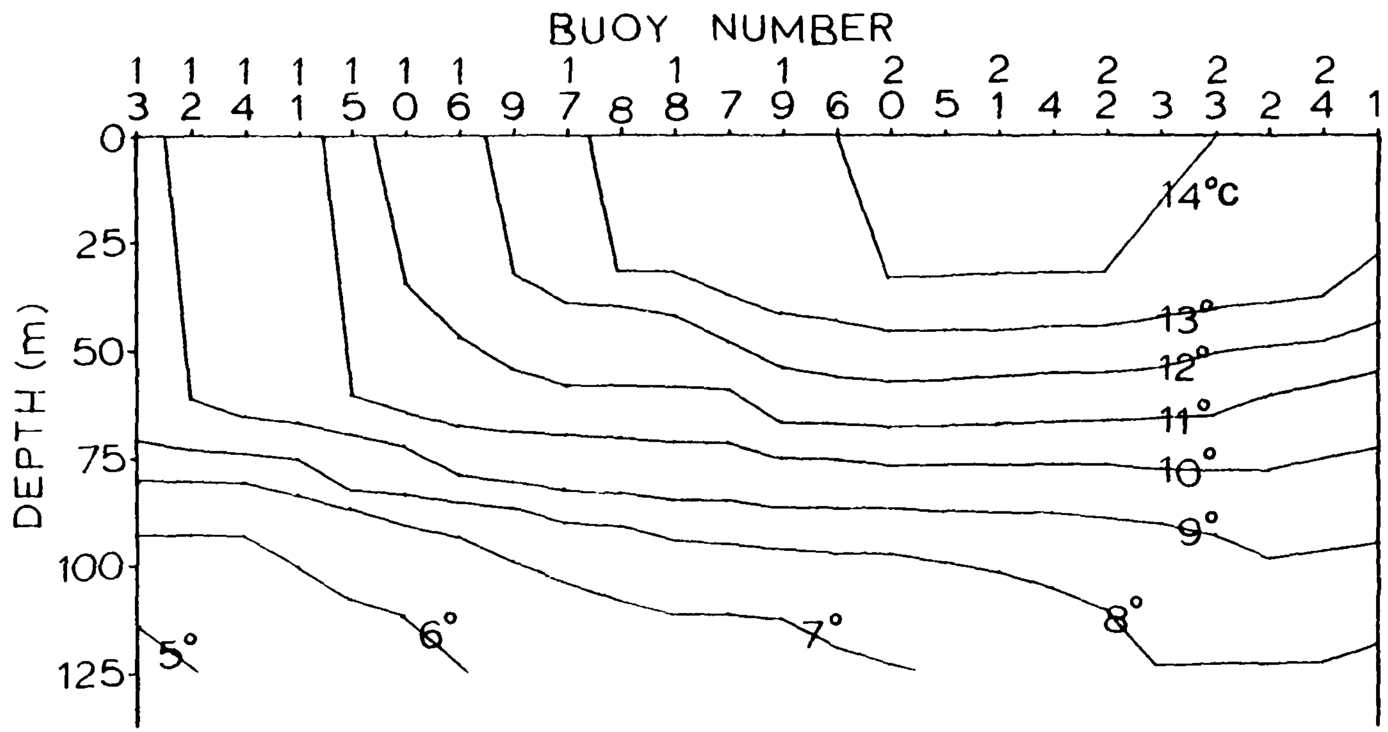

Figure 4. December mean vertical temperature structure in the project area (data from Robinson, 1976)

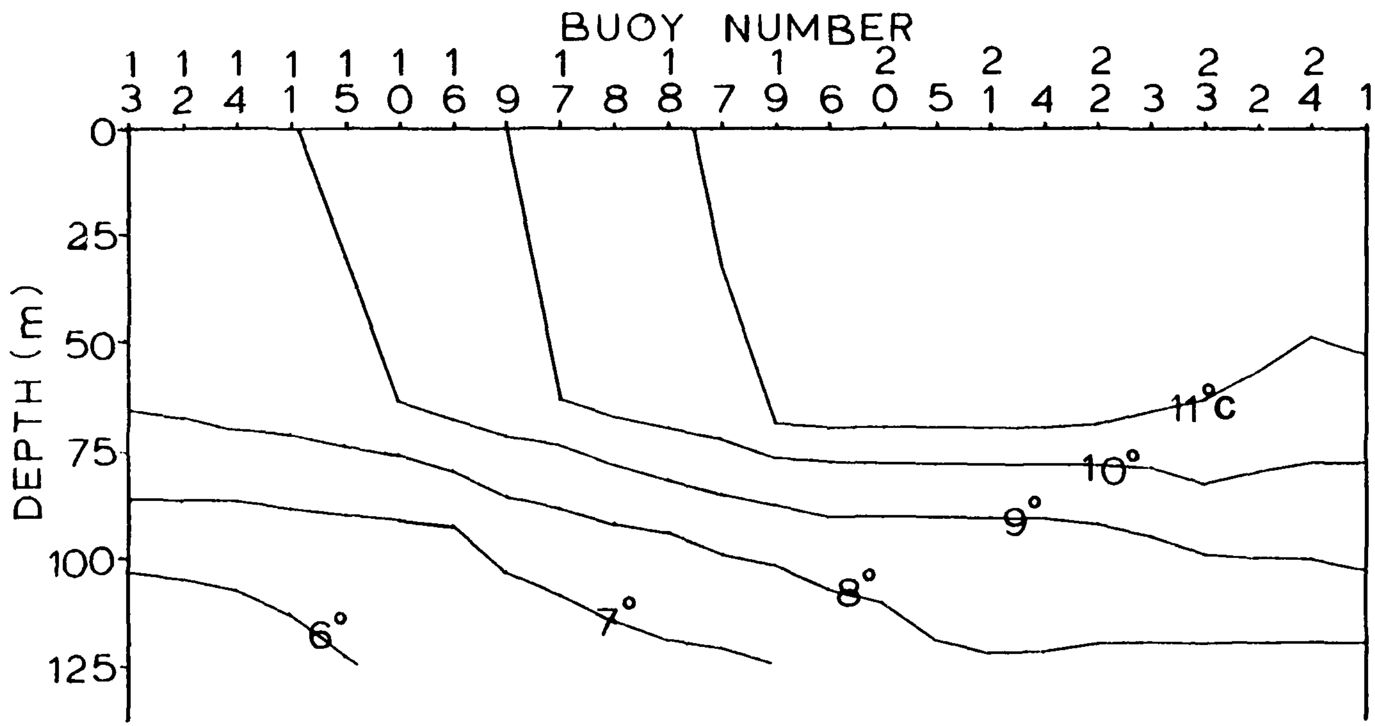

Figure 5. Annual surface salinity of the project area (from Robinson, 1976)

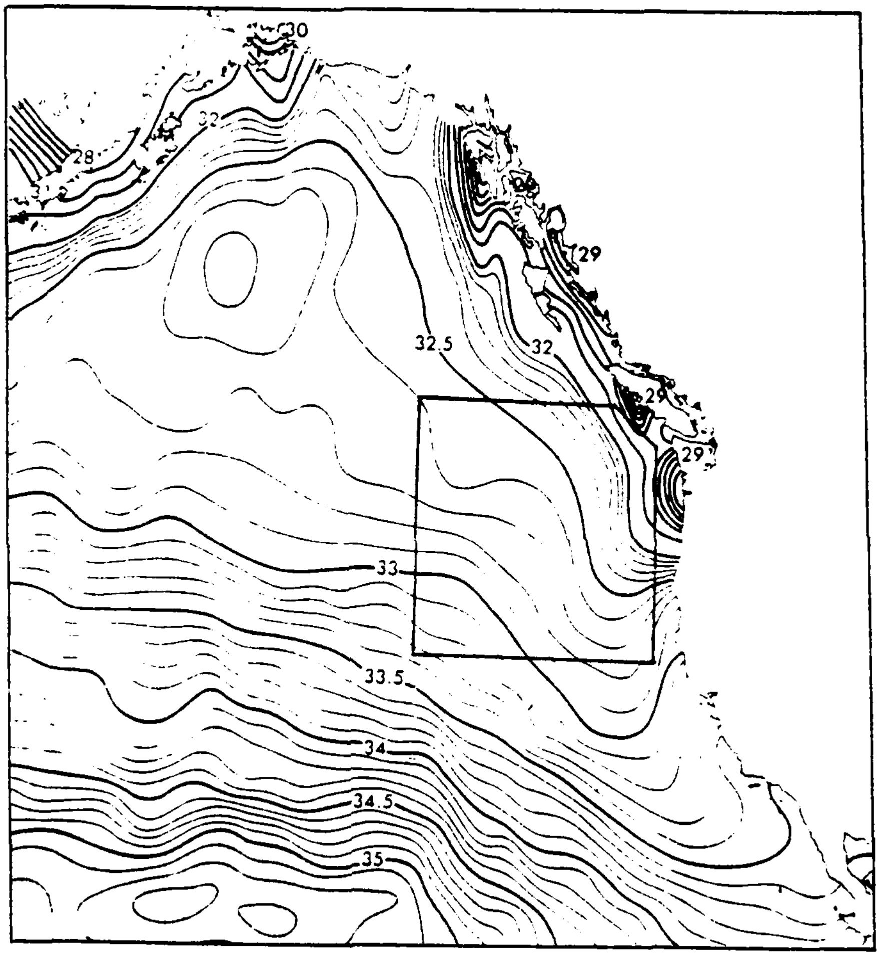

Figure 6. November mean layer depth in project area (from Robinson, 1976)

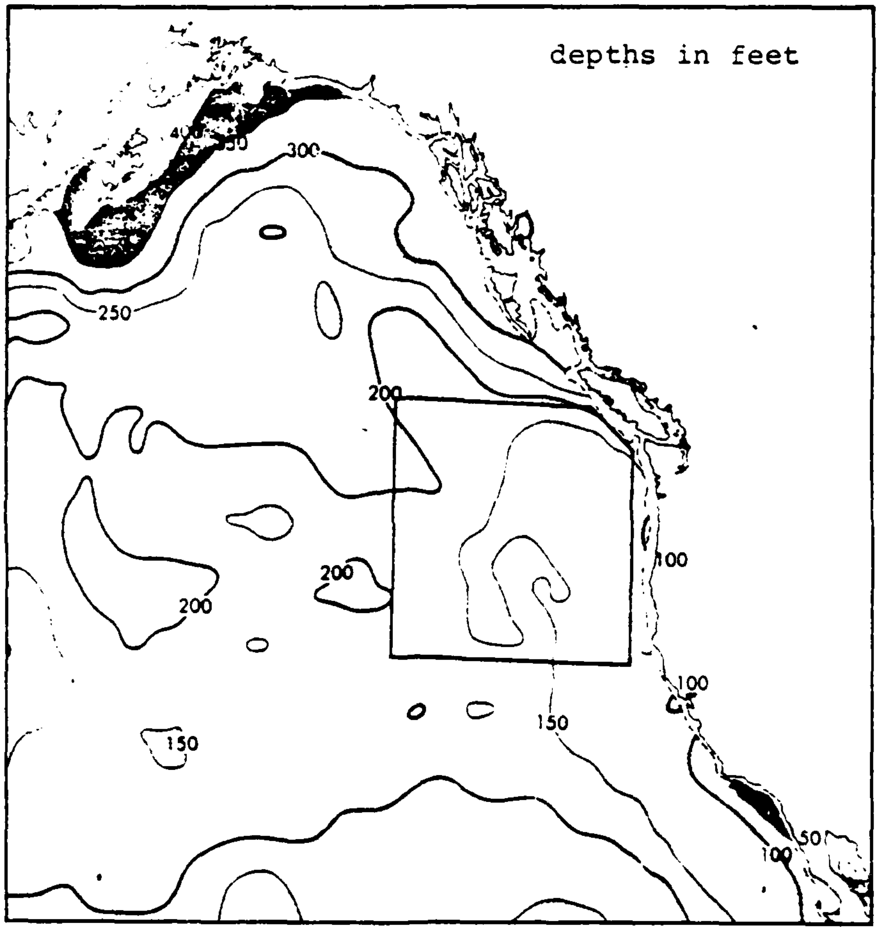

Figure 7. December mean layer depth in project area (from Robinson, 1976)

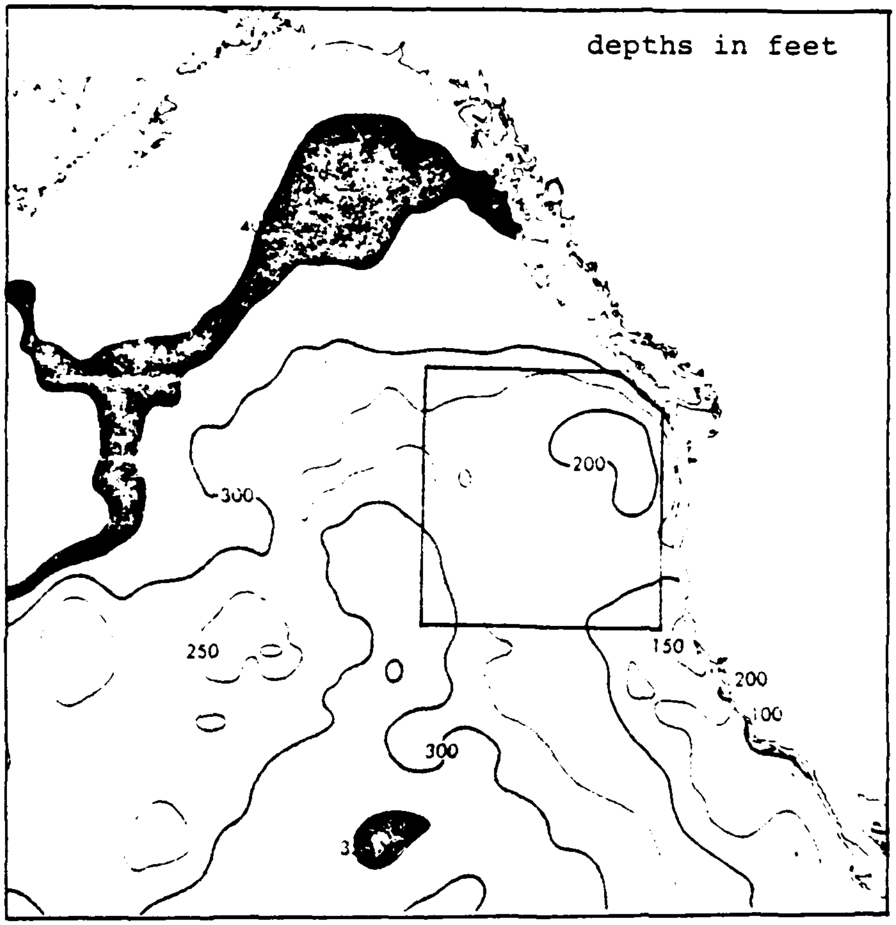

isotherms at the level of the halocline are five times greater than oscillations in the region of the thermocline.

3. Fronts and Eddies

The Subarctic Front, usually found between latitudes 40 N and 45 N, may be present in the center of this project area. This front is characterized by the lack of a density front in the upper 100 meters, by the region of the strongest surface baroclinic flow being to the south of the surface temperature and salinity fronts, and by the mixed layer depth extending to the top of the halocline at 100 meters on its northern edge (Roden, 1975). In the southern section of the project area, eddy formation may be present in that area influenced by the California Current which has been described as a relatively shallow meandering current with alternating warm and cold tongues (Bernstein *et al.*, 1977).

B. USE OF SATELLITES IN OCEAN THERMAL STUDIES

In 1968, a study was done comparing satellite-obtained sea surface temperatures with monthly mean surface temperatures with the result that the satellite values were anywhere from 3 to 8.3 degrees C lower than the mean (LaViolette and Chabot, 1968). The relative horizontal gradients observed in their satellite data, however, were fairly consistent with similar mean gradients from the historical data. This pattern of satellite-obtained sea surface temperatures being lower than the mean or the actually observed sea surface temperatures persists until today, except that technological advances have

reduced the differences in temperature between the two sets of data so they now are between 0.5 to 3.0 degrees C (Rao et al., 1972; Brower et al., 1975; McMillin, 1975; Cogan and Willard, 1976; Barnett et al., 1977; Tabata and Gower, 1980).

Prior to 1972, the oceanographic use of satellite-obtained sea surface temperature was severely limited by both the engineering characteristics of the satellite radiometers and by the environmental aspects causing atmospheric attenuation. Large instantaneous fields-of-view (IFOV) limited the resolution capacity of the satellite and the large values for the variations in the electronic signal (NEΔT) caused spatial and temporal errors, making it difficult to detect the gradients associated with oceanic fronts (Legeckis, 1978).

Several methods were proposed to remove the atmospheric contamination responsible for the majority of the difference between satellite and observed sea surface temperature values. The 3 to 8.3 degree difference found by LaViolette and Chabot (1968) came from satellite data that were not corrected for atmospheric attenuation, but in 1969 they developed a daily averaging method to lessen its impact (LaViolette and Chabot, 1969). Vukovich (1971) developed a filtering technique to accomplish the same purpose while Smith et al., (1970) used a statistical method which, when compared with ship observations, had both bias and random errors of less than 1 degree C using early NIMBUS satellite data. Maul and Sidran (1973) investigated the effects of the atmosphere, nadir angle, cloud amount, cloud height, and random noise which resulted in a

theoretical error (2 degrees C) for the NOAA satellite series, then soon to be launched.

In early 1970, NOAA launched ITOS-1 which was the first satellite in the NOAA series of satellites of which both NOAA-6 and NOAA-7 are now in orbit. In early 1970, NOAA-NESS began working on a satellite data processing model, to include the effects of atmospheric attenuation, which was the predecessor to the GOSSTCOMP (Global Operational Sea Surface Temperature Computation) model (Brower *et al.*, 1976). With the launch of NOAA-2 in 1972, a more advanced radiometer was put into use with an IFOV of about 1 kilometer and a much reduced system NEΔT of less than 3.0 degrees C (Legeckis, 1978). With this improved system, sea surface temperature fronts could be detected and monitored. Among the studies done during the following few years were those of LaViolette (1974) on upwellings off the west coast of Africa, Stumpf and Rao (1975) on tracking eddies in the Gulf Stream, and Bernstein *et al.*, (1977) on the comparison of eddies in the California Current with direct observations.

By the mid-1970's NOAA-NESS had refined their satellite data processing model; however, comparisons with observed data by NOAA itself and by others found that the quality of measurements varied with time and geographical area and were related to the temperature gradient field; good correlation came from regions of weak gradients and marginal results came from regions of strong gradients (Brower *et al.*, 1976). Klein (1979) found that NOAA-5 sea surface temperatures in the Northeast Pacific

Ocean that had been subjected to the GOSSTCOMP model were biased 3.5 to 3.9 degrees C and suggested that the error was a result of overcorrection by the model for atmospheric attenuation. With the launching of TIROS-N in 1978, NOAA-NESS updated GOSSTCOMP to take advantage of the Advanced Very High Resolution Radiometer (AVHRR) on this, and on the follow-on NOAA-6 and NOAA-7, satellites. Whereas NOAA-5 had a NEΔT of 1 to 1.5 degrees C, the TIROS-N/NOAA A-G satellite series has a NEΔT of 0.12 degrees C (Schwalb, 1978). The improvement in NEΔT should result in a better correlation between observed and satellite-derived sea surface temperatures. Chahine (1980) suggested that an absolute accuracy of 1 degree C in these differences could be obtained by simultaneous observations of atmospheric and surface emissions with multi-channel radiometers, using spectral regions of the 3.7 μm carbon dioxide windows as the main sounding channel. An instrument to accomplish this has yet to fly on a satellite.

1. Problems Associated with a Satellite Data Base

Briefly described below are three common problems associated with using satellites in thermal studies. Atmospheric attenuation is important when interpreting satellite-derived temperatures, while location accuracy is important when thermal comparisons are made between ship, satellite, and AXBT data. The depth to which present-day radiometers sense the thermal structure concludes the section.

a. Atmospheric Attenuation

As will be described in detail in Section II.C.2, data from the 10.5 to 11.5 μm infrared channel on NOAA-6 were used on this project. Radiation in this spectral region emitted from the earth's surface or from cloud tops is attenuated in its passage through the atmosphere to the radiometer. The major contribution to this attenuation is water vapor which can be responsible for up to a 9.0 degree C correction in the satellite data (Brower et al., 1976). The amount of water vapor in the atmosphere varies horizontally, vertically, and in time with the least amount of absorption around the 9.5 to 10.5 μm region (Fett and Mitchell, 1977). Other absorbers and their possible corrections are carbon dioxide (0.1 to 0.2 degrees), ozone (0.1 degrees), and aerosols (0.1 to 0.95 degrees). Details on the physics of this absorption process can be found in Roberts et al., (1976) and Weinreb and Hill (1980).

Many atmospheric correction techniques have been tried in an attempt to correct satellite data. Some of these were discussed previously. A knowledge of the vertical moisture field would help significantly in reducing the attenuation effects but these data are not generally available. In any case, the multispectral approach to this problem seems to offer the best chance to reduce this type of error significantly (Chahine, 1980; Deschamps and Phulpin, 1980).

b. Location Accuracy

A major portion of this project was devoted to locating geographic positions correctly on satellite imagery.

Sen[illegible] a

[illegible] c

[illegible]

layer. This layer is subject to the processes of net upward heat flux, infrared and solar radiation, and turbulence with the resulting temperature difference between the top and bottom of this layer of up to 1.0 degrees C (Katsaros, 1980). Typical radiometers sense only the radiation emitted from a depth of about 50 μm.

Direct measurement by satellites of the deeper vertical thermal structure is not possible with the instruments carried onboard the satellites in orbit today. Techniques using Raman lidar systems have been developed theoretically and prototypes experimentally tested with reported accuracies within 0.2 degrees C (theoretical best value) to depths of 30 meters (Leonard et al., 1979). Conclusions from this study suggest that the structure to depths of 100 meters may be detectable. The physics of the Raman spectra used in this process can be found in Murphy and Bernstein (1972).

C. NOAA-6 OPERATION

The NOAA-6 satellite is the second satellite in a series of third generation, polar-orbiting satellites that began with the launch of TIROS-N on 13 October 1978 at the Air Force Western Test Range, Vandenberg Air Force Base, California. The TIROS-N/NOAA A-G satellite series, of which NOAA-A became redesignated NOAA-6 upon its successful launch, is a joint research effort of the United States, the United Kingdom, and France and is operated by the National Environmental Satellite Service of the National Oceanic and Atmospheric Administration

(NOAA-NESS) under the U.S. Department of Commerce. The United Kingdom provided one of the three sounding units onboard the satellite, France supplied the onboard data collection system (DCS), the National Aeronautics and Space Administration (NASA) funded the development and launch of TIROS-N, and NOAA supplied the funds for the NOAA-6 satellite. The mission objective of this satellite series that directly relates to this thesis is the continuous monitoring of the environmental features in the western hemisphere which is accomplished in conjunction with a second satellite system, also operated by NOAA, the Geostationary Operational Environmental Satellite (GOES) System. It should be noted that TIROS-N ceased operation in late 1980. NOAA-6 was still functioning at the writing of this thesis and NOAA-7 began operating in June 1981.

For the purposes of this project, only those spacecraft systems that were extensively used or are important to the understanding of the results are explained below. The reader is referred to Schwalb (1978), Hussey (1979), Lauritson, et al., (1979), and ITT Aerospace (undated) for a fully detailed description of the many instruments onboard NOAA-6. Sections of these references, especially the works of Schwalb and Hussey, were used extensively below.

1. The Spacecraft

NOAA-6 used an Atlas-F launch vehicle which is a comparatively small rocket approximately 28 meters tall and weighing about 600,000 kilograms. See Figure 8. The main body of the rocket detaches after launch and a second stage solid

Figure 8. Atlas-F launch vehicle (from Hussey, 1979)

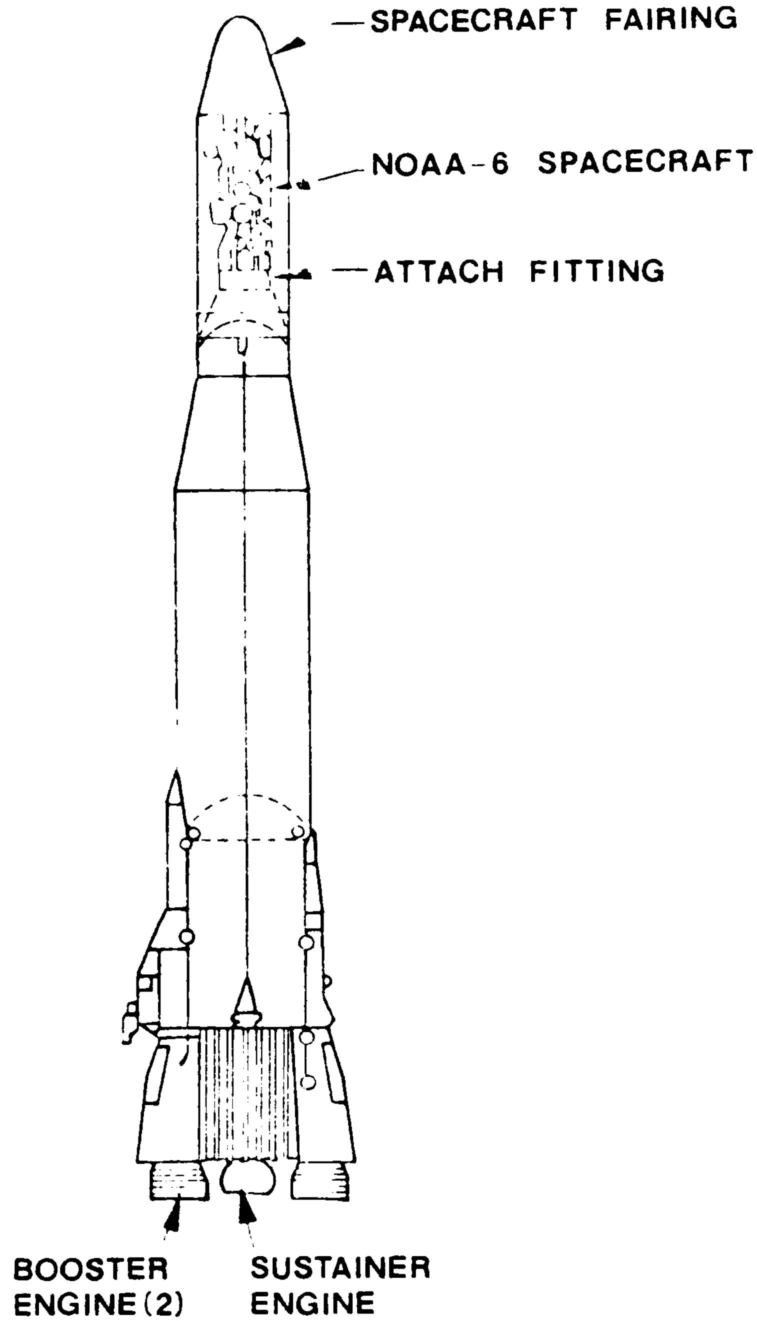

rocket motor, an integral part of the NOAA-6 satellite itself, burns until depletion putting the satellite into a nominal 833-kilometer orbit.

a. Physical Structure

The satellite itself, as shown in Figure 9, consists of three sections. The Reaction Support Structure (RSS) includes the injection motor mentioned above, the attitude control propulsion system, and an 11.6 square-meter solar cell array. The Instrument Mounting Platform (IMP) includes the attitude control sensors and the Advanced Very High Resolution Radiometer (AVHRR). The five-sided central structure, located between the RSS and the IMP, includes twelve thermal control louvres and the earth-facing communications antennae. The satellite is 3.71 meters long and 1.88 meters in diameter. Its weight at launch was 1420 kilograms which reduced to 737 kilograms once established in its orbit.

b. The Attitude Determination and Control Subsystem (ADACS)

When a satellite sensor, such as the AVHRR, scans the surface of the earth, the attitude of the spacecraft is extremely important in determining during data analysis just where the sensor looked. Any roll, pitch, or yaw on the satellite will make the application of scan geometry extremely difficult and significant errors would result. Because of this, the ADACS system was designed to maintain the attitude of the spacecraft to within 0.2 degrees (3-sigma) of the local geographic reference (Schwalb, 1978). This value is obtained

Figure 9. NOAA-6 Spacecraft (from Hussey, 1979)

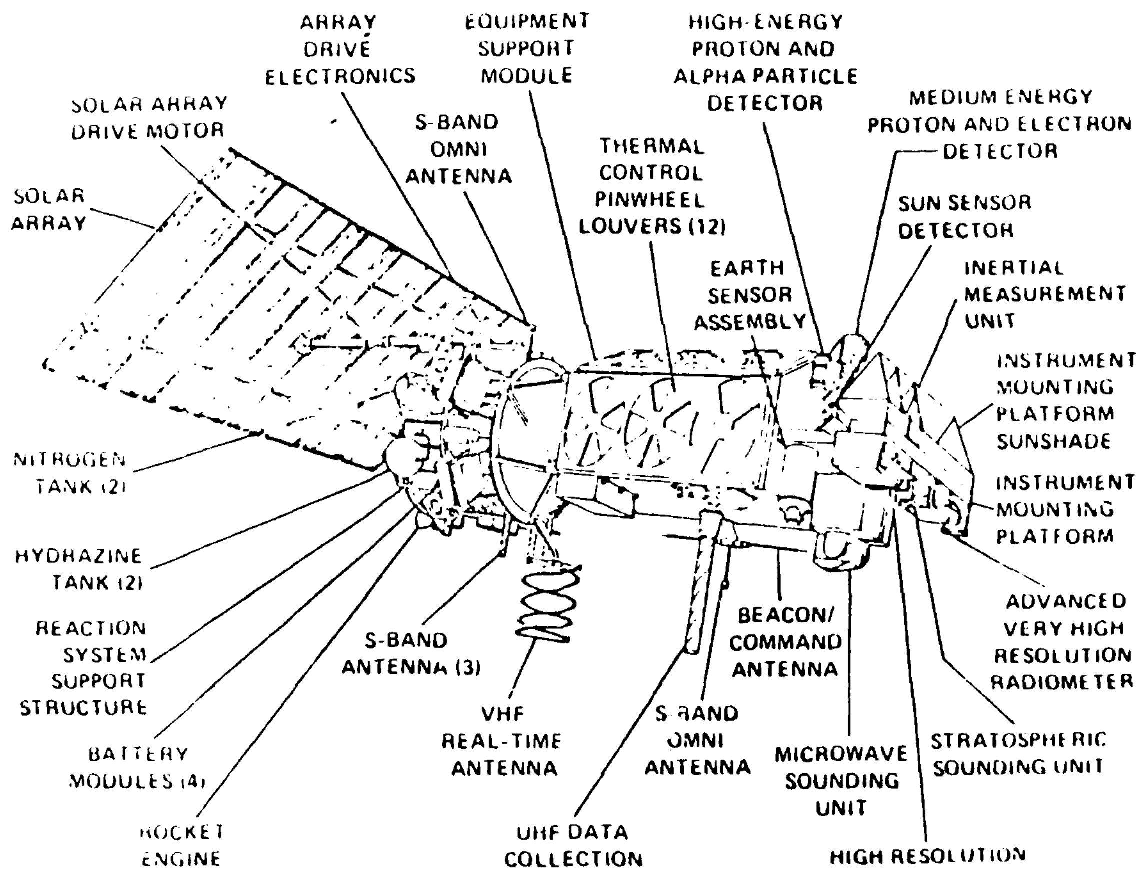

through the use of three mutually-orthogonal torque wheels which receive input from the Earth Sensor Assembly (ESA) for pitch and roll and, for yaw, an inertial reference source with sun-sensor updates. The ESA is an infrared (IR) sensor that views the entire earth and supplies torque input to keep the earth centered between four independent detectors. The sun sensor uses multiple data inputs from various mechanisms to provide the yaw input.

c. Data Handling Subsystem

There are four primary components in the data handling system onboard NOAA-6; the TIROS Information Processor (TIP), the Manipulated Information Rate Processor (MIRP), the Digital Tape Recorders (DTR), and the Cross Strap Unit (XSU). All the information eventually received on the ground from NOAA-6 has to be processed by at least one of these four components. Figure 10 is the data flow diagram for NOAA-6; attention is drawn to the path followed by the AVHRR data via the MIRP to the switching unit for subsequent transmission at 0.66 megabits per second to the earth station antenna as real-time High Resolution Picture Transmission (HRPT) data. The AVHRR-HRPT data stream was the only one used on this project. An explanation of the various other sensors shown in the diagram can be found in Schwalb (1978).

The MIRP formats the AVHRR data and adds synchronization, identification, telemetry, and time code information. It senses a pulse at the start of each AVHRR scan line and initiates a data sampling process that divides the arriving

Figure 10. NOAA-6 data flow diagram (from Hussey, 1979)

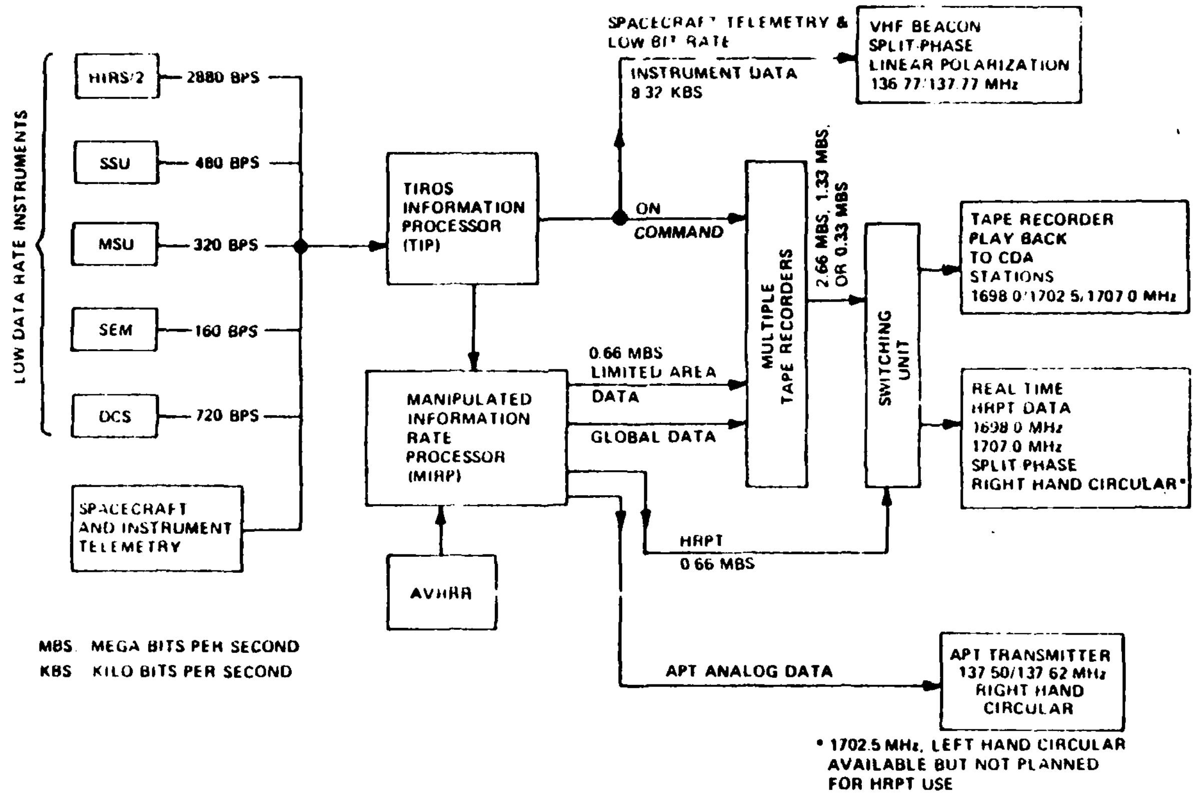

earth scan data into 2048 computer data words per scan line. The pulse that is sensed at the initiation of each scan line originates when the AVHRR scan mirror, which rotates at 360 RPM producing 6 scan lines per second, reaches a precise position in its sweep just prior to scanning across the surface of the earth. The data are stored in memory and then subsequently read out at a rate suitable for the HRPT on a first-in first-out basis. Any one of the 2048 data words or samples, along with the number of the scan line on which it is located, defines a pixel. Throughout this project, the term pixel will be defined by the designation (scan line number,sample number) or, in short, (NL,NS). A more comprehensive discussion of this process can be found in Section III.B below.

2. NOAA-6 Onboard Sensors

There are three primary environmental sensors onboard NOAA-6. The TIROS Operational Vertical Sounder (TOVS) consists of the High Resolution Infrared Radiation Sounder (HIRS/2) whose purpose is to provide data to allow calculation of vertical temperature profiles and atmospheric water and ozone concentrations, the Stratospheric Sounding Unit (SSU), and the Microwave Sounding Unit (MSU). The second sensor, the Space Environment Monitor (SEM), consists of a Total Energy Detector (TED), the Medium Energy Proton and Electron Detector (MEPED), and the High Energy Proton and Alpha Detector (HEPAD). The last of the three systems, the AVHRR, was the sensor system extensively used on this project and will be described in detail below. For an in-depth discussion of the first two

sensor systems mentioned above, the reader again is referred to Schwalb (1978).

The AVHRR aboard NOAA-6 is a *four-channel scanning* radiometer that is sensitive to energy in four regions of the electromagnetic spectrum. Table 1 below is a summary of NOAA-6 channelization.

Table 1

NOAA-6 AVHRR Channelization
(adapted from Schwalb, 1978)

CHANNEL	WAVELENGTH (μm)	REGION	PURPOSE
1	0.58 - 0.68	visible	cloud coverage land-water bound. snow-ice extent
2	0.725 - 1.1	visible- near-ir	as above
3*	3.55 - 3.93	mid-ir	sea surface temp. cloud mapping
4	10.5 - 11.5	far-ir	sea surface temp. cloud mapping

*On NOAA-6, channel 3 is very noisy and usually not used

An afocal 20.3 cm-aperture telescope, which produces a field of view of 1.3 ± 0.1 milliradians and an instantaneous field of view (IFOV) ground resolution of 1.1 kilometers at nadir (Lauritson, et al., 1979), separates the radiant energy into the four spectral regions with the help of secondary optics. The radiant energy in each of these regions is then focused on its respective detector. The quantity of energy

sensed by the detector then is converted to a count value from 0 to 255 in the format used for this project. Channel 4 was the main channel from which information was gathered and it uses a mercury cadmium teluride ($H_gC_dT_e$) detector optimized for best sensitivity between 10.5 and 11.4 micrometers (Schwalb, 1978). The spectral response curve for channel 4 is shown in Figure 11. The noise equivalent differential temperature (NEΔT), a measure of the random or coherent two-dimensional noise patterns superimposed on the data signal broadcast to earth, is less than 0.12 degrees Kelvin at 300 degrees Kelvin.

Pre-launch AVHRR calibration is covered in a report by ITT Aerospace (undated) and post-launch thermal calibration of channel 4 is covered extensively in a report by Laurtison, et al., (1979). For every scan line, the radiometer views deep space (0 radiance) and then a blackbody target designed into the radiometer housing and kept heated to 15 degrees centigrade. To a first order approximation, the radiometer output is linear with input energy (Schwalb, 1978) so a two-point linear calibration, using the above values, is done during every scan sequence. Channel 4 with its $H_gC_dT_e$ detector, however, has a not-quite-linear response due to the physical properties of the $H_gC_dT_e$. Lauritson, et al., (1979) have generated a table of errors for this channel, which represents the difference between the actual target temperature and the temperature derived from the two-point calibration. Table 2 is a summary of these data. Note particularly the small errors around 285 degrees Kelvin, for this is the sea surface temperature range

Figure 11. NOAA-6 AVHRR channel 4 spectral response curve (from Kidwell, 1979)

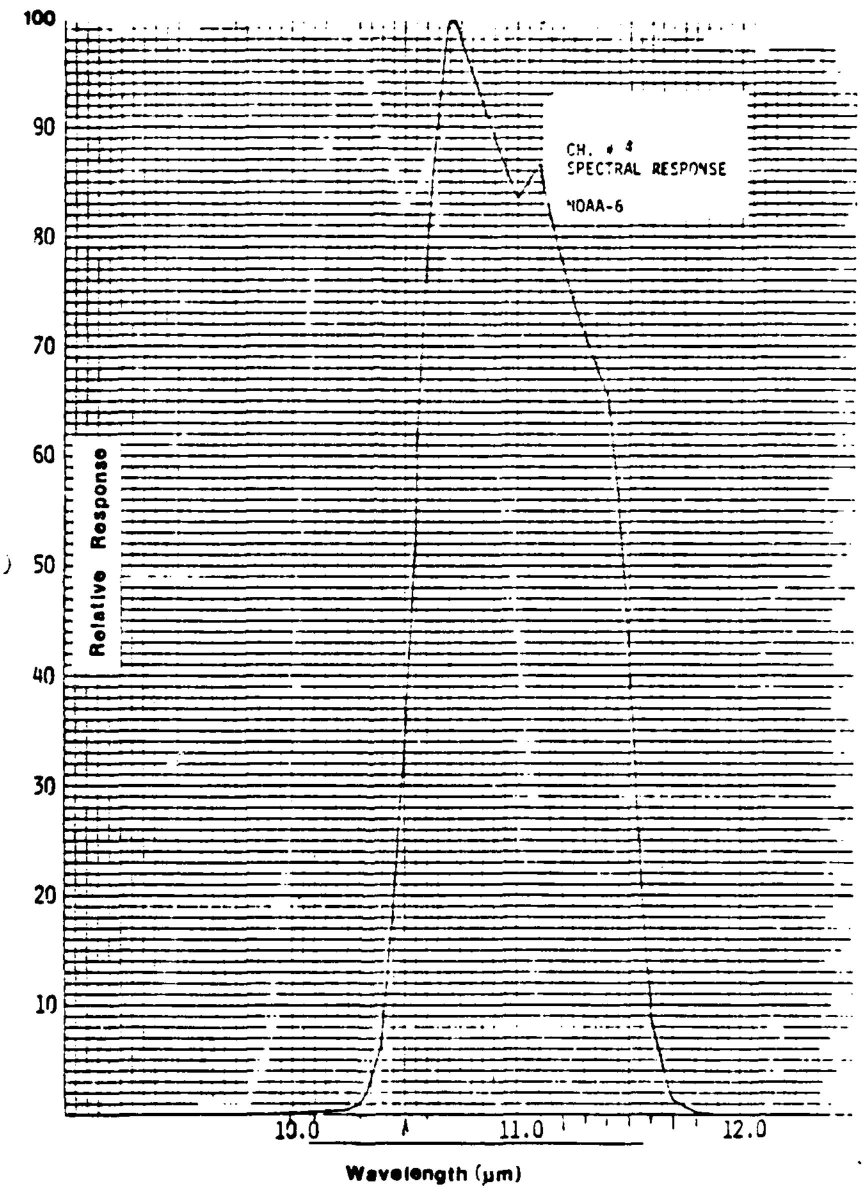

determined by the AXBT drops. With this information, a table of count-value-to-temperature conversions was generated for the time of this project by NOAA-NESS and is included in Appendix A.

Table 2

NOAA-6 AVHRR Channel 4 Nonlinearity Errors
(from Lauritson *et al.*, 1979)

TARGET TEMPERATURE (degrees K)	ERROR
305	0.5
295	0.3
285	0.0
275	-0.4
265	-0.8

3. NOAA-6 Orbital Parameters

Because the development of the satellite data set was so closely intertwined with the NOAA-6 orbital parameters, their discussion is included in Section III.B.3.c below.

III. DATA COLLECTION AND PROCESSING TECHNIQUES

The use of satellite data on any research topic introduces extensive data processing problems, especially when one considers that a typical NOAA-6 infrared satellite image contains over nine million pieces of data. This section explains the procedures used on this project to collect, process, and analyze NOAA-6 satellite imagery with emphasis in the area of geographic location accuracy. Also included in this section are the procedures to collect and process the AXBT data as well as the collection of the GOSSTCOMP product.

A. AXBT COLLECTION AND PROCESSING

As part of the data base for this project, a series of six Navy P-3C aircraft flights were staged out of NAS Moffett Field, California, for the purpose of dropping a pattern of bathythermographic sonobuoys (AXBT). The dates of these flights were 15, 17, and 19 November and 1, 3, and 5 December 1980. These flights were scheduled as part of the Naval Postgraduate School's research effort on behalf of the joint U.S.-Canadian Storm Transfer and Response Experiment (STREX).

Eact of the nine-hour flights flew northwestward from Cape Mendocino, California and proceeded to drop a series of AXBT's along a track 1333 kilometers (720 nm) long as shown in Figure 12. The spacing between the buoys was 55.6 kilometers (30 nm). The first four flights flew out and back on the center track dropping AXBT's on positions 1 through 24. Flight 5 flew the

Figure 12. AXBT patterns for the project area

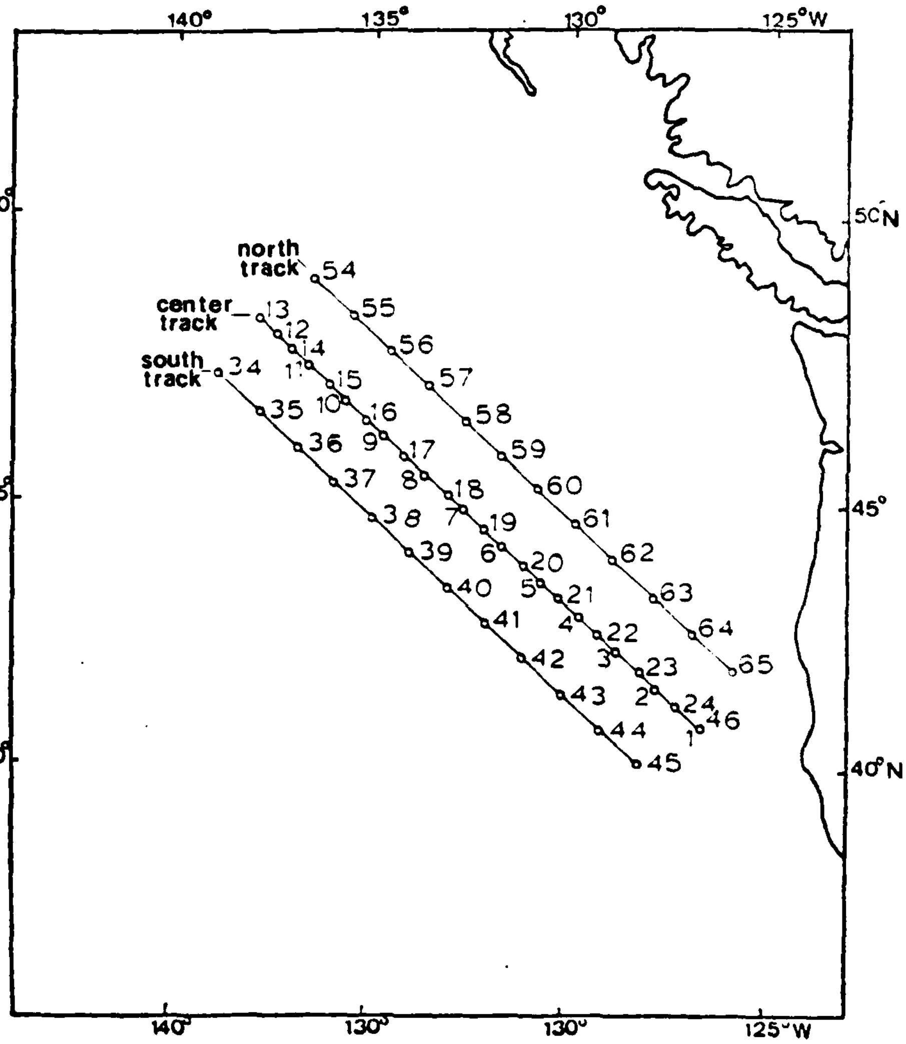

center track on the outbound leg and flew the southern track on the return leg dropping AXBT's on positions 1 through 13 and 34 through 46. Flight 6 repeated the center track outbound and flew the northern track inbound dropping AXBT's on positions 1 through 13 and 54 through 65. The northern and southern return tracks were designed to gather data on the horizontal thermal structure and were offset 111 kilometers (60 nm) either side paralleling the center track.

The complete navigation suite of the P-3C was used in calculating the position of each of the deployed AXBT's. At the end of each flight, the cumulative error of the inertial navigation system was checked and recorded. For the flights whose data were selected for the project, this error was less than 4 nautical miles.

Also important to note is the procedure that the P-3C onboard computer uses to calculate the splash points of the deployed AXBT's. Upon releasing the AXBT from the aircraft, the computer ballistics program uses the calculated wind speed and wind direction from the navigation system to provide a trajectory for the first 2000 feet of fall. After this 2000 feet of fall, the ballistics program assumes a straight descent to the water. This entry point becomes the so-called splash point for which geographical coordinates are calculated and displayed to the flight crews. Most of the AXBT's were dropped from an altitude of 2000 feet except when low clouds or icing conditions prevented flying at that altitude. It was felt

that the location error associated with the few high altitude drops was within the 4 nm aircraft navigation error.

1. The Air-Dropped Expendable Bathythermograph (AXBT)

The AXBT is an air-dropped expendable bathythermograph transmitter set deployed by Navy P-3C and S-3A aircraft. Its purpose is to provide an accurate profile of the vertical thermal structure from the ocean's "surface" to about 350 meters. Upon water entry, a seawater battery activates, powering a VHF transmitter, and approximately 30 seconds later a temperature probe begins a 5 foot/second descent (Sparton Electronics, 1976). The temperature probe and accompanying electronics within the sonobuoy package translate the sensed water temperature into a frequency broadcast by the radio transmitter using the formula

$$\text{frequency} = 800 + 20(\text{temperature deg. F.}).$$

This low-power broadcast from the sonobuoy is intercepted by the aircraft where it is electronically recorded on specially processed paper in real-time.

The accuracy of this process is governed by the accuracy of the thermal probe on the sonobuoy and this is claimed to be within 1.0 degrees C by the manufacturer (Sparton Electronics, 1976). Reports in the literature place the repeatable accuracy to within 0.2 degrees (Barnett et al., 1979). The detailed workings of this type of AXBT is described in Sessions and Wilson (1976) although the buoy described in their work was supplied by a different manufacturer.

It is also important to note that the temperature probe does not start at the surface of the ocean but begins its descent from a depth of about 0.2 meters (Barnett et al., 1979). The probe itself also may be subject to very low temperatures if the aircraft transports the buoys at a high altitude for a long period of time before deployment or if the buoys themselves are dropped from a high altitude. Both Navy aircraft described above have systems designed to prevent the freeze-up of the sonobuoys, and altitude launch restrictions do apply for the deployment of this buoy.

2. AXBT Data Processing

The thermal profiles were recorded using two different methods. As described above, the P-3C-produced paper copy of the thermal profile was used with a plastic overlay to read off the temperature for any depth. These readings were then transferred to paper logs by hand. The accuracy of this method is within the accuracy limits of the AXBT itself.

The second method involved the use of an AXBT-digitizer provided by the University of Hawaii and which was used also in the NORPAX Experiments. This piece of equipment was designed specifically to be used onboard the P-3C aircraft during flights. It connects into the equipment that receives the signal broadcast from the AXBT and digitally records on magnetic tape the signal representing the thermal profile at one second intervals. These tapes then are analyzed on a computer and various outputs produced. Figure 13 is an example of a group of AXBT profiles produced by this system. Figures 14 and

Figure 13. Digitizer AXBT profiles, an example (from Kilonsky, 1981)

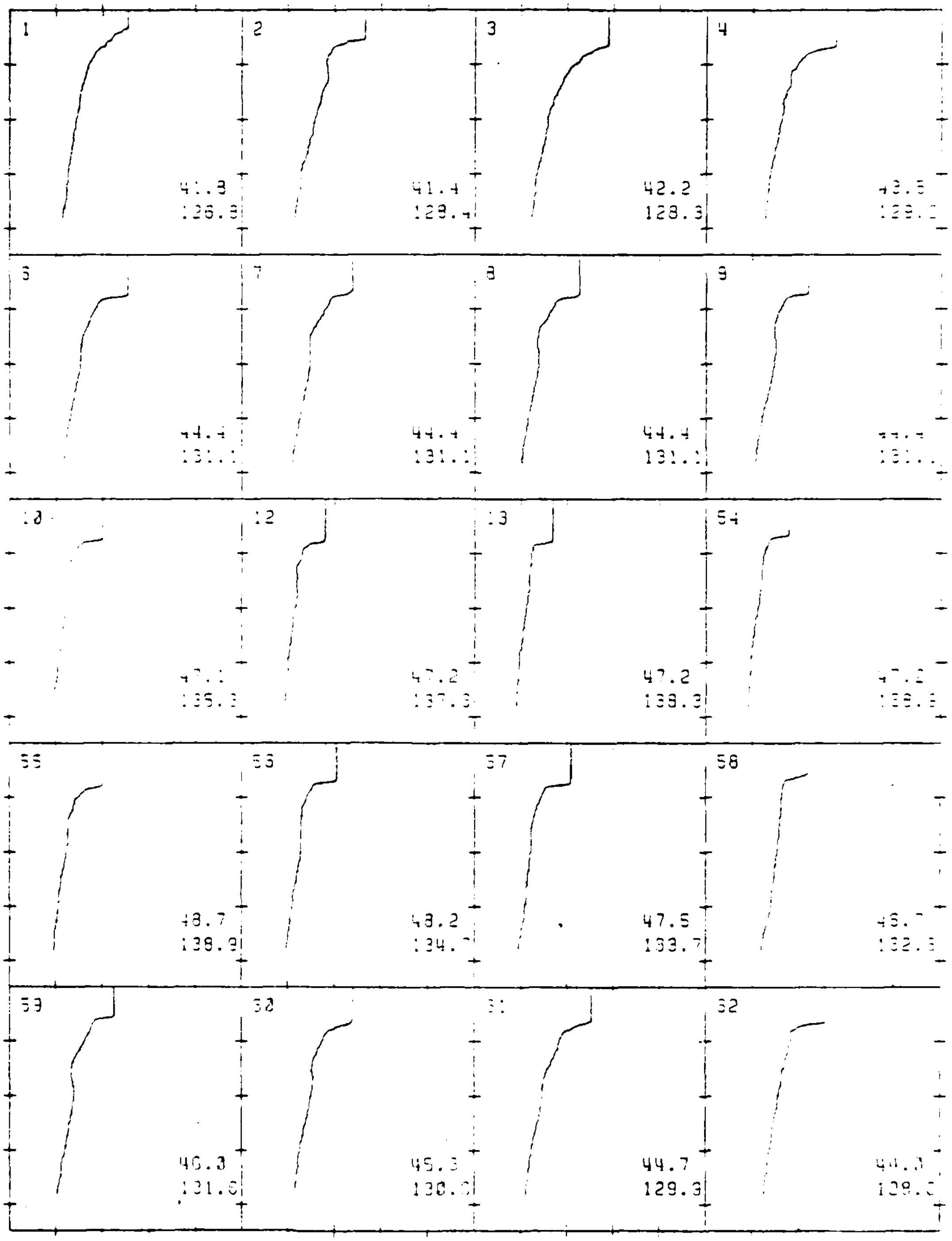

Figure 14. Digitizer depth-of-isotherm summary, an example (from Kilonsky, 1981)

CRUISE # -5

			DEPTHS OF ISOTHERMS IN METERS																									
LAT	LONG	YRMODAHRMN	30	29	28	27	26	25	24	23	22	21	20	19	18	17	16	15	14	13	12	11	10	9	8	7	SST	MLD
42.2	128.3	6912031909												67	72	81	87	101	164	204	295						14.64	70
42.9	129.2	6912031927												56	62	66	75	84	116	196	293						14.16	62
43.6	130.1	6912031944													37	41	47	68	111	152	256	335					13.38	42
44.4	131.1	6912032008													67	72	76	82	108	137	252	324					13.06	72
45.1	132.1	6912032025															65	69	83	121	201	304					11.77	69
45.8	133.1	[illegible]															80	83	88	116	152	275					11.42	83
46.5	134.2	[illegible]																75	78	105	223	323					10.99	77
47.2	135.3	[illegible]																59	60	63	91	226	336				[illegible]	62
48.5	137.5	[illegible]																		65	77	122	282				8.86	66
[illegible]	[illegible]	[illegible]																		79	81	111	237				8.16	52
47.9	[illegible]	[illegible]																	77	89	83	181	333				9.40	80
47.3	137.7	[illegible]																	81	86	102	261	350				9.54	86
[illegible]	131.5	[illegible]															68	70	80	111	210	312					11.11	70
44.6	[illegible]	[illegible]														58	63	68	94	131	221	297					12.01	64
[illegible]	[illegible]	[illegible]													60	74	79	93	136	177	277	356					[illegible]	74
[illegible]	[illegible]	[illegible]													41	43	48	53	117	179	294						11.16	43
41.8	[illegible]	[illegible]													44	47	57	69	109	160	[illegible]	335					13.89	46
41.1	[illegible]	[illegible]													51	59	69	75	116	168	263						[illegible]	54
40.7	[illegible]	[illegible]														38	51	70	89	113	205	331					[illegible]	45

[illegible]

15 show two additional products, a depth-of-isotherm summary and a listing of the temperature at 5 meter intervals for each AXBT. The accuracy of this system is also within the accuracy limits of the AXBT.

It should be noted also that the AXBT-digitizer had provisions for recording the raw received signal from the AXBT onto an analog tape recorder. These tapes then were used during the analysis phase as a direct input to the AXBT-digitizer in order to verify questionable temperature profiles.

B. SATELLITE DATA SET SELECTION AND PROCESSING

The decision criteria used to determine which satellite passes to examine were reviewed in the following order:

(1) the satellite pass coverage had to include the ocean area where the AXBT's were dropped;

(2) the time of the satellite pass should be as close as possible to the time when the AXBT's were dropped;

(3) the ocean areas containing the AXBT's should be relatively cloud-free; and

(4) there had to be at least one clearly identifiable landmark somewhere on the full satellite image.

Two outside government facilities were used in addition to the facilities at the Naval Postgraduate School in order to choose satellite passes which met these decision criteria.

1. NOAA-NESS

The facilities of the Satellite Field Services Station of the National Oceanic and Atmospheric Administration's National

Figure 15. Digitizer temperature-at-5-meter-intervals summary, an example (from Kilonsky, 1981)

date time lat. long. axbt no. depth (m) temp. (C)

```
1191180   3  192614  425500 1291200  38   4                                   77
  01481    51483   101483   151483   201481   251483   301481   351482   401482   431482
 501462   551421   601341   651217   701104   751071   801045   851032   901013    95 972
100 933 105 945 110 929 115 917 120 911 125 904 130 902 135 889 140 881 145 862
150 851 155 843 160 830 165 833 170 827 175 830 180 819 185 811 190 797 195 794
200 795 205 786 210 776 215 773 220 770 225 765 230 760 235 752 240 740 245 740
250 733 255 730 260 725 265 717 270 711 275 705 280 698 285 694 290 688 295 682
300 674 305 671 310 668 315 662 320 657 325 655 330 652 335 649 340 644 345 644
350 636 355 630 360 624 365 622 370 617 375 614 380 612
2191180   3  193818  433800 130 800  39   5                                   77
  01443    51445   101443   151446   201440   251438   301440   351442   401440   431442
 501446   551419   601311   651136   701091   751059   801049   851034   901021    95 996
100 980 105 959 110 943 115 928 120 912 125 897 130 900 135 894 140 886 145 878
150 855 155 843 160 829 165 822 170 816 175 811 180 893 185 797 190 789 195 783
200 772 205 768 210 770 215 770 220 768 225 762 230 757 235 754 240 751 245 745
250 723 255 735 260 727 265 722 270 719 275 713 280 708 285 700 290 692 295 687
300 676 305 671 310 663 315 652 320 644 325 634 330 625 335 614 340 609 345 604
350 596 355 589 360 587 365 584 370 579 375 574 380 571
3191180   3  195034  442100 131 700  55   6                                   77
  01295    51396   101397   151395   201395   251395   301397   351395   401394   451394
 501395   551222   601120   651039    70 991    75 967    80 959    85 949    90 932    95 918
100 995 105 909 110 878 115 870 120 862 125 853 130 838 135 827 140 814 145 781
150 773 155 765 160 761 165 752 170 744 175 738 180 735 185 738 190 733 195 734
200 723 205 735 210 727 215 727 220 727 225 719 230 717 235 702 240 694 245 692
250 624 255 632 260 671 265 663 270 663 275 651 280 646 285 644 290 639 295 636
300 623 305 617 310 606 315 600 320 596 325 593 330 588 335 582 340 574 345 571
350 571 355 565 360 561 365 555 370 550 375 547 380 545
4191180   3  20 253  45 400 132 700  58   7                                   77
  01314    51311   101314   151314   201317   251319   301317   351316   401316   451314
 501317   551300   601112   651013    70 988    75 952    80 933    85 929    90 900    95 889
100 870 105 854 110 835 115 814 120 794 125 783 130 769 135 754 140 744 145 735
150 723 155 733 160 733 165 733 170 733 175 735 180 733 185 735 190 735 195 733
200 724 205 732 210 727 215 727 220 732 225 722 230 722 235 718 240 712 245 710
250 701 255 695 260 590 265 684 270 682 275 677 280 667 285 657 290 617 295 639
300 631 305 623 310 620 315 613 320 608 325 601 330 599 335 582 340 574 345 571
350 563 355 557 360 550 365 547 370 543 375 536 380 536
5191180   3  201523  454600 133 800  63   8                                   77
  01220    51306   101306   151306   201306   251303   301303   351306   401305   451306
 501263   551306   601287   651029    70 964    75 922    80 906    85 885    90 870    95 859
100 754 105 813 110 827 115 796 120 769 125 742 130 719 135 703 140 698 145 698
150 693 155 701 160 702 165 702 170 698 175 702 180 705 185 706 190 706 195 703
200 702 205 701 210 693 215 695 220 699 225 687 230 684 235 679 240 674 245 668
250 663 255 600 260 652 265 649 270 649 275 641 280 635 285 631 290 628 295 625
300 629 305 612 310 612 315 601 320 593 325 599 330 582 335 574 340 571 345 369
350 563 355 557 360 553 365 546 370 542 375 539 380 531
6191180   3  202220  462800 1341200  66   9                                   77
  01193    51203   101204   151204   201204   251204   301204   351203   401203   451204
 501204   551205   601201   651136    70 883    75 850    80 837    85 824    90 811    95 805
100 820 105 797 110 734 115 769 120 738 125 742 130 695 135 684 140 679 145 684
150 690 155 694 160 701 165 701 170 793 175 703 180 701 185 703 190 701 195 698
200 695 205 686 210 679 215 682 220 682 225 674 230 671 235 667 240 665 245 663
250 660 255 655 260 649 265 641 270 639 275 628 280 623 285 617 290 612 295 606
300 601 305 596 310 590 315 581 320 576 325 569 330 566 335 555 340 553 345 547
350 545 355 539 360 534 365 527 370 529 375 518 380 512
7191180   3  204123  46 700 1334000  64  17                                   77
  01279    51282   101282   151282   201282   251282   301282   351282   401281   451281
 501272   551279   601271   651147   701031    75 948    80 905    85 885    90 870    95 857
100 845 105 852 110 819 115 898 120 738 125 772 130 757 135 751 140 744 145 730
150 722 155 721 160 721 165 724 170 730 175 727 180 727 185 735 190 730 195 719
200 719 205 718 210 719 215 717 220 717 225 714 230 711 235 704 240 697 243 690
250 637 255 682 260 671 265 666 270 657 275 657 280 652 285 637 290 636 295 631
300 628 305 620 310 617 315 609 320 605 325 601 330 593 335 588 340 583 345 577
350 574 355 568 360 564 365 557 370 553 375 545 380 542
```

Environmental Satellite Service (NOAA-NESS) in Redwood City, California, were used in initially selecting the satellite passes. The Redwood City facility is one of three NOAA-NESS stations that monitor NOAA-6; the other two are the Command and Data Acquisition (CDA) stations in Gilmore Creek, Alaska, and Wallops Island, Virginia. Redwood City differs from the CDA stations in that Redwood City records the digital High Resolution Picture Transmission (HRPT) readout consisting of three channels of AVHRR data in the 8-bit precision field-station format. These 1600 BPI, 9-track computer-compatible magnetic tapes then are archived in Redwood City on a 90-day rotating basis. The CDA stations record the various other data formats broadcast from NOAA-6 as well as recording the HRPT data in 10-bit precision which then are forwarded to the NOAA Suitland, Maryland, facility where processing and archiving on a more permanent basis occur. The precision loss in going from the 10-bit HRPT data to the 8-bit HRPT data is between 0.4 and 0.5 degrees when making thermal comparisons (Kidwell, 1979). The amount of data recorded per satellite pass depends on the satellite's elevation in relation to the receiving station antenna and can be limited by the 13-minute capacity of a standard length magnetic tape. Passing directly over Redwood City's antenna, NOAA-6 would be within reception range for 15.5 minutes, depending on orbital altitude, and could provide data from a circular area 6200 kilometers in diameter centered on the antenna (Schwalb, 1978). According to Schwalb, the satellite provides useful data only if it is

at least five degrees above the horizon. This reduces the contact time to 13 minutes and the circular area to 5200 kilometers.

a. Field-Station Format

The field-station format differs from the CDA-station format in that it is a combination ASCII-Binary format consisting of a single header record at the beginning of the tape followed by up to 15000 data records. Each of the data records is a sequential interleavening of the scan lines and the recorded channels as shown in Table 3 below:

Table 3

Field-Station Format

RECORD	CONTENTS
1	header
2	scan line 1--AVHRR channel A
3	scan line 1--AVHRR channel B
4	scan line 1--AVHRR channel C
5	scan line 2--AVHRR channel A
.	.
.	.
.	.
14998	scan line 5000--AVHRR channel A
14999	scan line 5000--AVHRR channel B
15000	scan line 5000--AVHRR channel C

channel A, B, or C = any sequence of channels 1, 2, 3, 4

The 40-byte header record, all in ASCII, contains the ground station identification (SFO for Redwood City), the channel numbers identifying which three of the four available AVHRR channels were recorded, the time (GMT) of the first scan line, the duration of the pass, and the orbit number. See Figure 16 for an example of the header record. Each of the remaining 15000 or so data records have identical 2138-byte formats beginning with a 14-byte ASCII "mini-header" consisting of an identification sequence, the specific AVHRR channel number from which the data in the record originated, the Julian date of the scan line, and the time (GMT) of the scan line. Following the "mini-header" are 10 bytes of telemetry data, 6 bytes of back scan data, 10 bytes of space view data, and 50 bytes of space data, all in binary format. The remaining 2048 bytes, also in binary, are the video data from which estimates of the sea-surface temperature are derived. See Figure 17 for an example of one of these data records.

b. Ephemeris Data Set

A set of ephemeris data for NOAA-6 also is maintained at Redwood City. An ephemeris data set consists of tracking information so that the field station can capture the satellite's data stream as the satellite rises above the horizon and passes overhead to the opposite horizon. See Figure 18 and Figure 19 for examples of an ephemeris data set. More importantly to this project, the ephemeris also contains the subsatellite points for the pass calculated at one minute intervals. A subsatellite point is that point on the earth's

Figure 16

Header record--field-station format
(adapted from Kidwell, 1979)

WORD	BYTE	CONTENTS	BYTE	CONTENTS	TYPE
1	1	station ID	2	station ID	ASCII
2	3	station ID	4	blank	ASCII
3	5	blank	6	channel A	ASCII
4	7	channel B	8	channel C	ASCII
5	9	hours	10	hours	ASCII
6	11	minutes	12	minutes	ASCII
7	13	seconds	14	seconds	ASCII
8	15	duration-min	16	duration-min	ASCII
9	17	duration-sec	18	duration-sec	ASCII
10	19	orbit	20	orbit	ASCII
11	21	orbit	22	orbit	ASCII
12	23	orbit	24	blank	ASCII
13-20	25-40	blank			

channel A, B, or C = channel 1, 2, 3, or 4

As an example, a pass selected for the project may have a header record as follows:

SFO 1340333481300 7244

indicating a Redwood City tape (SFO) containing AVHRR channels 1, 3, and 4. Time of the first scan line was 03 hours 33 minutes and 48 seconds (GMT) while the duration of the pass recorded was 13 minutes and 00 seconds. The orbit number was 7244.

Figure 17

Data record--field-station format
(adapted from Kidwell, 1979)

WORD	BYTE	CONTENTS	BYTE	CONTENTS	TYPE
1	1	ID	2	ID	ASCII
2	3	ID	4	ID	ASCII
3	5	channel no.	6	day	ASCII
4	7	day	8	day	ASCII
5	9	hours	10	hours	ASCII
6	11	minutes	12	minutes	ASCII
7	13	seconds	14	seconds	ASCII
8-12	15-24	telemetry data (average)			Binary
13-15	25-30	back scan data (average)			Binary
16-20	31-40	space view data (average)			Binary
21-45	41-90	space data (raw)			Binary
46-1078	91-2138	video			Binary

Figure 18. Ephemeris data set, an example (from Breaker, 1980).

TIROS-N NAVIGATION SYSTEM POLAR SPACECRAFT EPHEMERIS ACCESS ROUTINE

INITIALIZATION REPORT AT NOV 28,1980 VER 3.0

KEPLERIAN		ORBITAL ELEMENTS	
SEMI-MAJOR AXIS	7199.1555973122	SEMI-MAJOR AXIS =	1.12733638
ECCENTRICITY	0.0006027081	ECCENTRICITY =	0.00114034
INCLINATION	98.6912265338	INCLINATION =	98.69562637
RT ASC OF ASC NODE	1.5502936649	R.A. OF ASCEND. NODE =	1.54938308
ARG OF PERIGEE	153.0766804545	MEAN ANOMALY =	142.83669892
MEAN ANOMALY	202.2727505348	ARGUMENT OF PERIGEE =	212.52125960

ANOMALISTIC PERIOD .... = 101.130840 MINUTES

GHA OF ARIES AT EPOCH TIME .... = 370.6652 DEGREES

REVOLUTION NUMBER AT EPOCH TIME .. = 7381

Figure 19. *Ephemeris data set, an example (from Breaker, 1980)*

REV.NO. 7507 ASC NOD: TIME 1515/477 ASC NODE LONG 56.65 DEG

DAY	HR	MIN	SUBPOINT LAT	SUBPOINT LONG	STA SFC	ELEV	AZ	X AXIS	Y AXIS
6	15	43	60.4N	56.1W					
6	15	44	73.[illegible]N	72.4W					
6	15	45	75.8N	83.5W					
6	15	46	72.9N	91.2W					
6	15	47	69.8N	96.7W					
6	15	48	66.5N	100.9W					
6	15	49	63.3N	104.1W					
6	15	50	59.5N	106.7W	CC	2.3	16.9	80.0	70.8
6	15	51	56.4N	108.9W		7.5	20.9	69.7	67.9
6	15	52	53.0N	110.7W		12.6	23.5	60.7	63.5
6	15	53	49.5N	112.3W		19.0	27.3	53.1	57.2
6	15	54	46.1N	113.9W		27.4	33.3	46.7	48.0
6	15	55	43.6N	115.1W		38.6	44.3	41.1	34.0
6	15	56	39.1N	116.3W		51.6	68.2	36.3	13.3
6	15	57	35.6N	117.4W		55.8	113.3	31.9	-12.8
6	15	58	32.1N	118.4W		45.0	148.3	27.8	-37.0
6	15	59	28.5N	119.4W		32.3	164.1	23.5	-54.4
6	16	0	[illegible]	120.3W		22.5	171.9	18.6	-66.1
6	15	1	21.5N	121.3W		15.2	176.5	12.6	-74.4
6	16	2	17.9N	122.0W		9.6	179.5	2.9	-80.4
6	15	3	14.4N	122.9W		4.9	181.7	-18.5	-84.8
6	16	4	10.9N	123.7W	3C	1.0	183.3	-73.4	-86.6

surface directly beneath the spacecraft and represents the middle of the scan line for the AVHRR. All the subsatellite points for each scan line taken together represent the ground track that the satellite followed in its orbit. It should be noted that any alignment errors made when the AVHRR module was attached to the spacecraft during construction may result in the subsatellite point not being the center of the AVHRR scan line. A summary of alignment data may be found in an undated report prepared by ITT Aerospace for NASA. For the purposes of this project it was decided that any alignment errors were so slight as to be negligible and therefore that the sub-satellite point would represent the center of each AVHRR scan line. Other information in the ephemeris data set important to this project were the orbital elements listed in the preface to each ephemeris including orbital period, semi-major axis, eccentricity, and inclination. This information was vital to the orbital calculations made further on in this project and will be explained there.

c. Initial Satellite Pass Selection

Each AVHRR scan line is approximately 2840 kilometers long with 1420 kilometers on each side of the subsatellite point. With this information as well as the ephemeris data sets for the dates of the P3-C flights and a chart of the Northeast Pacific Ocean, it was relatively easy to determine specific passes which viewed the ocean areas where the AXBT's were dropped, thus satisfying the first decision criterion

mentioned above. Twenty-two satellite passes were thus selected for further screening.

The selection from these 22 passes of orbits whose time matched as closely as possible the time of the AXBT drops was done in conjunction with the investigation of cloud coverage over the ocean area of interest. As the project relied solely on the use of the infrared channels of the AVHRR and because cloud cover effectively prevents AVHRR scan coverage of the ocean surface, the absence of cloud cover in the ocean area of interest was a major factor in pass selection. Also, as will be discussed below, NOAA-6 is a sun-synchronous satellite that circles the earth 14.2 times every 24 hours. As a result, NOAA-6 views the same earth location at the same local sun time each day. This translated to our ocean area of interest as between 0330 and 0400 (GMT) for ascending passes and between 1650 and 1720 (GMT) for descending passes. Since Redwood City maintains hourly pictures taken from the visual channels of the geostationary GOES-WEST satellite, examination of these pictures for cloud coverage in the ocean area of interest resulted in the selection of one pass for each of the six flight dates that represented the best compromise between matching times and cloud coverage. The six passes chosen for further examination are listed in Table 4 below.

2. NASA-Ames Research Center

The last criterion to be satisfied, identification of a landmark on each image, was done on the Interactive Digital Image Manipulation System (IDIMS) located at the Technology

Table 4

Selected Satellite Passes

AIRCRAFT FLIGHT	PROJ. NO.	AXBT DROP TIMES (DTG)	ORBIT NO.	ORBIT TIMES (DTG)	TYPE PASS
15 Nov 80	1	151905-160049	7209	151658-151711	D
17 Nov 80	2	171932-180236	7244	180331-180346	A
19 Nov 80	3	191843-192232	7266	191712-191716	D
01 Dec 80	4	011826-020031	7429	010344-010358	A
03 Dec 80	5	031826-040127	7465	031656-031710	D
05 Dec 80	6	051816-060013	7486	050355-050408	A

where D = descending and A = ascending

Applications Branch of the Airborne Missions and Applications Division under the Director of Astronautics, NASA Ames Research Center, Moffet Field, California.

a. IDIMS

The IDIMS system is a software package that interacts with a minicomputer (HP-3000), a display terminal, a 25-inch COMTAL display screen, a Dunn Instruments color camera recorder, and a high-speed printer, and is used extensively to work with satellite data, especially LANDSAT imagery. Options are available that allow the user to manipulate interactively satellite imagery so that specific topics of interest may be investigated like land use with LANDSAT data, sea surface temperature, cloud cover, or ice pack coverage as examples from TIROS-NOAA imagery or the many other applications available from NIMBUS-7 imagery. The mechanics behind specific options

are proprietary data owned by Electromagnetic Systems Laboratory, Inc. (ESL) of Sunnyvale, California, who developed IDIMS and to whom the reader is referred for more detailed information (ESL, Inc., 1978). A second IDIMS system is located at the Scripps Institution of Oceanography in La Jolla, California, where initial training was done by the author in the use of the IDIMS system. A third IDIMS system, also operated by NASA Ames, is located in a mobile van that tours the Western United States; its facilities were used upon one of its stops at the Naval Postgraduate School.

b. Landmark Identification

The basic procedure for landmark identification used by this project on the IDIMS system was as follows:

(1) run a short tape routine on each of the selected pass's magnetic tapes to identify the number of data records, hence the number of scan lines per pass (number of data records minus 1 header record, all divided by 3);

(2) read the 3-channel AVHRR data from the magnetic tape into computer memory and initiate IDIMS processing;

(3) recall that data comprising the infrared channel from memory and display it on the COMTAL display screen;

(4) enhance the displayed infrared imagery for temperature using false colors;

(5) use the Dunn color camera recorder to produce an 8 by 10-inch color Polaroid photograph of the enhanced image;

(6) use the ZOOM option of IDIMS to enlarge selected sections of the displayed image in order to locate landmark pixels by scan line number and sample number; and finally,

(7) use the PICPRINT option of IDIMS to dump to the high-speed printer the count values of all pixels within a specified area surrounding the landmark.

An explanation of certain aspects of this procedure is explained in the sections below.

(1) Count Values. In order to display a satellite image on the COMTAL display screen, the IDIMS system sequentially unpacks the video data read into memory from the magnetic tape. These data consist of count values between 0 and 255 which represent the difference in detected energy between a look at deep space and a look at a radiating surface such as the earth or clouds (Schwalb, 1978). These count values are used by the IDIMS system to produce an image with a grey-scale intensity range from 0 to 255 in order to match the same range of count values. Options available on the IDIMS system allow various color assignments based on these count values including an automatic full-spectrum false color assignment where red is "hot" and blue is "cold" or vice versa. Also available are options allowing a single color to vary in its saturation over the full count range of 256 values or the assignment of a specific color to an individual count as "blue=count 125" or to a range of counts as "blue=counts 125 through 130". Assigning colors in this manner tends to produce

a confusing image if many hues are used indiscriminantly. For purposes of this project, the automatic full-spectrum false color assignment of red "cold" and blue "hot" was used so that the oceans were blue and the cloud tops, being much colder, were red in all the photographs.

c. Pixel Identification

The identification of a landmark pixel and the subsequent assignment of a scan line number and sample number are made easy by the IDIMS system but the principles behind their assignment had to be understood so that other landmarks and buoy positions could be located as needed later on in the project.

As seen in Table 4 above, three of the six selected NOAA-6 passes were ascending passes and three were descending passes. An ascending pass is one where the satellite in its orbit crosses the earth's equator heading northwards while a descending pass is one where the satellite crosses the equator heading southwards. As the satellite is moving, the AVHRR scan mirror sweeps from right to left perpendicularly across the satellite's velocity vector six times per second with each sweep defining a single scan line. Although the scanning mirror rotates in a complete circle, only the data located 55.4 degrees either side of nadir is retained. Nadir is a term similar in meaning to the subsatellite point in that nadir represents that point on the sweep of the scanning mirror when the mirror is pointed at the spot on the earth's surface directly underneath the spacecraft. The radiometer data

stream from this 110.8-degree arc is electronically divided by the MIRP into 2048 equal samples each representing 0.054 degrees of the total arc (110.8 divided by 2048). Therefore, when the satellite transmits its data stream to the earth receiving station, the first 2048 bytes of video data taken together is intrinsically labeled scan line number 1 while the first byte is intrinsically labeled sample number 1 or, as used throughout this project, (1,1). The second byte of the first scan line is labeled (1,2). Sample number 1505 from scan line number 3520 would be labeled (3520,1505). Sample number 1 through 1024 are located to the right of the sub-satellite point when looking in the direction of the satellite's velocity vector while samples 1025 through 2048 are to the left. Because of this right-to-left pixel numbering system, when an image is displayed on the COMTAL unit by the IDIMS system, an ascending pass image looks reversed and upside down while a descending pass image looks normal where normal is defined as having Alaska to the north or top of the image, Hawaii to the west or left of the image, and California to the east or right of the image. An ascending pass image, when displayed on a display screen or when stored into computer memory for further processing, has Alaska on the bottom, Hawaii on the right, and California on the left of the image. This occurs because IDIMS always displays pixel (1,1) in the upper left corner of the COMTAL unit. Although landmark identification can be easily done on either type of pass, the geometry involved further on in this project rests heavily on a clear understanding of which

type of pass you are analyzing and on which side of the sub-satellite point is the landmark or buoy. Figure 20 is an example of an ascending pass while Figure 21 is an example of a descending pass. In each figure, the satellite would travel directly up or down the center of the image respectively.

The IDIMS system automatically keeps track of this numbering system and conveniently displays the scan line number, sample number, and count value for the pixel you have identified on the COMTAL unit using a movable cursor. By use of the ZOOM feature on IDIMS and with reference to a chart of the local area, it is usually easy to identify landmarks. In most of the passes used on this project, the San Francisco Bay Area was identified readily and its (scan line number, sample number) determined. For purposes described later on, up to 20 landmarks per satellite pass along the west coast of the United States from Glacier Bay, Alaska, south to Mexico and from San Francisco east to Pyramid Lake, Nevada, were identified. Only one of these landmarks is needed to navigate the image as will be explained later on.

The PICPRINT feature of IDIMS allowed the dumping to a high-speed printer of the count values of the pixels surrounding the landmark. This was done as a method of verifying the accurate position of the feature chosen for landmark identification. Figure 22 is an example of a PICPRINT output where by using a variation of the game of connecting the dots one can connect count values in order to recognize features. This method of verification will not work, or is made more difficult,

Figure 20. NOAA-6 ascending pass, from IDIMS processing

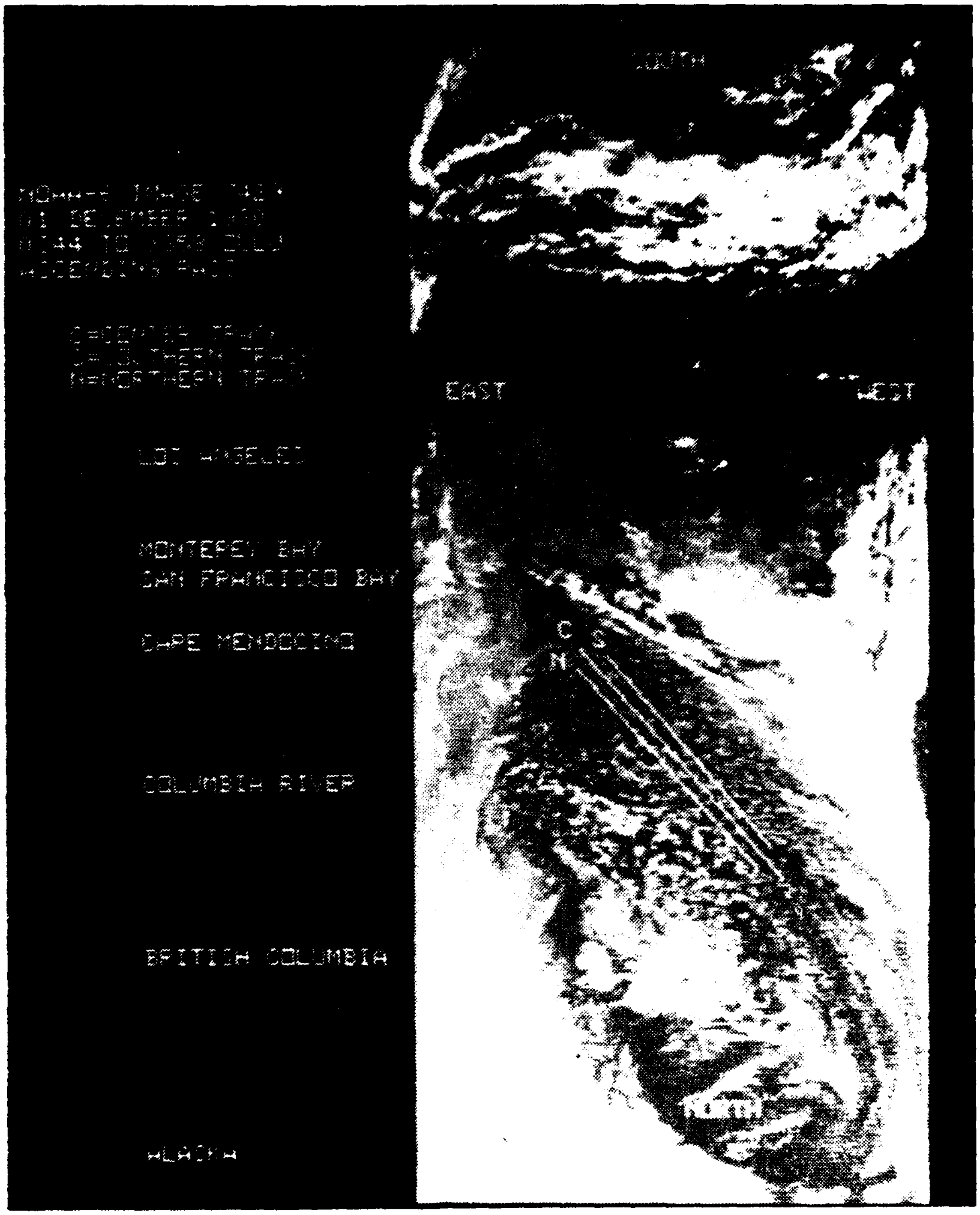

Figure 21. NOAA-6 descending pass, from IDIMS processing

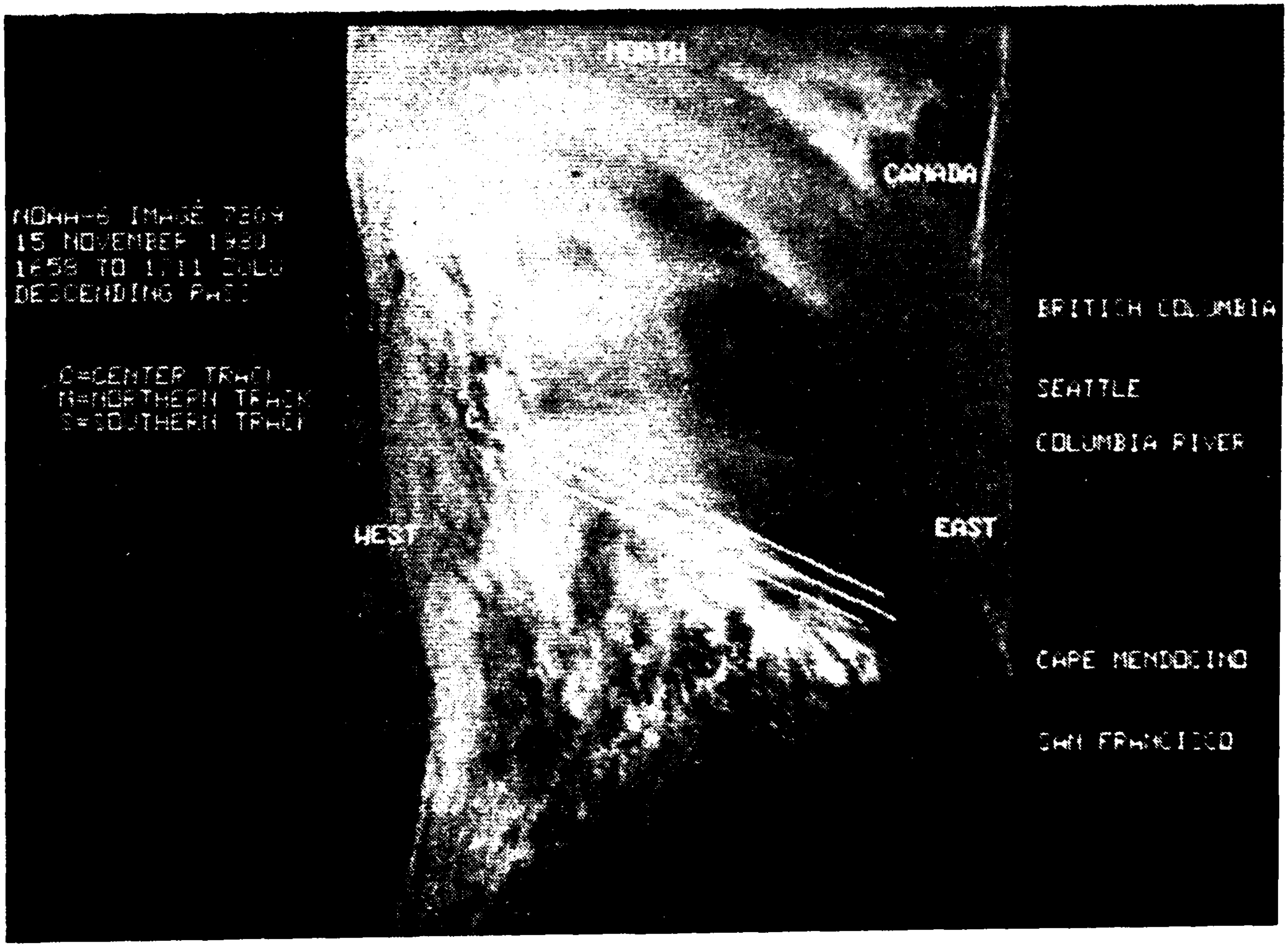

Figure 22. PICPRINT output of count values, San Francisco Bay entrance; cloud-free image

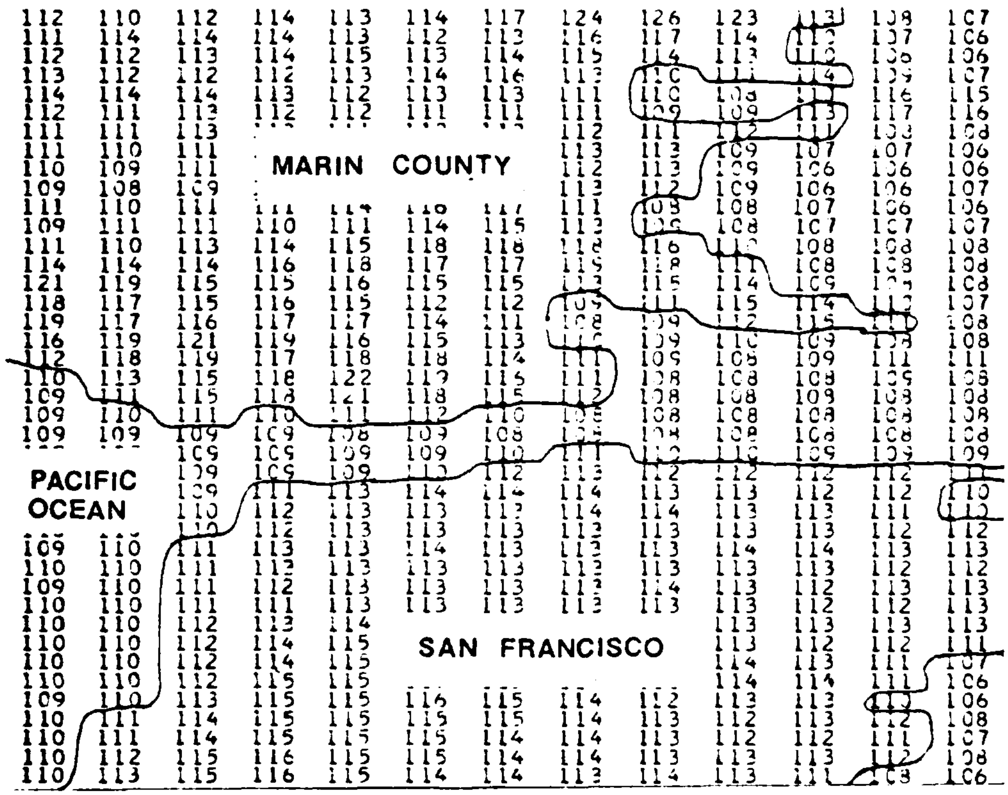

if the temperature of the land is the same as the water, if any low-lying clouds (fog) have similar temperatures as either the water or land, or if clouds obscure sections of the land. Normally, the visual channels of the spacecraft are used but since many of the passes occurred at night, only the infrared channels were usable. Figure 23 is an example of a case where clouds interfered with the landmark identification process.

Because an average pass contained 4680 scan lines each with 2048 samples or about 9.6 million pixels per pass, a convenient method of matching pixel numbers (hence count values) to AXBT positions was necessary; thus a system was needed to "navigate" the image.

3. Satellite Image Navigation

As mentioned in the introduction, there are many sources of error when one wants to compare satellite-derived sea surface temperatures and AXBT-derived sea surface temperatures. It was decided at the beginning of this project that an attempt would be made to reduce as much as possible one of these, that being the earth location errors associated with transferring AXBT drop positions to a satellite image, so that temperature comparisons could be made. Several methods were tried and three of those methods that produced the smallest errors are described below. For the purposes of developing procedures for locating AXBT's on the satellite image only, an assumption was made that the geographical location of the AXBT's was accurate; hence any aircraft navigation errors,

Figure 23. PICPRINT output of count values, San Francisco Bay entrance; cloud-covered image. (Note: This image is from an ascending pass hence it appears upside down.)

131	128	125	124	125	124	121	121	122	123	125	125	120
130	130						120	120	119	120	120	119
129	125	SAN FRANCISCO					119	118	118	118	117	114
128	126	124	122	121	119	118	118	118	117	117	116	113
126	126	125	124	124	122	121	119	118	117	116	114	112
127	128	127	126	127	127	124	122	119	116	114	113	112
130	129	127	125	125	125	123	120	118	117	115	114	114
134	134	132	128	125	126	129	126	123	120	118	116	116
130	130	130	128	127	126	127	126	126	127	127	125	123
135	132	130	128	127	128	127	126	126	130	130	129	125
132	137	[illegible]	131	130	131	130	129	128	131	132	131	128
135	134	CLOUDS	134	133	132	130	129	129	132	134	134	131
141	[illegible]	[illegible]	134	130	129	130	130	127	129	132	131	131
143	[illegible]	139	137	134	133	134	133	129	129	132	136	134
146	146	144	141	138	136	137	136	132	132	135	136	133
149	147	144	142	139	136	133	133	MARIN COUNTY				131
154	152	148	143	139	135	132	132					128
156	152	147	144	143	140	136	132	132	133	134	137	135
154	152	150	145	143	140	138	136	134	135	134	134	134
149	148	148	147	146	144	141	138	136	140	141	137	133
149	142	142	143	141	141	143	142	141	138	137	138	137
149	146	142	138	130	128	133	140	146	146	144	141	138
143	142	140	137	132	130	130	133	139	143	143	143	144
135	136	136	137	137	135	133	132	132	134	136	138	139
127	128	129	130	131	134	135	134	134	133	133	133	132

ballistic errors on the falling AXBT's once launched from the aircraft, drift errors on the floating AXBT, or human errors in transcribing positional data from aircraft displays to logs were ignored. These sources of error will be discussed later.

a. Zoom Transfer Scope

A Bausch and Lomb Zoom Transfer Scope was used initially in an attempt to transfer the AXBT positions to the satellite image. A zoom transfer scope allows one optically to overlay a chart, on which the AXBT positions have been plotted, onto a satellite image where enough distinguishing features (landmarks) are evident so that by optically stretching, condensing, or rotating the chart, landmarks on both chart and image coincide. Once the landmarks coincide, the operator manually marks with a pencil the AXBT positions onto the satellite image. While the system works fine with small area images consisting mostly of land, it could not be used satisfactorily on this project for a number of reasons. First, each of the selected NOAA-6 passes covered an area extending from Northern Mexico to Alaska and [illegible] mid-Pacific to the western United States. Reducing [illegible] of this area to a size suitable for use on a zoom transfer scope (about 10 by 10 inches) necessarily requires reduction in the accuracy of plotting geographical coordinates. Second, on each of the NOAA-6 passes, approximately 30 to 90 percent of the coverage area was open ocean with any visible landmass only on the edge of the image. Landmasses on the edges of these images are much more distorted than landmasses near the subsatellite

points due to a combination of satellite scan geometry, earth curvature, and the transfer of these images to a flat medium like a photograph or chart. Third, the AXBT's were dropped along a line over 1300 kilometers long stretching northwestard from Cape Mendocino, California. There are no landmarks in the Northeast Pacific Ocean between Cape Mendocino and the Aleutians; therefore location accuracy decreased the farther away from the coast the AXBT's were dropped. Fourth, marking a chart manually with a pencil necessarily involves inaccuracies especially when one is trying to locate geographically an item as small as an AXBT. Last, and the hardest to overcome, is that once the buoy position is marked on the satellite image, some method must be found to determine the pixel number and hence the count values of the AXBT's position. Remembering that there are 9.6 million pixels per image, determining the exact pixel to choose for a count value would involve some guesswork and possibly even large-scale pixel averaging. Satellite images unfortunately do not come marked with latitude and longitudes, nor do charts contain scan line numbers and sample numbers.

b. IDIM's TRNSFORM

A second method of trying to locate an AXBT on the satellite image involved the use of an ESL, Inc-developed IDIMS function called TRNSFORM. TRNSFORM is used mainly in registering LANDSAT imagery and involves the calculation of a transformation matrix between matching sets of control points using a least-squares fit method (ESL, Inc., 1978). A first,

second, or third order transformation is possible. TRNSFORM was not designed to navigate NOAA-6 imagery mainly because TRNSFORM requires 15 to 20 landmarks spread over the entire image in order to obtain a small pixel error. Therefore, use of this function also failed to provide the accuracy desired for this project for one of the same reasons that the zoom transfer scope failed, in that landmasses were present only on the edges of the images.

The method finally used, and from which a location accuracy of less than 2 pixels resulted, was the development of a computer program that determined a satellite's orbit referenced to a single landmark in the image and from this, when given an AXBT latitude and longitude, could determine the scan line number and sample number of the AXBT. The development of the program required a basic understanding of the orbital dynamics of NOAA-6 as well as a working knowledge of spherical geometry.

c. NOAA-6 Orbital Dynamics

For orbital information in this section, the work by Stewart (1979) and Schwalb (1978) was used extensively.

The NOAA-6 satellite is a sun-synchronous satellite which means that its orbital plane rotates at the same rate as the rotation of the earth about the sun. As a result, the satellite views a point on the Earth's surface at the same local sun time each day. Table 4 above listed those times that NOAA-6 viewed the AXBT drop area. According to Schwalb (1978), the orbital plane precession rate is approximately

equal to 0.000000199 radians per second or 0.986 degrees per day eastwards. This rate is achieved by placing the satellite in an orbit with a suitable inclination. In the case of the NOAA-6 satellite, the inclination was determined prior to launch to be 98.739 ± 0.15 degrees, where inclination (i) is defined as the angle the satellite's orbital plane makes with the earth's equatorial plane measured counterclockwise from east. A retrograde inclination (i_-) is the supplement of the inclination. See Figure 24.

Figure 24

NOAA-6 orbital plane inclination

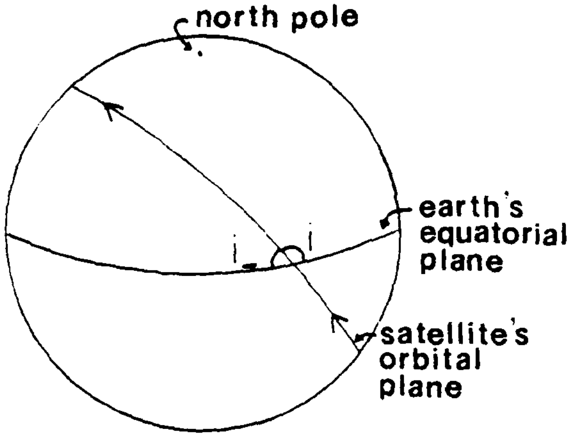

i = inclination (from ephemeris)

i_- = retrograde inclination

The period of the satellite, obtainable from the ephemeris data set (as is the inclination), is the amount of time it takes the satellite to make one orbit of the Earth.

The predetermined launch value for the NOAA-6 period was 101.58 minutes; therefore, NOAA-6 orbits the Earth 14.18 times per 24 hours. For each orbit the earth rotates 25.40 degrees eastward. See Table 5 for a summary of NOAA-6 orbital parameters.

Table 5

NOAA-6 Orbital Parameters

orbital plane precession rate	0.986 deg/day east
inclination (i)	98.739 ± 0.15 deg
retrograde inclination (i_-)	81.261 ± 0.15 deg
period	101.58 minutes
orbits per day	14.18
earth rotation per orbit	25.40 degrees east
orbital altitude	833 ± 18.5 km

The predetermined launch altitude of the satellite was 833 ± 18.5 kilometers. The orbit of NOAA-6, to a first approximation, is an ellipse. From the ephemeris data set the semi-major axis of the ellipse and its eccentricity can be found, thus making the satellite's altitude on any pass simple to calculate as shown in Figure 25 below. The mean satellite altitude (H) is that distance measured from the center of the Earth and can be derived using Equation (1).

Using the above orbital information, the data in Table 6 below was derived for the six selected NOAA-6 passes used in this project.

Figure 25

Satellite Altitude Determination

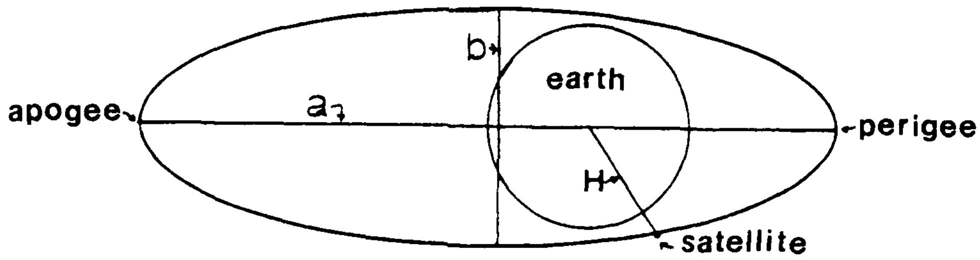

a = semi-major axis (from ephemeris) in nm

e = eccentricity (from ephemeris)

b = semi-minor axis = $a[(1-e^2)]^{1/2}$

H = mean satellite altitude = $(2b+a)/3$ (Eq. 1)

Table 6

Satellite Data Set Orbital Parameters

PARAMETER	7209	7244	7266	7429	7465	7486
inclination (degrees)	98.69708	98.69708	98.69708	98.69123	98.69123	98.69123
retrograde inclination	81.30292	81.30292	81.30292	81.30877	81.30877	81.30877
period (minutes)	101.13285	101.13285	101.13285	101.13084	101.13084	101.13084
semi-major axis (km)	7185.4875	7185.4875	7185.4875	7199.1856	7199.1856	7199.1856
eccentricity	0.001187	0.001187	0.001187	0.000603	0.000603	0.000603
mean satellite altitude	7185.4841	7185.4841	7185.4841	7199.1847	7199.1847	7199.1847

The reason that the orbital parameters are not constant for each pass is that the satellite is subject to many forces that tend to cause its orbit to vary. The largest of these forces is the fact that the earth is not a perfect sphere but an oblate spheroid. King-Hele (1958) and Brouwer (1959) developed mathematical solutions to describe this perturbation whose primary effects on the orbit include changing the orbital plane precession rate and changing the period. A secondary influencing factor is the effect of atmospheric drag on the satellite which acts to change the eccentricity and is a function of the satellite's altitude. A third influence is the effect of solar wind and radiation. It should be noted that during 1980, the International Solar Maximum Year, solar flare and sunspot activity reached some of the highest levels recorded (Ponte, 1981). Lesser influences include the gravitational effects of the sun and the moon on the satellite.

d. Computer Navigation Program

The main computer navigation program was developed under the following premise: given the orbital parameters of NOAA-6, the latitude and longitude of an AXBT, and a satellite image upon which one landmark has been identified as to (scan line number, sample number) and latitude and longitude, calculate the (scan line number, sample number) of the AXBT so that the count value, hence the sea surface temperature, of that pixel can be identified readily either on IDIMS or any other

computer system. Procedural methods were outlined by Mueller (1981).

(1) Preliminary Programs. Three preliminary computer programs were designed to be run on the IBM 3033. The first program, SCANLINE, was a simple block counter that counted the number of data records on each magnetic tape. The number of data records minus the header record divided by 3 gives the total number of scan lines per pass. The program listing can be found in Appendix B. The second program, TAPEDUMP, was a routine designed to dump from the magnetic tape any number of bytes per data record and to translate their ASCII-Binary formats into decimal notation. This program was used to verify that there were indeed six scan lines per second and its listing can be found in Appendix C. The third program, AREAMAP, was designed to function in a manner similar to the IDIMS' PICPRINT function in that it would extract from the magnetic tape the count values of a selected grouping of pixels around the landmark or AXBT pixel. This program was used to verify landmark locations and to determine the surface thermal structure around the position of the AXBT. Its listing can be found in Appendix D.

(2) Common Case Geometry. In the development of the main computer program, it was necessary to consider four cases in the process of predicting an AXBT pixel. These four cases are:

(a) an ascending pass where the landmark has a sample number greater than 1024 (Case 1);

(b) an ascending pass where the landmark has a sample number less than or equal to 1024 (Case 2);

(c) a descending pass where the landmark has a sample number greater than 1024 (Case 3); and

(d) a descending pass where the landmark has a sample number less than or equal to 1024 (Case 4).

Common to each of these four cases was the assumption of a spherical earth with a radius equal to the earth's radius at the landmark latitude. This local radius can be calculated using Equation (2)

$$R = \left[\frac{\cos^2(L_o)}{(3443.925)} + \frac{\sin^2(L_o)}{(3432.381)}\right]^{-1/2} \qquad \text{(Eq. 2)}$$

where:

R = local earth radius in nm

L_o = landmark latitude in degrees.

Also common to all four cases were the calculations to determine the great circle distance between the subsatellite point and the pixel containing the landmark. These calculations refer to Figure 26 below.

These calculations are made possible under the assumptions that the subsatellite point is directly beneath the satellite on the earth's surface, that the scanning mirror of the AVHRR forms a scan line perpendicular to the satellite's velocity vector, and that the earth is a perfect sphere.

Figure 26

Determination of great circle distances

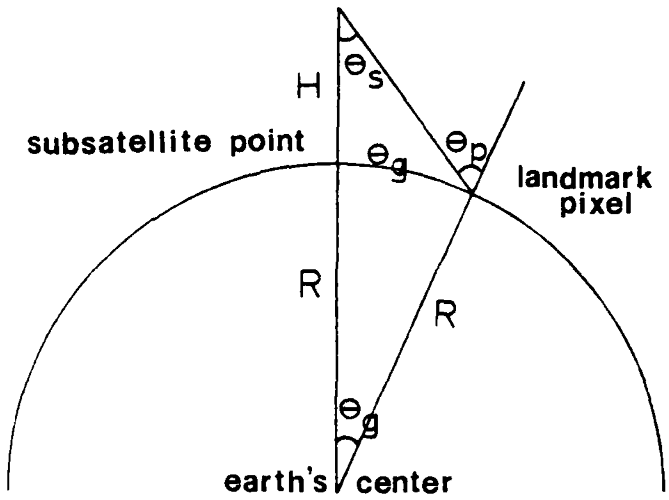

where: H = mean satellite altitude from Eq. 1

R = local earth radius from Eq. 2

θ_s = scan angle

θ_g = great circle distance

θ_g = geocentric angle

θ_p = zenith angle

Determination of the scan angle (θ_s) in degrees assumes an equal division of the arc viewed by the radiometer (110.8 degrees) into 2048 samples, thus

$$\theta_s = \begin{cases} (\text{landmark sample}-1024)(110.8/2048) & \text{if sample} > 1024 \\ (1025-\text{landmark sample})(110.8/2048) & \text{if sample} \leq 1024 \end{cases} .$$

The zenith angle (θ_p) in degrees now can be found:

$$\theta_p = \sin^{-1}\left[\frac{(R+H)(\sin \theta_s)}{R}\right] .$$

The geocentric angle (θ_g) in degrees is found from Equation (3).

$$\theta_g = \theta_p - \theta_s \qquad \text{(Eq. 3)}$$

If desired, the geocentric angle in degrees can be expressed as the great circle distance in nautical miles from Equation (4).

$$\rho_g = 60\ \theta_g \qquad \text{(Eq. 4)}$$

(3) Units and Notation. Because the IBM 3033 and the Fortran computer language were used heavily during this project, all angles were converted to or used in radians. Table 7 lists the common conversion factors used. Notations on all figures included in this project were designed to have the same definition whenever possible so comparisons could be made between the four cases.

Table 7

Program Conversions

45 degrees $= \frac{\pi}{4}$ radians $=$ (8)[(tan^{-1}(1.0 radians)]

any angle in radians $= \frac{\text{(same angle in degrees)}}{45}(\pi/4)$

any geocentric angle in radians expressed as a great circle distance in nautical miles $= \frac{45}{\pi/4}$ (geocentric angle)(60)

1 nautical mile = 1.835 kilometers

(4) <u>Nodal and Subsatellite Point Calculations.</u> The main program, LOCATE, is divided into two sections. The first section calculates the orbital characteristics referenced to the previously-identified landmark. The desired output is the time and longitude of the ascending or descending node. Their calculation is dependent on the four cases enumerated above and described in detail below. Once the time and longitude are known, the second part of the program can proceed to calculate the pixel number for an AXBT. To begin, the calculation of the ascending or descending node and time follows for each of the four cases.

Case 1. Ascending pass with landmark sample number greater than 1024.

The derivation of orbital characteristics referenced to a single landmark in Case 1 made use of Figure 27 below.

At time equal 0, the satellite is directly over the subsatellite point that has an unknown latitude (L_s) and longitude (λ_s). The only known quantities are that the scan line that includes the subsatellite point also includes the landmark with known latitude (L_o); longitude (λ_o); and from IDIMS, a known scan line number (NL); and sample number (NS). From the ephemeris data set for this pass, the inclination (and hence retrograde inclination (i_)) and the period are known. From Equation (3) or (4), the great circle distance θ_g is known. The goal of this orbital set of calculations is to find the latitude and longitude of the subsatellite

Figure 27

Case 1--orbital characteristics

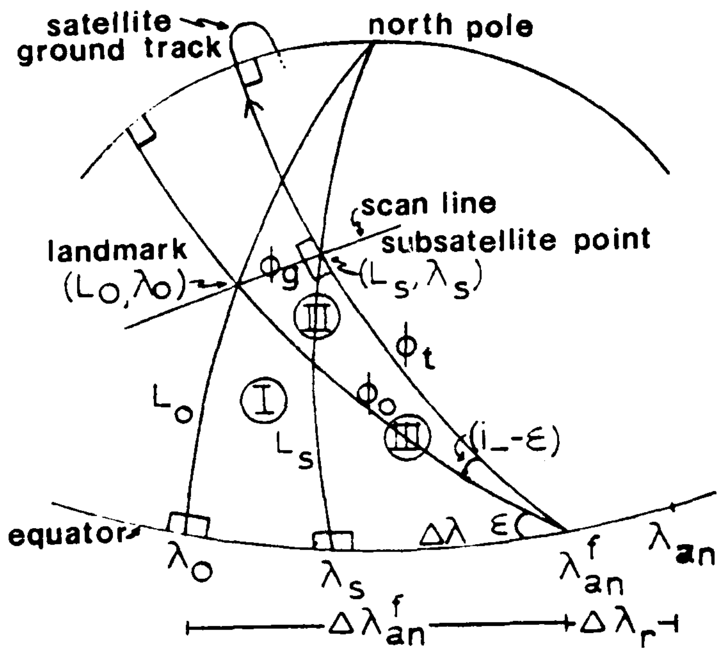

point, the longitude of the ascending node (λ_{an}) and the time of the ascending node.

By using similar triangles and the Law of Sines, the angle (ε) can be determined as follows:

from triangle I $\quad \dfrac{\sin \varepsilon}{\sin L_o} = \dfrac{1}{\sin \phi_o}$;

from triangle II $\quad \dfrac{\sin (i_- - \varepsilon)}{\sin \phi_g} = \dfrac{1}{\sin \phi_o}$;

hence, $\quad \varepsilon = \tan^{-1}\left[\dfrac{\sin i_-}{\dfrac{\sin \phi_g}{\sin L_o} + \cos i_-}\right]$.

From triangle I

$$\beta_o = \sin^{-1}\left[\frac{\sin L_o}{\sin \theta}\right] .$$

From triangle II, the distance over which the satellite travelled between the ascending node and the subsatellite point is

$$\beta_t = \cos^{-1}\left[\frac{\cos \beta_o}{\cos \beta_g}\right] .$$

Finally the latitude of the subsatellite point (L_s) can be determined using Equation (5) and triangle III

$$L_s = \sin^{-1}[\sin(i_{-})\sin(\beta_t)] . \qquad \text{(Eq. 5)}$$

For the moment, the rotation of the Earth is ignored, so the change in longitude at the equator between the landmark longitude (λ_o) and the fixed ascending node longitude (λ_{an}^{f}--where the "f" indicates a fixed or non-rotating earth derived term) can be found by solving triangle I as follows:

$$\Delta\lambda_{an}^{f} = \cos^{-1}\left[\frac{\cos \beta_o}{\cos L_o}\right] .$$

The change in longitude at the equator between the subsatellite point and the fixed ascending node longitude can also be found from triangle III

$$\Delta\lambda = \cos^{-1}\left[\frac{\cos \beta_t}{\cos L_s}\right] .$$

Now, the longitude of the subsatellite point (λ_s) can be calculated easily using Equation (6)

$$\lambda_s = \lambda_o - (\Delta\lambda^f_{an} - \Delta\lambda) \quad . \qquad \text{(Eq. 6)}$$

The fixed ascending node longitude is now found by

$$\lambda^f_{an} = \lambda_o - \Delta\lambda^f_{an} \quad .$$

To account for the earth's rotation during the time the satellite traveled from the ascending node to the subsatellite point, the longitude change due to rotation ($\Delta\lambda_r$) is calculated and subtracted from the fixed ascending node longitude as follows:

$$\Delta t \text{ (seconds)} = \frac{\theta_t}{2\pi} \text{ (period in seconds)} \ , \qquad \text{(Eq. 7)}$$

where Δt is the time the satellite took to travel between the ascending node and the subsatellite point. Continuing,

$$\Delta\lambda_r = \frac{2\pi}{24} (1.002738)(\Delta t) \qquad \text{(Eq. 8)}$$

where 1.002738 is the sidereal day correction factor. Finally,

$$\lambda_{an} = \lambda^f_{an} - \Delta\lambda_r \quad . \qquad \text{(Eq. 9)}$$

The time of the ascending node can be found by subtracting the Δt in seconds from the landmark time in seconds. Landmark time can be read from the magnetic tape using the tape dump program mentioned above to dump the data record containing the scan line of the landmark.

Case 2. Ascending pass with landmark sample number less than or equal to 1024.

The orbital calculations for this case are very similar to those of Case 1 and have the same goals. Figure 28 shows the geometry applicable in this case. As in Case 1, the known values are the great circle distance ϕ_g from Equations 3 or 4 and the landmark's latitude (L_o), longitude (λ_o), and the scan line number and sample number (NL,NS).

Figure 28

Case 2--orbital characteristics

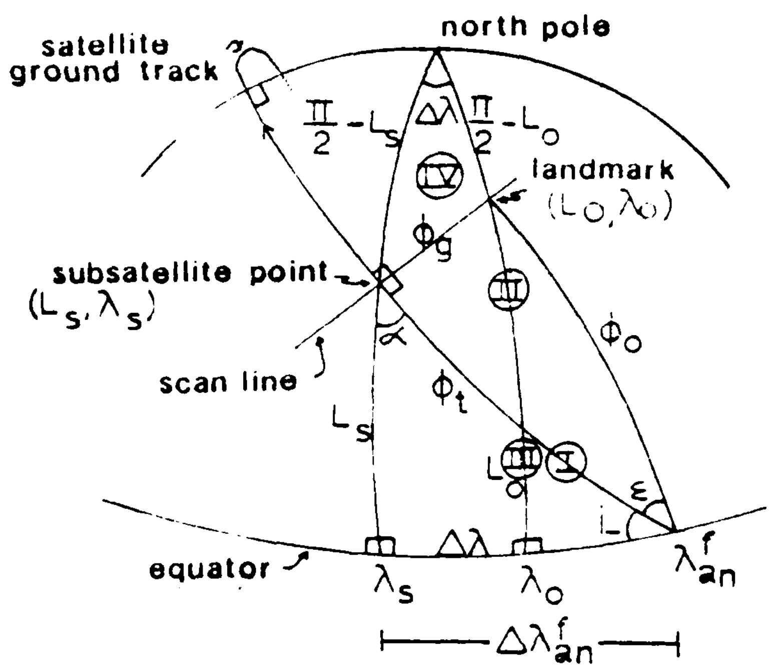

Using spherical triangles I and II, the angle (ϵ) can be determined as follows:

from triangle I $\quad \dfrac{\sin(i_- + \epsilon)}{\sin L_o} = \dfrac{1}{\sin \theta_o}$;

from triangle II $\quad \dfrac{\sin \epsilon}{\sin \theta_g} = \dfrac{1}{\sin \theta_o}$;

therefore, equating the two equations and solving for ϵ yields

$$\epsilon = \tan^{-1}\left[\frac{\sin i_-}{\dfrac{\sin L_o}{\sin \theta_g} - \cos i_-}\right] .$$

Continuing with triangle II

$$\theta_o = \sin^{-1}\left[\frac{\sin \theta_g}{\sin \epsilon}\right] ,$$

and the distance the satellite travels from the ascending node longitude to the subsatellite point of the landmark's scan line (θ_t) also can be found by

$$\theta_t = \cos^{-1}\left[\frac{\tan \theta_g}{(\sin \epsilon)(\tan \theta_o)}\right] .$$

From spherical triangle III, the latitude of the subsatellite point can be found using Equation 10

$$L_s = \sin^{-1}[(\sin i_-)(\sin \theta_t)] . \qquad \text{(Eq. 10)}$$

The change in longitude between the longitude of the ascending node and the longitude of the subsatellite point now can be found from triangle III, ignoring the earth's rotation.

$$\Delta\lambda_{an}^{f} = \cos^{-1}\left[\frac{\tan L_s}{(\sin i)(\tan \theta_t)}\right] .$$

The angle (α) from triangle III is

$$\alpha = \sin^{-1}\left[\frac{\sin \Delta\lambda_{an}^{f}}{\sin \theta_t}\right]$$

which can be used in triangle IV to find the change in longitude between the subsatellite point and the landmark ($\Delta\lambda$):

$$\Delta\lambda = \sin^{-1}\left[\frac{(\cos \alpha)(\sin \theta_g)}{\cos L_o}\right] .$$

The longitude of the subsatellite point (λ_s) now is found using Equation 11

$$\lambda_s = \lambda_o + \Delta\lambda . \qquad \text{(Eq. 11)}$$

The fixed earth ascending node longitude is

$$\lambda_{an}^{f} = \lambda_s - \Delta\lambda_{an}^{f} . \qquad \text{(Eq. 12)}$$

Using Equations (7) and (8) from Case 1 to determine the degrees of longitude through which the earth turns during the time the satellite travels from the ascending node to the

subsatellite point (L_r), the ascending node longitude (λ_{an}) can be found using Equation (9). The time of the ascending node is found exactly as in Case 1.

Case 3. Descending pass with the landmark sample number greater than 1024.

The case for the descending pass is slightly different from the ascending pass cases in that the satellite is travelling from north to south. The goals and the known factors are identical with the ascending pass cases. Figure 29 below pertains to the spherical geometry applicable in this case. Note that the ascending node becomes the descending node (dn) in descending pass calculations.

Figure 29

Case 3--orbital characteristics

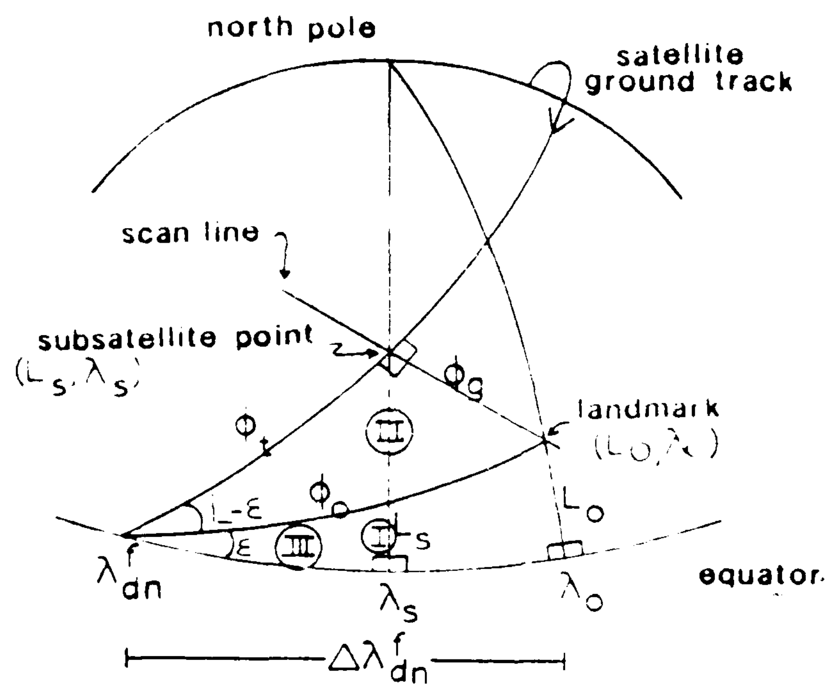

AD-A111 005 NAVAL POSTGRADUATE SCHOOL MONTEREY CA F/G 8/10
RAPID OCEANOGRAPHIC DATA GATHERING: SOME PROBLEMS IN USING REMO--ETC(U)
SEP 81 G W LUNDELL
UNCLASSIFIED NPS68-81-006 NL

2 OF 2
AD
A111005

END
DATE
FILMED
DTIC

The calculations for this case are exactly the same as those for Case 1 with some exceptions as noted below. The fixed earth change in longitude between the landmark longitude and the descending node longitude ($\Delta\lambda^f_{dn}$) can be determined from

$$\Delta\lambda^f_{dn} = \cos^{-1}\left[\frac{\cos \phi_o}{\cos L_o}\right] . \qquad \text{(Eq. 13)}$$

The change in longitude between the subsatellite point longitude and the descending pass longitude ($\Delta\lambda$) can be found from triangle III

$$\Delta\lambda = \cos^{-1}\left[\frac{\cos \phi_t}{\cos L_s}\right] .$$

The longitude of the subsatellite point (λ_s) can be determined from Equation 14

$$\lambda_s = \lambda_o + (\Delta\lambda^f_{dn} - \Delta\lambda) , \qquad \text{(Eq. 14)}$$

and the fixed earth descending node longitude now also can be determined

$$\lambda^f_{dn} = \lambda_o + \Delta\lambda^f_{dn} .$$

Using Equations (7) and (8), the degrees of longitude through which the earth turns while the satellite travels between the subsatellite point and the descending node can be determined ($\Delta\lambda_r$), and from this the rotating earth descending node

longitude can be found using Equation (15)

$$\lambda_{dn} = \lambda^{f}_{dn} + \Delta\lambda_{r} \quad . \qquad \text{(Eq. 15)}$$

The time of the descending node now can be determined by adding the time calculated in Equation (7) to the landmark time.

Case 4. Descending pass with landmark sample number less than or equal to 1024.

In this final case, the goals and the known quantities are the same as in the other cases described above. Figure 30 is used to describe the geometry associated with this case.

Figure 30

Case 4--orbital characteristics

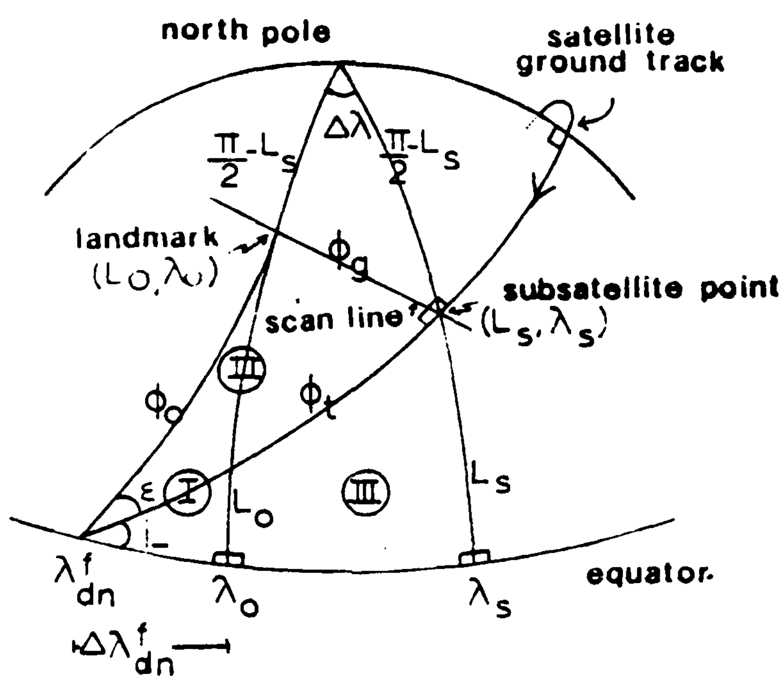

The calculations for this case are exactly the same as those for Case 2 with some exceptions as noted below. The distance the satellite travels from the subsatellite point to the descending node, ϕ_t, becomes

$$\phi_t = \cos^{-1}\left[\frac{\cos \phi_o}{\cos \phi_g}\right] .$$

The latitude of the subsatellite point, L_s, now can be found using Equation (16) as follows:

$$L_s = \sin^{-1}[(\sin i_{-})(\sin \phi_t)] . \qquad \text{(Eq. 16)}$$

The fixec earth change in longitude between the landmark longitude and the descending node longitude, $\Delta\lambda^f_{dn}$, now can be found by

$$\Delta\lambda^f_{dn} = \cos^{-1}\left[\frac{\cos \phi_o}{\cos L_o}\right] ,$$

and the change in longitude between the subsatellite point longitude and the descending pass longitude, $\Delta\lambda$, can be found from triangle III

$$\Delta\lambda = \cos^{-1}\left[\frac{\cos \phi_t}{\cos L_s}\right] .$$

The longitude for the subsatellite point, λ_s, is now found using Equation 17

$$\lambda_s = \lambda_o - (\Delta\lambda - \Delta\lambda^f_{dn}) , \qquad \text{(Eq. 17)}$$

and the fixed-earth descending node longitude becomes

$$\lambda_{dn}^{f} = \lambda_{o} + \Delta\lambda_{dn}^{f} \quad .$$

Again, using Equations (7) and (8), earth rotation is considered now, with the rotating earth descending node longitude described by Equation (18)

$$\lambda_{dn} = \lambda_{dn}^{f} + \Delta\lambda_{r} \quad . \qquad \text{(Eq. 18)}$$

The time of the descending pass is determined by adding the time calculated in Equation 7 to the landmark time.

(5) Buoy Pixel Identification. With the calculation of the time and longitude of the ascending or descending node, the second part of the program can proceed to calculate the (NL,NS) of the AXBT. The previous set of calculations referenced the orbital characteristics to the landmark pixel (remember pixel = (NL,NS)). The geographical relationship between the latitudes and longitudes of the landmark and the AXBT are known so the purpose of the remaining part of the program is to transform this geographical relationship into satellite image coordinates of (NL,NS). Besides the quantities calculated above, the only other known quantity is that the AXBT has a unique (NL,NS).

As a first guess, any arbitrary scan line can be chosen to be the "true" scan line containing the AXBT. One of the 2048 samples along the "true" scan line could be the

sample number of the AXBT. The aim of the calculations below is to prove or disprove, geometrically, that the arbitrary scan line is the true AXBT scan line and, once the true scan line is selected correctly, to calculate the correct sample number.

The procedure to determine the time that the satellite recorded the scan line containing the landmark was described above. Since the time of the ascending or descending node was calculated in the earlier part of the main program, subtracting the two times describes the satellite flight time between the particular node and the subsatellite point of the landmark scan line. The assumption was made earlier that the satellite's orbit can be considered circular with a mean altitude (H) and that the period of the satellite was the amount of time it takes the satellite to complete one orbit; then the flight time between the node and the landmark scan line can be described as a great circle distance in radians by

$$\phi_s = \frac{2\pi(\text{flight time})}{\text{period}} \quad . \qquad \text{(Eq. 19)}$$

Another assumption was made earlier, which was proved by using one of the preliminary computer programs described above, that the satellite records six scan lines per second. Combining these factors, it is simple to determine the difference in scan lines between the landmark scan line and the first-guess, arbitrarily-chosen scan line; divide by 6 to get the time difference between the two scan lines; either add to (ascending passes) or subtract (descending passes) this time difference

from the flight time; and use Equation (19) to determine the distance between the particular node and the subsatellite point of the arbitrarily-chosen scan line. The latitude and longitude of this subsatellite point now can be determined using spherical triangles.

Assuming that the arbitrary scan line is very close to the true AXBT scan line, the next step is to find the correct sample number along this line. Beginning with sample number 1, and then taking every 89th sample (1,90,179, ...,1959,2048) the distance between the subsatellite point and the center of the pixel can be found using Equations (1) through (4) for each of the 24 sample numbers. With this distance it is possible to calculate the latitude and longitude of the center of each of these 24 samples by using one of the four cases described below.

Case 1. Ascending pass with sample number greater than 1024.

This case uses the geometry of Figure 31. The angle (ε) can be found easily by

$$\varepsilon = \cos^{-1}\left[\frac{\cos i_{-}}{\cos L_s}\right] \quad ; \qquad \text{(Eq. 20)}$$

from which

$$i_s = \cos^{-1}[(\cos L_s)(\sin \varepsilon)] \quad . \qquad \text{(Eq. 21)}$$

The distance, in radians, of ϕ_s can be found by using

Figure 31

Case 1--pixel determination

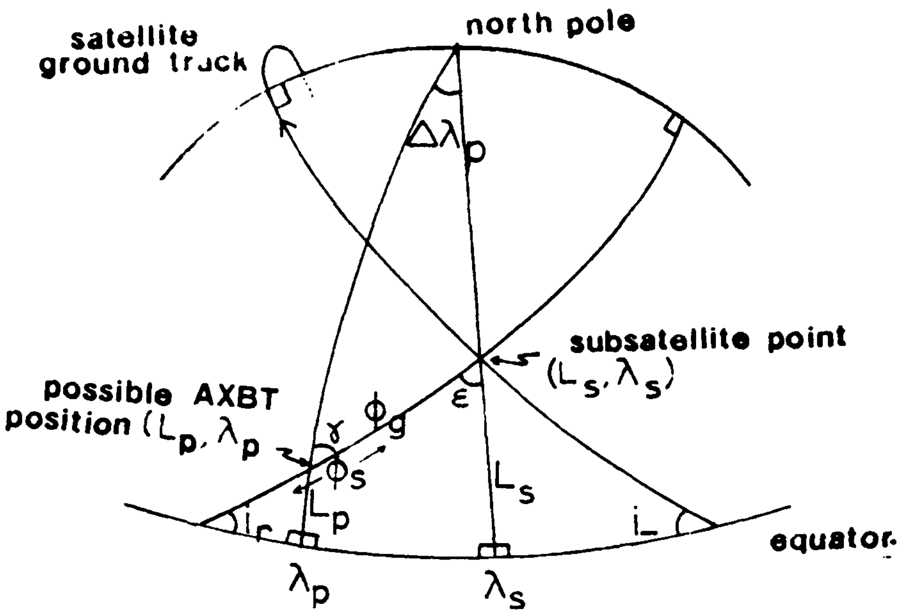

$$\phi_s = \sin^{-1}\left[\frac{\sin L_s}{\sin i_s}\right] \quad ; \qquad \text{(Eq. 22)}$$

hence the latitude of the possible AXBT position (L_p) can be calculated

$$L_p = \sin^{-1}[(\sin(\phi_s - \phi_g))(\sin i_s)] \quad .$$

The angles (γ) and ($\Delta\lambda_p$) now can be determined by

$$\gamma = \sin^{-1}\left[\frac{\cos i_s}{\cos L_p}\right] \quad ,$$

and

$$\Delta\lambda_p = \sin^{-1}\left[\frac{(\sin\gamma)(\sin\phi_g)}{\cos L_s}\right] ;$$

thus the longitude of the possible AXBT position (λ_p) is determined simply by

$$\lambda_p = \lambda_s + \Delta\lambda_p .$$

Case 2. Ascending pass with sample number less than or equal to 1024.

Case 2 geometry uses Figure 32.

Figure 32

Case 2--pixel determination

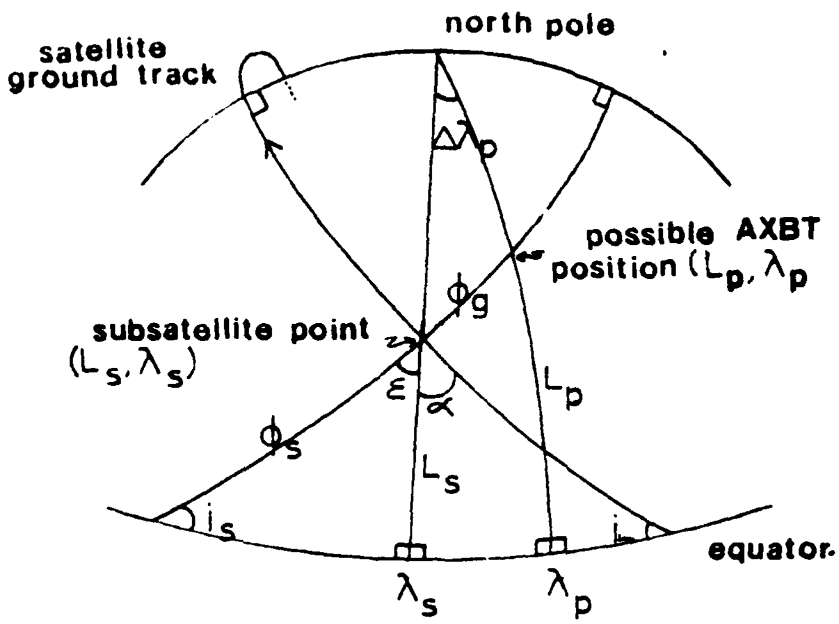

The angles (ε) and (i_s) and the distance (ϕ_s) are found using Equations (20), (21), and (22) respectively. The latitude of the possible AXBT position becomes

$$L_p = \sin^{-1}[\sin(\phi_s + \phi_g)\ \sin(i_s)] \quad .$$

The angle ($\Delta\lambda_p$) now is found by

$$\Delta\lambda_p = \sin^{-1}\left[\frac{(\sin\ \varepsilon)(\sin\ \phi_g)}{\cos\ L_p}\right] \quad ,$$

and therefore the longitude of the possible position is

$$\lambda_p = \lambda_s - \Delta\lambda_p \quad .$$

Case 3. Descending pass with sample number greater than 1024.

Case 3, although using Figure 33 for its geometry, uses exactly the same equations as in Case 1 with the exception that the longitude of the possible AXBT position is found by

$$\lambda_p = \lambda_s - \Delta\lambda_p \quad .$$

Figure 33

Case 3--pixel determination

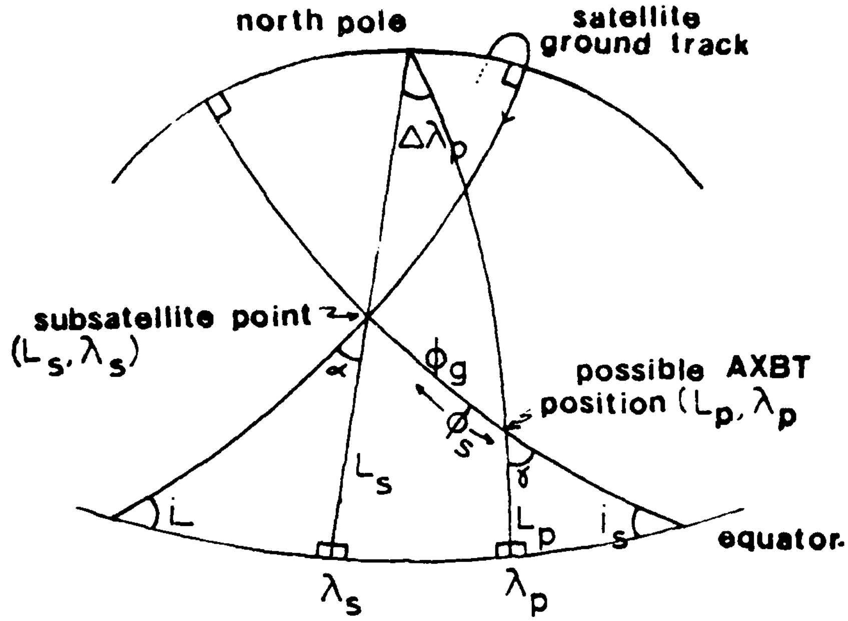

Case 4. Descending pass with sample number less than or equal to 1024.

Case 4, although Figure 34 represents its geometry, uses exactly the same equations as in Case 2 with the exception that the longitude of the possible AXBT position is found by

$$\lambda_p = \lambda_s + \Delta\lambda_p \ .$$

In addition to calculating latitude and longitude for each of these 24 samples along the arbitrary scan line, it also is necessary to calculate the great circle

Figure 34

Case 4--pixel determination

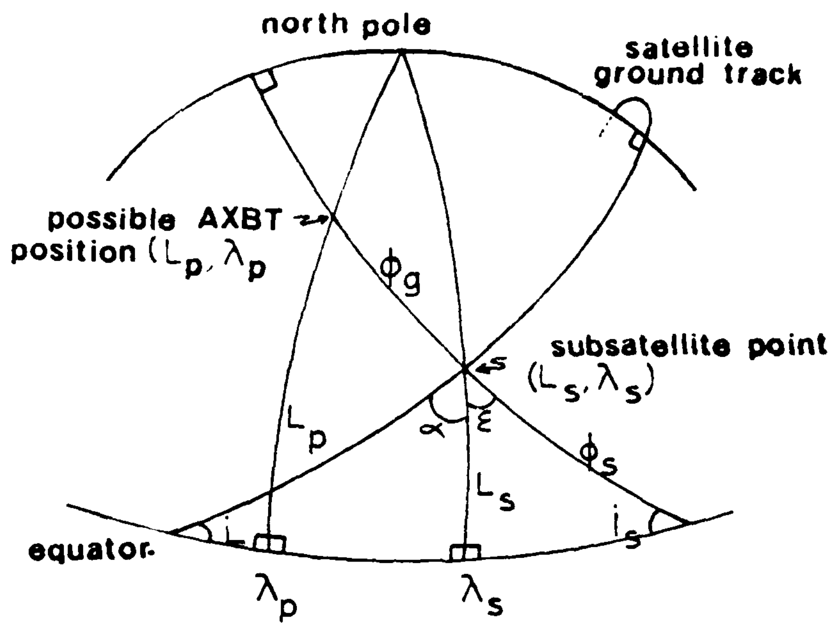

distance (d) between the AXBT geographical position and those of the 24 samples using Equations 23

$$d = \cos^{-1}[(\sin L_b \sin L_p) + (\cos L_b \cos L_p)\cos(\lambda_p - \lambda_b)], \quad \text{(Eq. 23)}$$

where:

L_b = true AXBT latitude

λ_b = true AXBT longitude . (Eq. 23)

By taking the sample number that has the smallest of these great circle distances, creating a bracket

89 samples wide on either side of this center sample, and proceeding as before through the appropriate case number for each of the 180 samples in this bracket, the sample that has the shortest great circle distance between itself and the AXBT position can be selected. The reason for the wide bracket is to allow for earth rotation and curvature whose effects are especially noticeable on the edges of the satellite image. If, as before, we assume that we had a scan line very close to the true AXBT scan line, a 10 by 10 pixel "square" box is created around the sample with the smallest great circle distance. In reality, this box is not perfectly square due to the curvature of the earth and the motion of the satellite during the scan sequence. Those boxes near the subsatellite point would be more perfectly "square" than those boxes on the edges of the image.

The scan lines on the top and bottom of the box as well as the samples on each of the four corners are subjected to the same calculations described above to find the latitude and longitude of each of the samples on the four corners. The geometry of this box is shown in Figure 35.

The calculations to find the (NL,NS) of the AXBT begins with finding the change in the latitudes and longitudes with respect to the changes in the sample and scan line numbers.

$$\frac{\partial L}{\partial (NL)} = \frac{1}{2}\left[\frac{L_3 - L_1}{10} + \frac{L_4 - L_2}{10}\right]$$

Figure 35

Box geometry

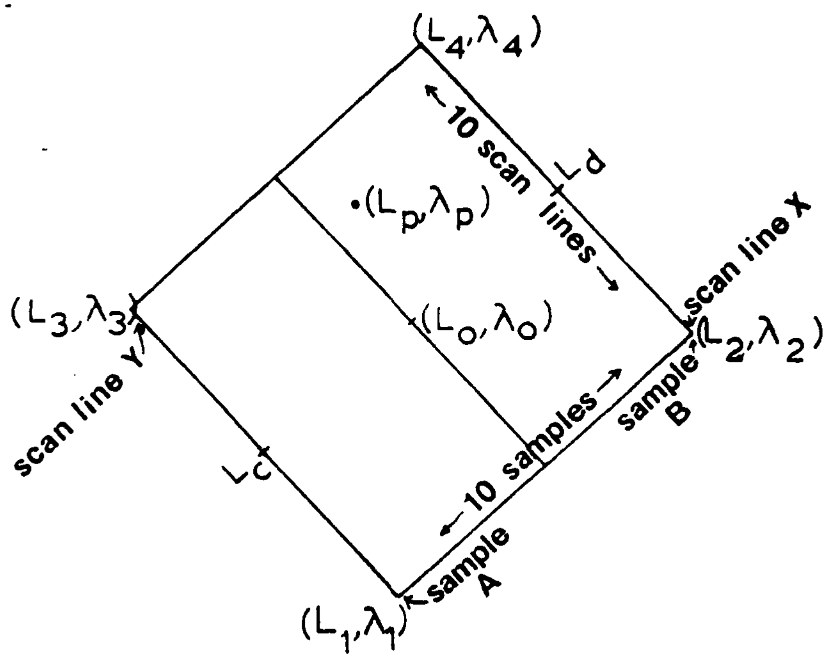

where L_i = latitude of sample on i-th corner

λ_i = longitude of sample on i-th corner

L_o, λ_o = latitude and longitude of the sample having the smallest great circle dist.

L_p, λ_p = AXBT latitude, longitude

L_c, L_d = check procedure latitudes

$$\frac{\partial L}{\partial (NS)} = \frac{1}{2}\left[\frac{L_2 - L_1}{10} + \frac{L_4 - L_3}{10}\right]$$

$$\frac{\partial \lambda}{\partial (NL)} = \frac{1}{2}\left[\frac{\lambda_3 - \lambda_1}{10} + \frac{\lambda_4 - \lambda_2}{10}\right]$$

$$\frac{\partial \lambda}{\partial (NS)} = \frac{1}{2}\left[\frac{\lambda_2 - \lambda_1}{10} + \frac{\lambda_4 - \lambda_3}{10}\right]$$

Continuing, two intermediate equations are required

$$A = (\lambda_p - \lambda_1) + \frac{\partial\lambda}{\partial(NS)} \text{ (sample A)} + \frac{\partial\lambda}{\partial(NL)} \text{ (scan line x);}$$

$$B = (L_p - L_1) + \frac{\partial L}{\partial(NS)} \text{ (sample A)} + \frac{\partial L}{\partial(NL)} \text{ (scan line x).}$$

Finally, determination of the (NL,NS) of the AXBT can be made

$$NL = \frac{\dfrac{A}{\partial\lambda/\partial(NS)} - \dfrac{B}{\partial L/\partial(NS)}}{\dfrac{\partial\lambda/\partial(NL)}{\partial\lambda/\partial(NS)} - \dfrac{\partial L/\partial(NL)}{\partial L/\partial(NS)}} \quad ;$$

$$NS = \frac{A}{\partial\lambda/\partial(NS)} - \left[\frac{\partial\lambda/\partial(NL)}{\partial\lambda/\partial(NS)} (NL)\right] \quad .$$

Rarely will the arbitrary scan line chosen as a first guess be close to the true scan line of the AXBT. In this case, after the great circle distances have been calculated between the initial 24 samples and the AXBT position, and the "square" box has been set up, a check is made to see how "small" is the smallest great circle distance. As described earlier, the satellite follows a ground track as it travels poleward that cuts across meridians of latitude at an angle set up by its inclination. This means that scan lines are not oriented east-west along degrees of longitude but are oriented northwest-southeast (descending pass) or northeast-southwest (ascending pass) crossing many degrees of longitude and latitude. The check involves comparing the latitude of the AXBT

with the latitudes L_c and L_d as shown on Figure 35 above. If the arbitrary scan line is very close to the true AXBT scan line, for ascending passes, latitude L_c will be south of the AXBT latitude while latitude L_d will be north of the AXBT latitude. The reverse is true for descending passes. If the arbitrary scan line is far away from the true AXBT scan line, both L_c and L_d will be either north or south of the AXBT latitude. In this case, the smallest great circle distance is converted to an integral number of scan lines which are added to or subtracted from the first-guess arbitrary scan line number depending on whether L_c and L_d were both south or north of the AXBT's latitude respectively. The jump to a new scan line initiates the entire procedure again beginning with the steps necessary to calculate Equation (19). This jump process terminates when the number of scan lines to be jumped is 5 or less at which time the boxing procedure begins with the eventual determination of the AXBT's (NL,NS).

The main program, whose listing may be found in Appendix E, was initially set up to be run interactively on a display terminal. The program was used to locate all the AXBT's that were dropped from the P-3C. Verification of the accuracy of the program was done by selecting 15 to 20 landmarks per image and asking the program to predict the (NL,NS) even though they were known already from the IDIMS system. Results of this verification will be discussed below in Section IV.A.

C. GOSSTCOMP

The GOSSTCOMP sea surface temperature charts were obtained for the period of this project from NOAA-NESS. These charts are produced on a weekly basis by NOAA-NESS using procedures outlined by Brower et al., (1976) and since updated to take advantage of the AVHRR on NOAA-6.

IV. RESULTS

A. NAVIGATION ACCURACY

A major effort was made on this project in an attempt to reduce the effects of geometric distortion associated with locating landmarks or open-ocean positions on satellite imagery. Previously published works with earth location errors in excess of 10 kilometers at nadir were suitable for regional location and analysis of mesoscale features; however, it was believed that accurate comparisons of thermal data were significant only if the products being compared were co-located in the same geographical position. The location of thermal features is especially important in naval tactical applications. If a submarine were taking advantage of the unique acoustical properties of an eddy or ocean front, then acoustical prosecution by the opposing forces would be more successful if the sensors employed by this group were located so as to take advantage of the thermal feature also. If pre-mission information mislocated the edge of the front or eddy due to the geometric distortion inherent in satellite imagery, then the results could be disastrous to one of the parties. Ultimately, any error in sensor placement could prove disastrous whether caused by satellite imagery or not; part of the purpose of this project was to make the location error as small as possible.

Using the main computer program, the (NL,NS) of each AXBT was predicted. The error in this prediction was determined to be within 2 pixels of the true AXBT (NL,NS). The procedure

to verify this accuracy began with the identification of the (NL,NS) of up to 20 landmarks on each satellite image. Each of the landmarks then was treated like an AXBT and its geographical coordinates were input to the computer to see what the program would predict for each landmark's (NL,NS). These predictions then were compared to the IDIMS-determined (NL,NS), and the separations in pixels were determined. The results are summarized in Table 8 below.

Table 8

Statistical Summary of Navigation Accuracy

SCAN LINE ERROR	
mean	1.32 scan lines
standard deviation	0.93 scan lines
99% confidence level	0.88-1.90 scan lines
SAMPLE ERROR	
mean	1.35 samples
standard deviation	1.17 samples
99% confidence level	0.81-1.90 samples

The conclusion drawn from this statistical summary was that the predicted AXBT (NL,NS) is within 2 pixels of the true AXBT (NL,NS). Because of earth curvature, pixels close to nadir are not as wide as those out on the edges of the image. Sample number 1 and 2048, on the right and left edge of the image respectively, are 4.3 kilometers wide whereas sample number 1024 and 1025, located to the right and left of nadir

respectively, are only 0.77 kilometers wide. As a result, the 2-pixel error can be as small as 1.9 kilometers, if the predicted (NL,NS) is at nadir; or as large as 10.7 kilometers, if the predicted (NL,NS) is at the edge of the image. Table 9 lists the navigation error associated with selected sample numbers. Notice that the error is not linear with distance from nadir but is less than 5 kilometers over 80% of the image and less than 3 kilometers over 50% of the image. Only on the outer 10% of the image does the error balloon from 4.8 to 10.7 kilometers.

Table 9

Navigation Errors Associated with a 2-Pixel Error

SAMPLE NUMBER	ERROR (km)
1	10.7
200	4.8
400	3.0
600	2.5
800	2.0
1024	1.9
1200	2.0
1400	2.3
1600	3.0
1800	4.3
2048	10.7

There are some other sources of navigation error that should be kept in mind when using data developed by this method. Alignment of the AVHRR module during its assembly prior to launch could be the source of constant offset error. This type of error was described previously in this paper; analysis of the navigation results did not show any consistent offset bias that could be attributed to module alignment errors.

Through the process of verifying the 2-pixel accuracy, many landmarks were identified on the IDIMS system as explained above. The data from NOAA-6 infrared channel number 4 were used for landmark identification and their use could introduce errors in assignment of the (NL,NS). These errors arise from trying to identify landmarks whose surface temperature may not be very different from the surrounding surfaces. This effect would become even more pronounced if ground fog were present. When selecting these landmarks, the best contrast was effected by land-water boundaries, examples of which were Point Lobos west of Monterey, the San Francisco Bay entrance, Alcatraz Island, Point Reyes, the Columbia River mouth, Lake Tahoe, and Glacier Bay among others. Many possible landmarks were not considered if there were insufficient contrast to identify the feature. A good example of this was the Seattle-Tacoma-Olympia area where the numerous bays and tributaries had surface temperatures close to land temperatures, thus making it very difficult to distinguish a specific pixel as being some peninsula or promontory.

A third source of error involved the number of significant figures used in the mathematics of this project. Single-bit precision was used during computer processing. Although this may have had an effect after numerous computations (the average program run to calculate 24 AXBT positions per image executed 475,000 statements), it was felt that the number of significant figures was more critical. An example of this was the determination of decimal geographical coordinates. The navigation system on the P-3C supplied the computer-calculated coordinates of the AXBT's to seconds of latitude or longitude. One second of latitude error is equal to 0.1 kilometers, which in itself is not so large; however, most landmarks were identified using charts with scales of 1:2,000,000. After determination of the coordinates, a decimal conversion to three decimal places was completed. If errors in this procedure were compounded by weak land-water contrast on the infrared image used for landmark identification, it could contribute significantly to the 2-pixel error.

A fourth source of error has to do with the resolution of the AVHRR itself. As discussed earlier, the 1.1 kilometer resolution would necessarily make it difficult to identify something like the Transamerica Building in downtown San Francisco. An example of where this could be a contributing factor to the 2-pixel error would be in using the most western point of Point Reyes. If the scan sequence is such that the radiometer does not resolve this point, then the first pixel it does identify as being land would be to the east of the

point. The user of the satellite image would have a very difficult time in trying to determine whether or not this has occurred. As a result, the user would assign the geographical coordinates of the most western point, introducing a 1-pixel error immediately before any computer processing begins. It is felt that if landmark's could be identified using sharper land-water contrast or using a visible channel vice the infrared channel if it is available, and if geographical coordinates could be assigned with greater accuracy, the majority of the 2-pixel bias would be eliminated.

Another error to be considered is that the satellite may not be perfectly stable in its orbit. It is likely that small amounts of pitch, roll, or yaw occur from time to time although the ADACS system was designed to keep these attitudes to a minimum.

The last error to be discussed is the use of several assumptions made during this project. The Earth was assumed to be spherical and although the radius was calculated to be that radius at the latitude of the landmark, a small error will be introduced in calculations involving the earth radius term at the latitude of the buoys. Similar small errors arise with the assumptions made concerning the satellite orbit during scan line calculations, and with the calculation of the mean altitude of the satellite above the earth's surface.

In conclusion, it is believed that the 2-pixel error found on this project could be reduced further to sub-pixel accuracies if some of the errors described above were eliminated

or refined. Since the development of LOCATE, a program using most of the same techniques as LOCATE has been developed to predict the geographical coordinates of open ocean images with similar accuracies (Mueller, 1981).

B. THERMAL COMPARISONS

1. Horizontal Distribution

As usually can be expected when satellite-derived sea surface temperatures that are uncorrected for atmospheric attenuation are compared with AXBT values of sea surface temperature, the satellite temperatures were colder than the AXBT data by a mean difference of 2.9 degrees C. Table 10 lists the mean temperature difference values and the corresponding standard deviations for this and following comparisons. Figures 36, 37, 38, and 39 show sea surface temperature comparisons of this and other methods to be described below along the buoy line. The majority of the 2.9-degree error can be attributed to the effects of the intervening atmosphere between the ocean's surface and the satellite radiometer. Cloud contamination of the satellite values was not considered a major factor due to the screening process that went into selecting the data. Out of the six satellite passes selected for study at the beginning of this project, only three met the full requirements that were required for processing. Two of the passes were not considered due to scattered clouds over enough buoy positions to make any comparisons useless and one pass was not considered because it contained no clearly

Table 10

Temperature Comparison Statistics

COMPARISONS	MEAN (C)	STANDARD DEVIATION
satellite vs. AXBT		
17 November	-3.0	0.5
01 December	-2.6	0.4
05 December	-3.0	0.6
overall	-2.9	0.5
satellite vs. GOSSTCOMP		
17 November	-2.0	0.9
01 December	-3.2	0.6
05 December	-4.3	0.9
overall	-3.2	1.1
GOSSTCOMP vs. AXBT		
17 November	-0.7	0.7
01 December	0.5	0.6
05 December	1.2	0.6
overall	0.3	1.0

Figure 36. Sea surface temperature comparisons, 17 November 1980, center track

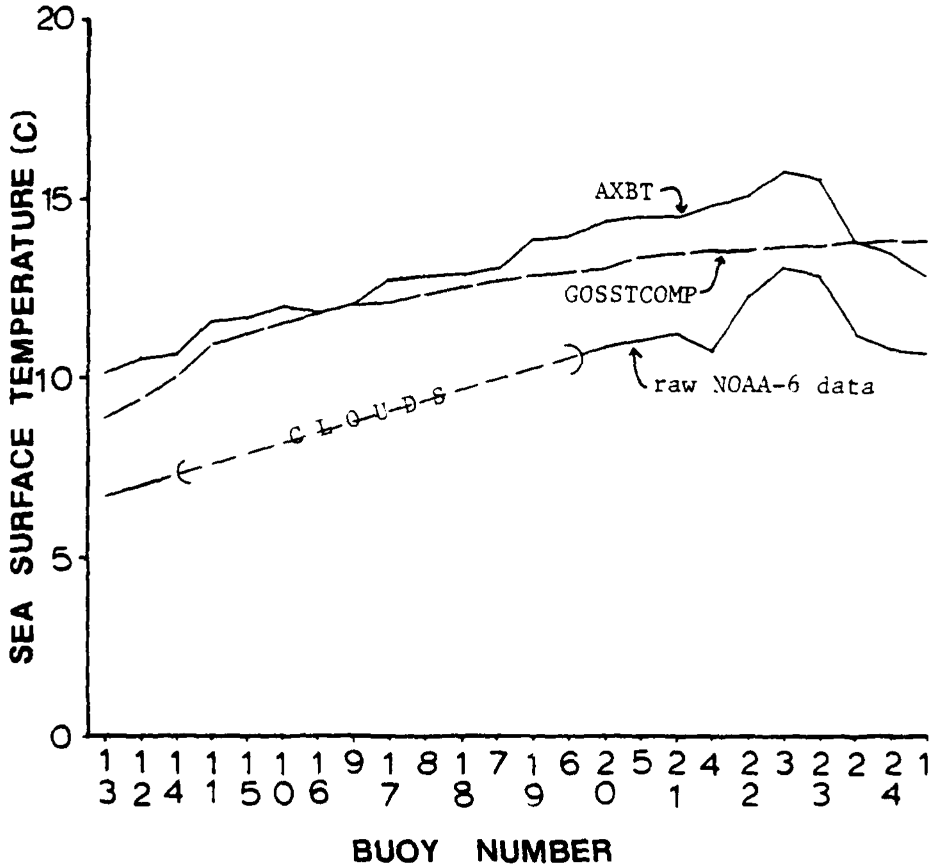

Figure 37. Sea surface temperature comparisons, 1 December 1980, center track

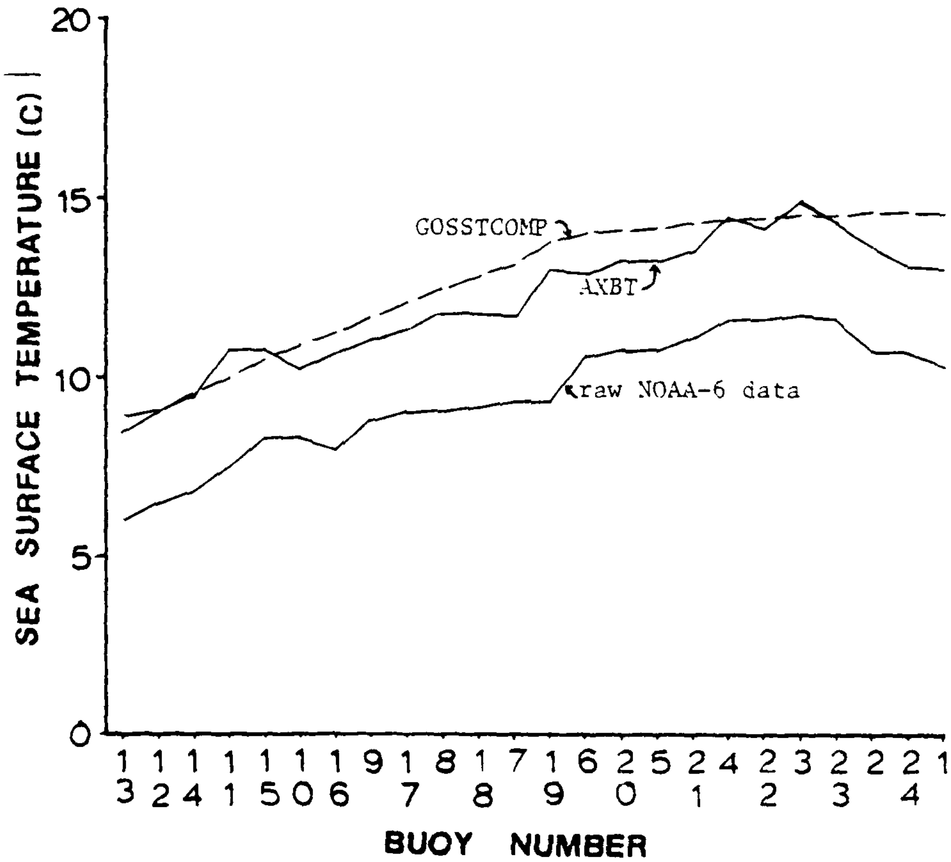

Figure 38. Sea surface temperature comparisons, 5 December 1980, center track

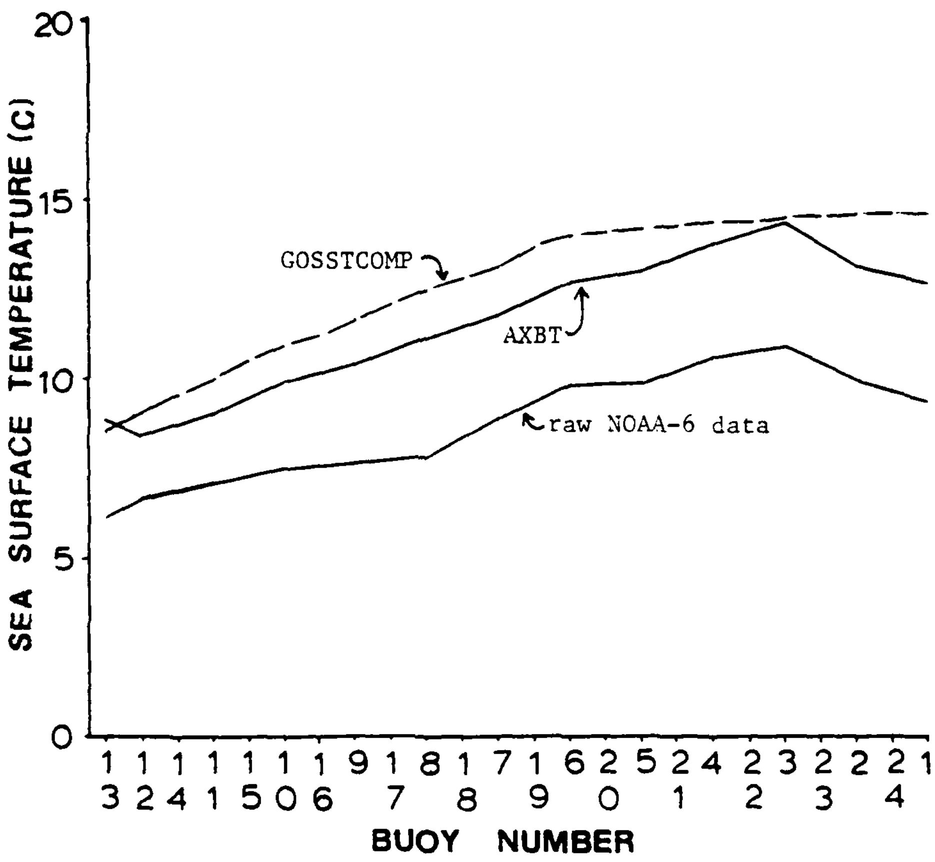

Figure 39. Sea surface temperature comparisons, 5 December 1980, northern track

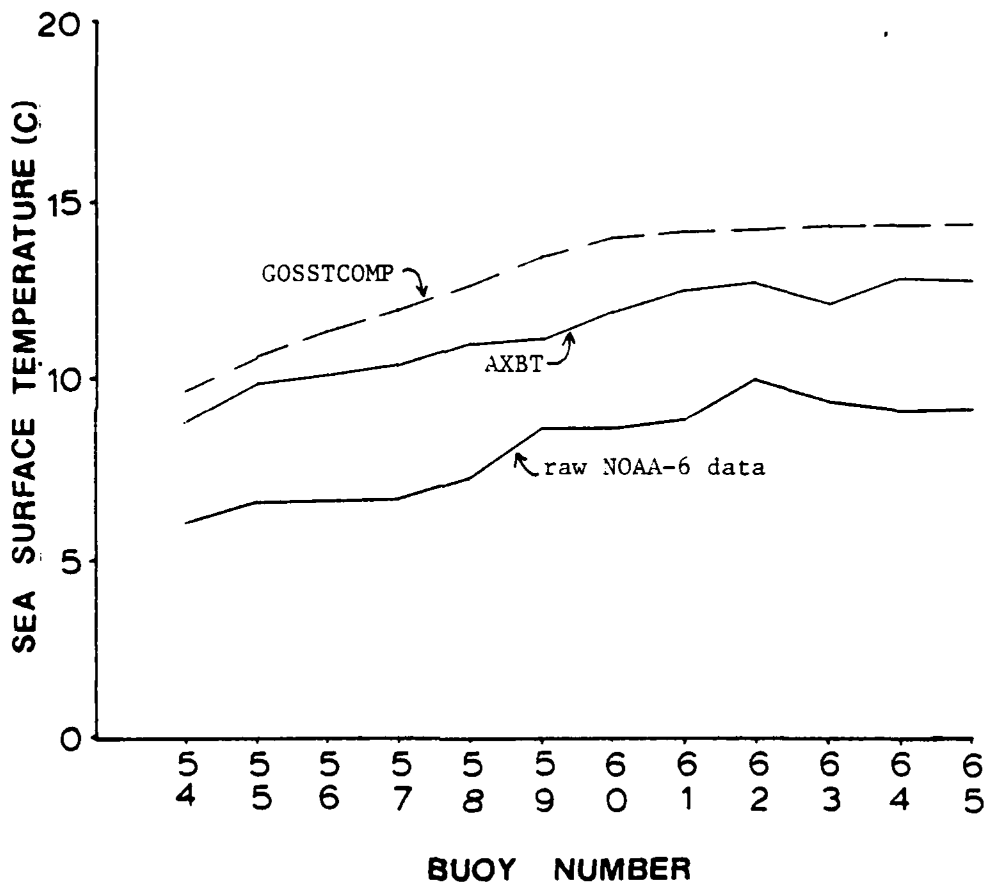

identifiable landmarks. Passes selected for complete processing were 17 November, 1 and 5 December 1980. From personal observations onboard the P-3C during AXBT deployment, it was noted also that there was no ground fog to interfere with satellite measurements of the AXBT positions. The time difference of one, three, and three hours between the last buoy drop and the satellite flyover for 17 November, 1 and 5 December, respectively, probably is not a factor as the lowest and highest mean error values were found on 1 and 5 December with 17 November having an intermediate value. If there were a correlation, one would expect 17 November to have the smallest error but this was not the case. The transient warming of the surface waters during the afternoon, the so-called afternoon effect, did not occur due to the weather conditions during the three-week project period; hence, this process also was ruled out as a source of the error. Constant wind speeds in excess of 20 knots from the south on 17 November, in excess of 25 knots from the northeast on 1 December, and in excess of 15 knots from the westnorthwest on 5 December (National Weather Service, 1980a) along the buoy line kept the surface waters under constant wind-mixing conditions. In addition to the winds, ship observations of the sea state at the northern end of the buoy pattern found four to ten foot swell and two to six foot waves. These turbulent mixing conditions are diametrically opposed to the formation of the afternoon effect (James, 1966).

A method of "field-calibrating" the satellite data to eliminate the effects of the atmosphere was suggested by Tabata and Gower (1980). Using a simple linear regression technique, they plotted numerous ship-obtained surface temperatures versus satellite count values and found that over a limited area and a limited time period between satellite and ship observations (1.5 days), the error between satellite and ship values could be reduced to 0.5 degrees C. This technique was tried using the data from this project. An absolute mean difference of 0.3 degrees (s = 0.2 degrees) was found between satellite and AXBT values. The time period between satellite and AXBT observations was three to eight hours.

Flight crews usually will not have the luxury of expending 24 AXBT's on a tactical mission however, so the linear regression technique was tried using only two buoys. The rationale behind using two buoys was that this is the number of AXBT's usually carried on both S-3A and P-3 aircraft. Additionally, a scenario could exist whereby a satellite photo obtained prior to the flight could pinpoint two sections of the tactical operating area where thermal differences exist and those two locations could be designated for AXBT deployment. The point is to try and get a spread in temperature between the two AXBT's. Using the two-buoy method, the data from AXBT positions 1 and 13 on 1 December were used for the linear regression. Predictions of temperatures from count values found a mean difference error of 0.3 degrees (s = 0.3 degrees), the same value found using the 24-buoy method. When this same

regression formula with constants calculated from 1 December data was used to predict 5 December (4 days later) and 17 November (15 days earlier) temperatures, mean errors of 0.5 degrees (s = 0.3 degrees) and 0.4 degrees (s = 0.3 degrees), respectively, resulted. Although examination of all possible cases would be necessary before conclusive results could be stated, these preliminary estimates indicate that it should be possible to use two AXBT's and an infrared satellite image to predict sea surface temperatures within 0.5 degrees for at least two days after the original satellite pass, a prediction tool particularly helpful if clouds obscure the sea surface during those two days or if AXBT assets are in short supply. In addition, these procedures can be used in near real-time processing of current satellite images and do not rely on any atmospheric model processing. In any case, these thermal predictions that are very accurate in location and fairly accurate in temperature would be tactically significant, in place of mean values or best-guess values, when doing sound velocity calculations near meander, eddy, or frontal regions.

Relative temperature gradient analysis displayed the expected correlation between satellite and AXBT values. Both the AXBT and satellite gradients were 0.6 degrees per 60 nm on 17 November and 1 December while on 5 December the AXBT gradient was 0.56 degrees per 60 nm and the satellite gradient was 0.52 degrees per 60 nm.

An interesting thermal feature whose horizontal surface manifestation was detected by both the satellite and

the AXBT was a meander in the final stages of closing off from its parent body of water to form an eddy. See the darker region transected by the buoy line through buoy positions 23, 3, 22, and 4 in Figure 40. This warm-core meander had an approximate 100 nm diameter with the exception of an open arm extending southward into its parental water mass. The diameter was verified by the buoys dropped on the northern and southern tracks. These buoys were 60 nm away from the center rack and the warm meander did not show up on any ot the thermal traces. The satellite indication of this diameter resulted in a slightly larger radius, a fact attributed to the thermal resolution limitations of the satellite data in determining weak temperature boundaries. In the satellite images, this meander is surrounded on the west, north, and east by the Subarctic Current-California Current confluence. The center of the meander had a surface temperature of 15.8, 14.9, and 14.4 degrees C on 17 November, 1 and 5 December, respectively. A chart of the monthly mean surface temperature for November 1980 (Renner, 1981) clearly shows the intrusion of a large tongue of warm water from the area between San Francisco and Hawaii northward along the west coast of the United States.

The decrease in the surface temperature of the meander over the project time period was reflected by the decrease in the surface temperatures all along the buoy line. Both the satellite and the AXBT's recorded mean changes of 0.9 degrees between 17 November and 1 December and 0.7 degrees between 1 December and 5 December. This drop in temperature

Figure 40. Meander, 17 November 1980

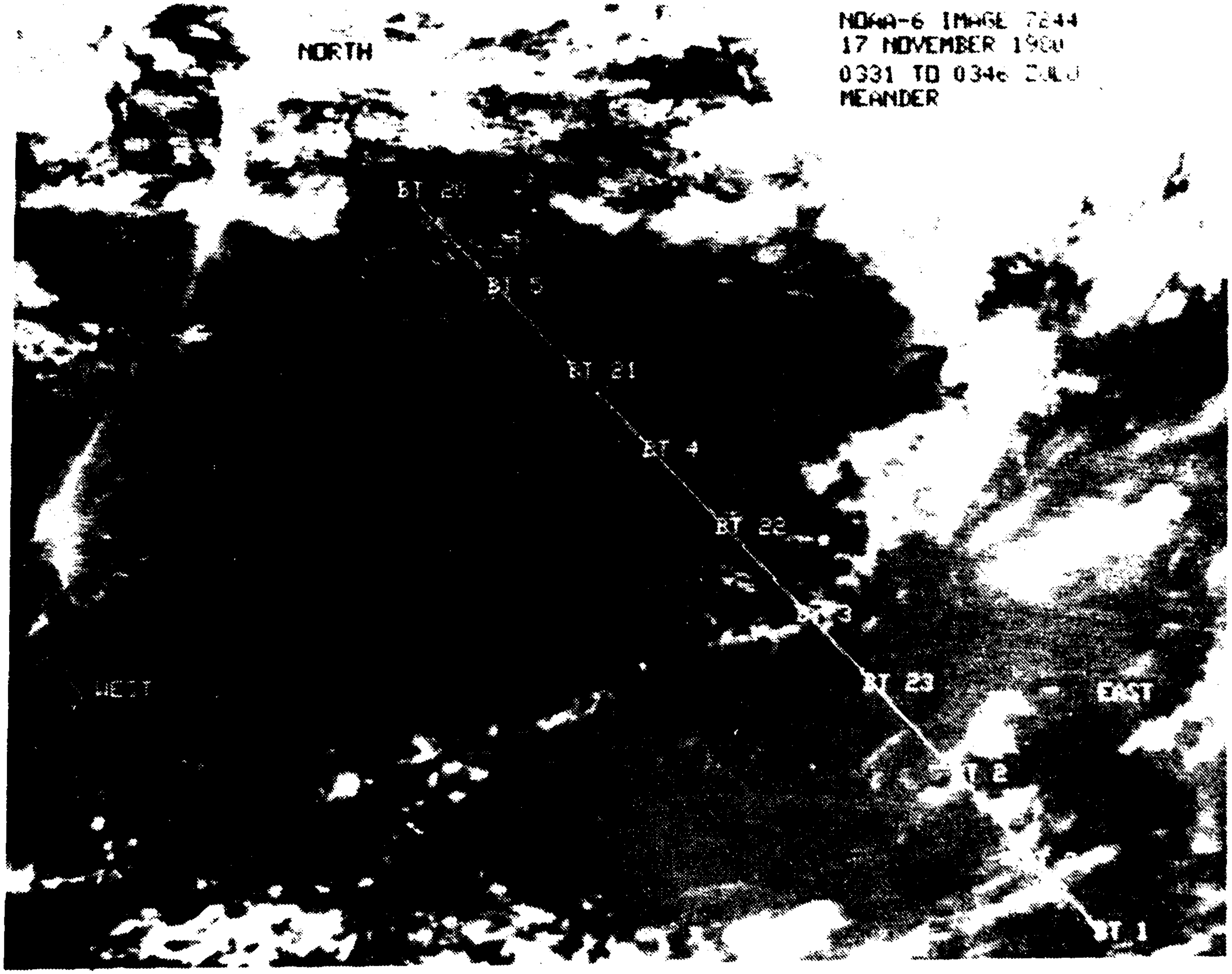

is to be expected considering the weather conditions as mentioned above. On 17 November, a low pressure system was firmly entrenched over the Aleutians while a high pressure system was anchored off of Southern California. This pressure pattern is typical of the Northeast Pacific in early winter. A cold front extending southward from the Aleutian low moved across the buoy line during the evening of 17 November and crossed the U.S. coastline during the morning of 18 November. Winds before passage were southerly at 25 knots while after passage the wind shifted northerly at 30 knots; hence the condition for considerable wind-mixing existed. A series of cold fronts on 20-22 November and 25 November also passed through the project area continuing to lower the sea surface temperature and drive the mixed layer depth deeper. On 1 December, low pressure cells were established west of the coast of Washington and about 500 nm west of the central California coast. The Washington low strengthened and centered near buoy positions 7 on 2 December. This low was accompanied by winds in excess of 35 knots on 3 December over the entire buoy area while a slow-moving cold front hugged the coastline. On 4 December, a high pressure area, previously established in the Gulf of Alaska, moved into the project area from the north pushing the cold front well inland although the low remained off the Washington coast. The high moved southerly on 5 December, influencing the weather over the entire buoy area (National Weather Service, 1980b). See

Figures 41, 42, and 43 for the surface weather depiction charts for 17 November, 1 and 5 December, respectively.

Because the linear regression model mentioned earlier was used to remove the effects of the atmosphere with fairly good results, a comparison was made between the satellite data and the GOSSTCOMP product. Sea surface temperature products from GOSSTCOMP have been subjected to an atmospheric correction model and are issued on a weekly basis. On all three days, the satellite data from this project were colder than the GOSSTCOMP values. The mean difference for 17 November, 1 and 5 December were 2.0 degrees (s = 0.9 degrees), 3.2 degrees (s = 0.6 degrees), and 4.3 degrees (s = 0.9 degrees) respectively with the overall mean of 3.2 degrees (s = 1.1 degrees). This overall mean agrees fairly well with the 3.5 to 3.9 degree bias enumerated by Klein (1979). The reason for the 3.2 degree bias can be attributed directly to the effects of the atmosphere, exactly the same situation as seen in the AXBT versus satellite comparisons mentioned previously. An interesting point to be made is that the 3.2 degree bias of GOSSTCOMP versus satellite data is higher than the 2.9 degree bias of AXBT versus satellite data. This led to a comparison between GOSSTCOMP and AXBT data with the result that GOSSTCOMP values were 0.3 degrees (s = 1.04 degrees) warmer overall than the AXBT values. Because the project area was never totally cloud-free during the period of observations, it is felt that the overcorrection for atmospheric effects described by Klein (1979) is still a factor in the warmer GOSSTCOMP values. It

Figure 41. Surface weather chart, 17 November 1980 (from Reed and Mullen, 1981)

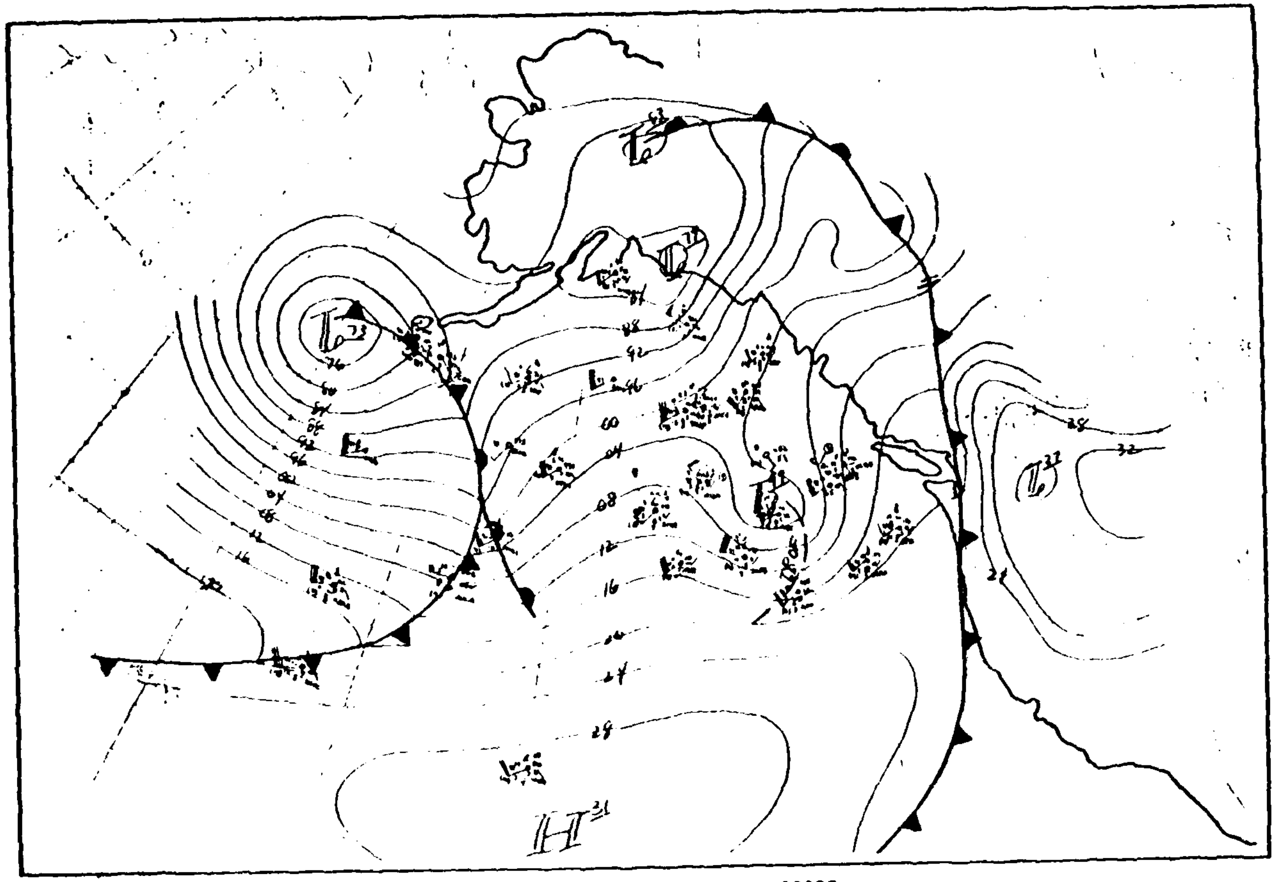

Surface Analysis for 17 NOV 80, 0000Z.

Figure 42. Surface weather chart, 1 December 1980 (from Reed and Mullen, 1981)

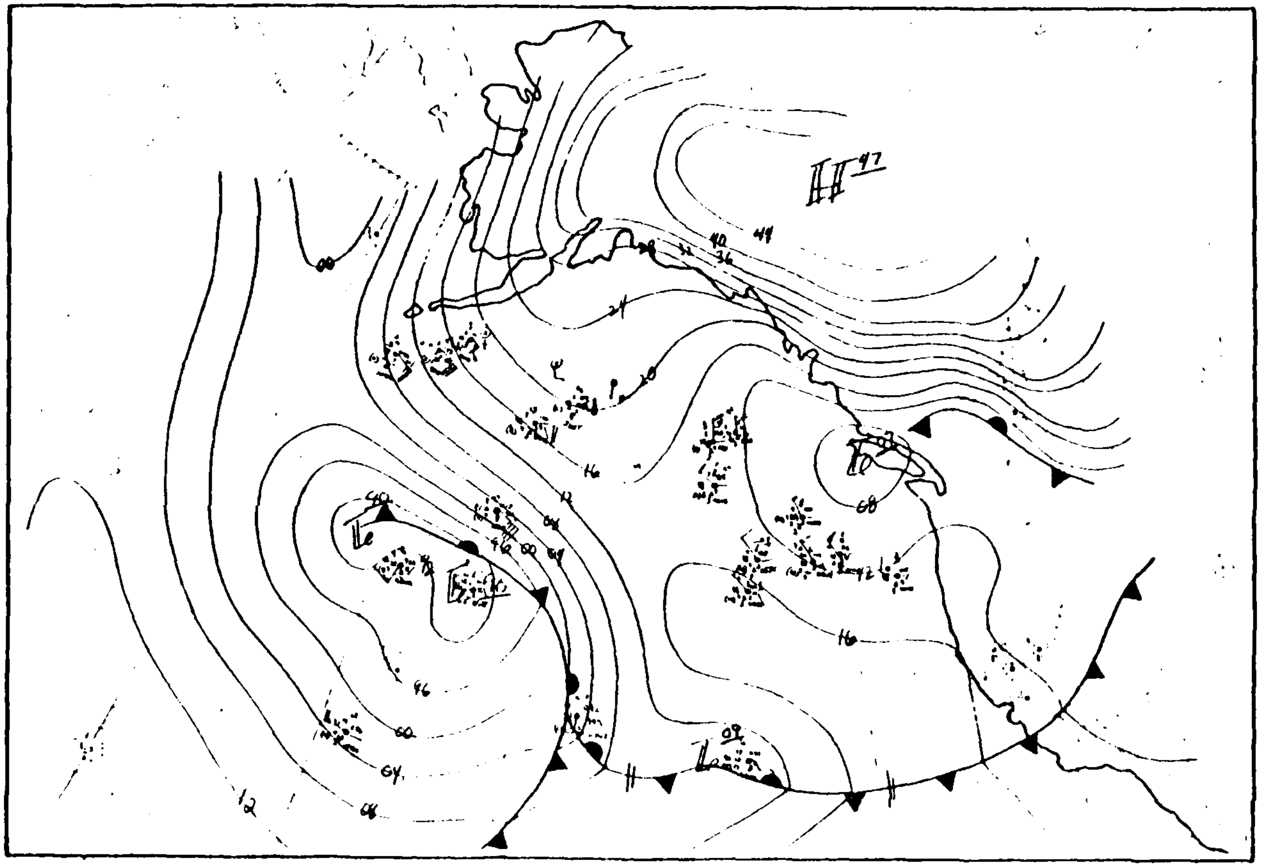

Surface Analysis for 1 DEC 80, 0000Z.

Figure 43. Surface weather chart, 5 December 1980 (from Reed and Mullen, 1981)

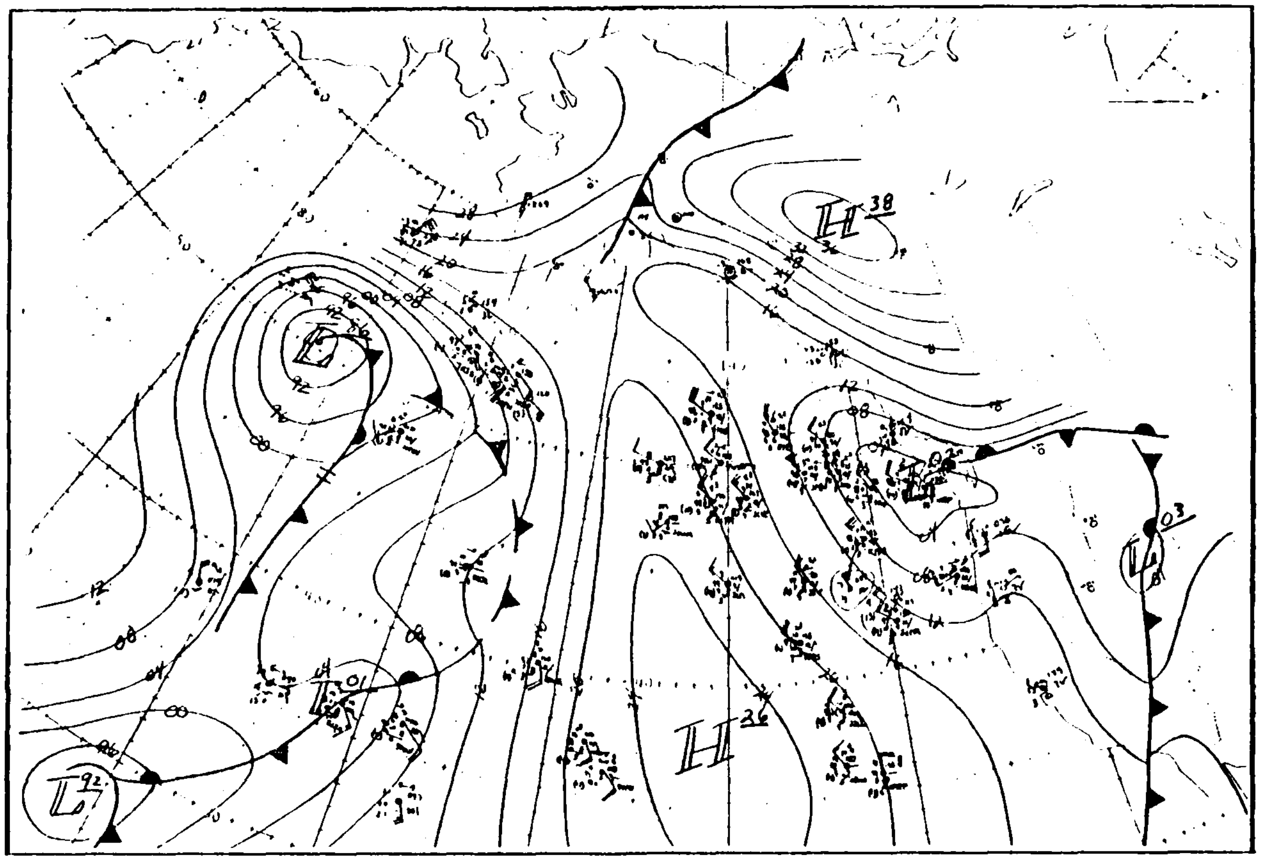

Surface Analysis for 5 DEC 30, 0000Z.

should be mentioned that the GOSSTCOMP product did not indicate the warm meander that the AXBT and satellite data located, probably due to the large grid structure used by GOSSTCOMP.

All three methods of sea surface temperature determination, AXBT, satellite, and GOSSTCOMP, were compared to the 20-year mean surface temperature values of Robinson (1976). AXBT values versus climatology resulted in the November AXBT's being 0.3 degrees colder than the mean while the December values were about the same as the mean. The reason for the cooler surface waters in November is probably a result of the high incidence of weather frontal passage with accompanying high winds through the project area. As was expected, climatology did not show the warm meander.

Comparison of satellite versus monthly mean data found the satellite data averaging 3.0 to 2.7 degrees colder than the mean for November and December. Comparison of GOSSTCOMP versus the mean resulted in GOSSTCOMP being 0.4 degrees warmer than the mean for November and 2.0 degrees colder than the mean for December.

2. Vertical Distribution

There is no known way at present to sense remotely the vertical thermal structure in the ocean; however, if one combines knowledge of the horizontal gradients with climatology, a fairly accurate synopsis of the upper ocean thermal structure is possible. A more accurate picture can be

formulated if the satellite data are augmented with well-placed AXBT drops.

From climatology, the expected mean surface temperature and the mean layer depth for November were 12.9 degrees and 50 meters (s = 5 meters) respectively over the project area. The AXBT mean surface temperature and mean layer depth for 17 November were 12.6 degrees and 58 meters (s = 6 meters). For December, climatology means were 10.8 degrees and 67 meters (s = 6 meters) and the AXBT means were 10.8 degrees and 71 meters (s = 7 meters). Figures 44, 45, 46, and 47 show the vertical structure along the buoy line on 17 November, 1 and 5 December (center track and north track) respectively. From the numerous oceanographic studies in the area (Tully, 1961; Tabata, 1961; etc.), it is known that during this period of the year, the layer depth is deepening towards the maximum limit of the top of the permanent halocline at 100 meters. The 100-meter depth is not reached usually until February. The deepening of the layer is directly attributable to the turbulent mixing conditions caused by the sustained high wind speeds and by the convective mixing caused by the surface cooling during the calmer periods. The weather pattern for late-November and early-December was discussed previously. A general rule of thumb is that warm surface waters generally exhibit shallow layer depths while colder surface waters exhibit deeper layer depths. This pattern held true throughout the project area. Although definitive sea surface temperature-layer depth relationships were not within the scope of this

Figure 44. Vertical thermal structure, 17 November 1980, center track

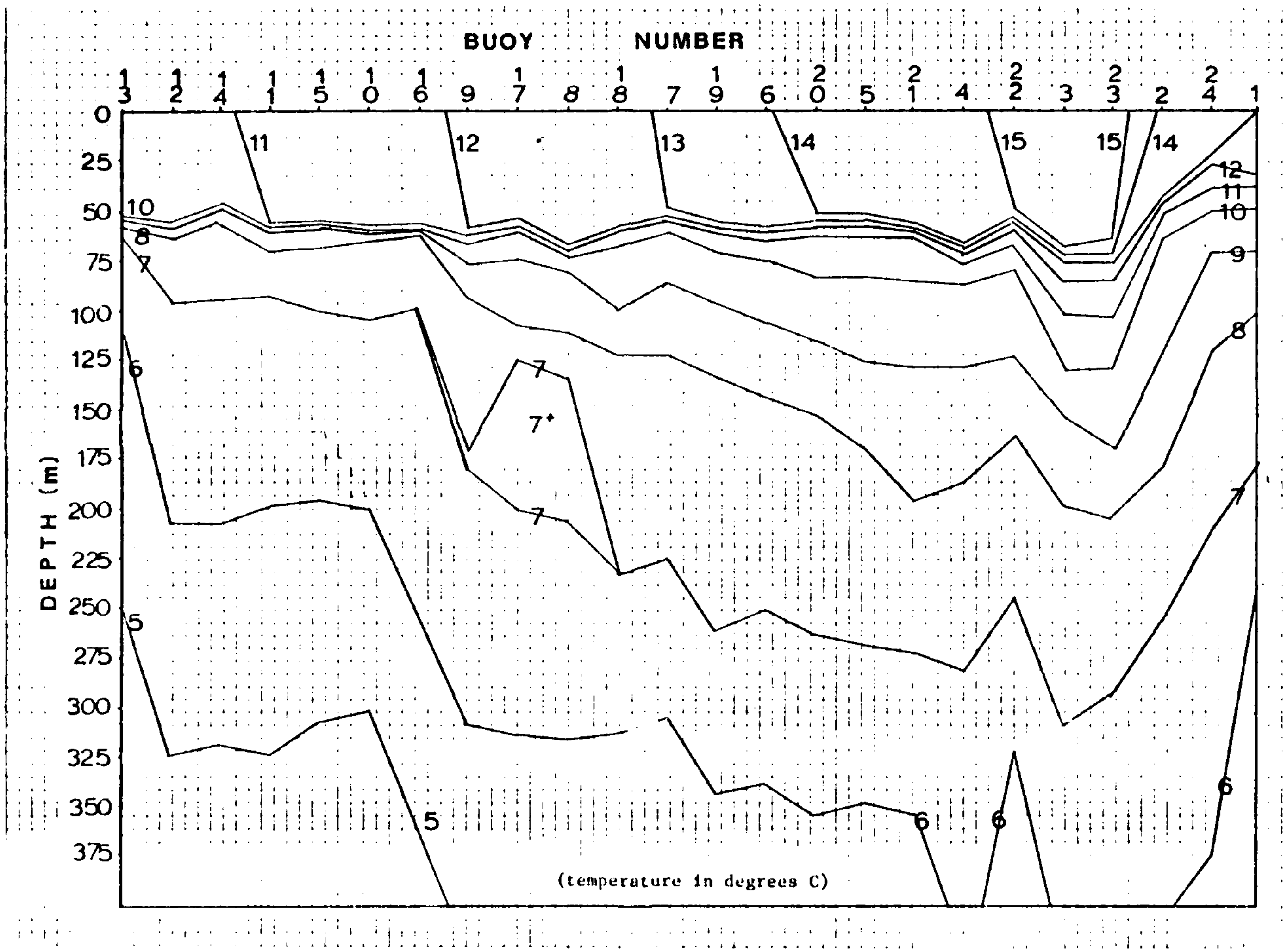

Figure 45. Vertical thermal structure, 1 December 1980, center track

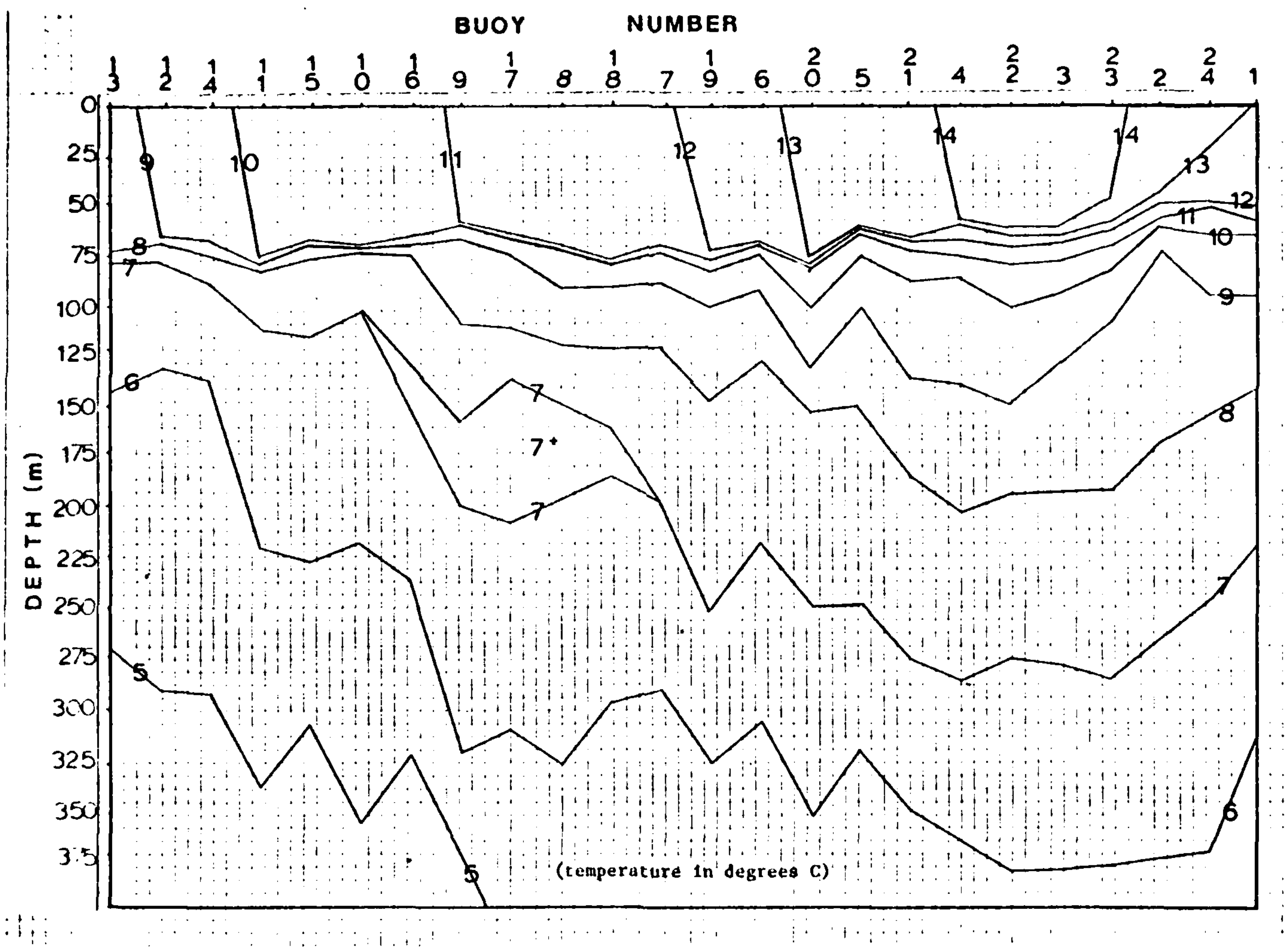

Figure 46. Vertical thermal structure, 5 December 1980, center track

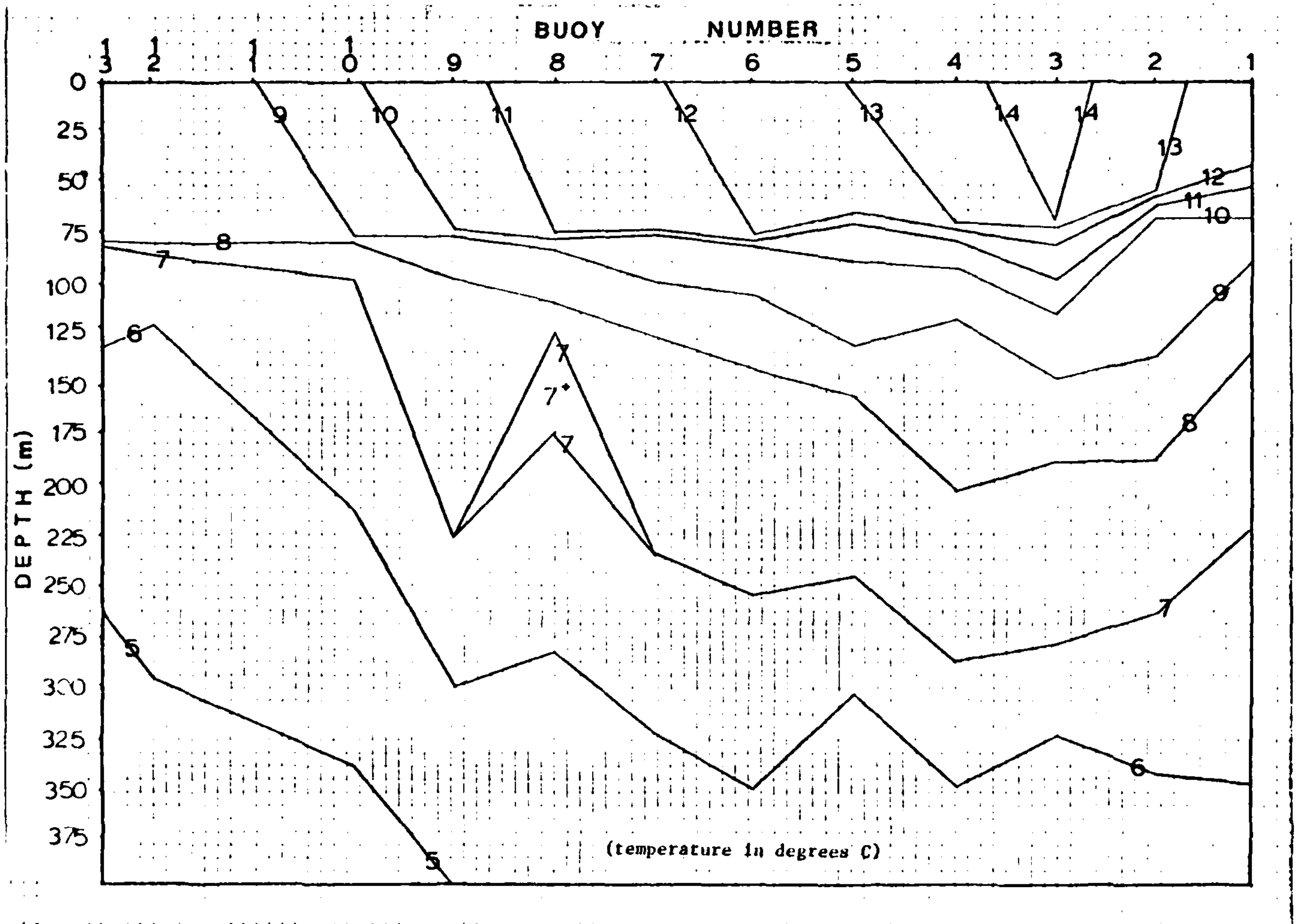

Figure 47. Vertical thermal structure, 5 December 1980, northern track

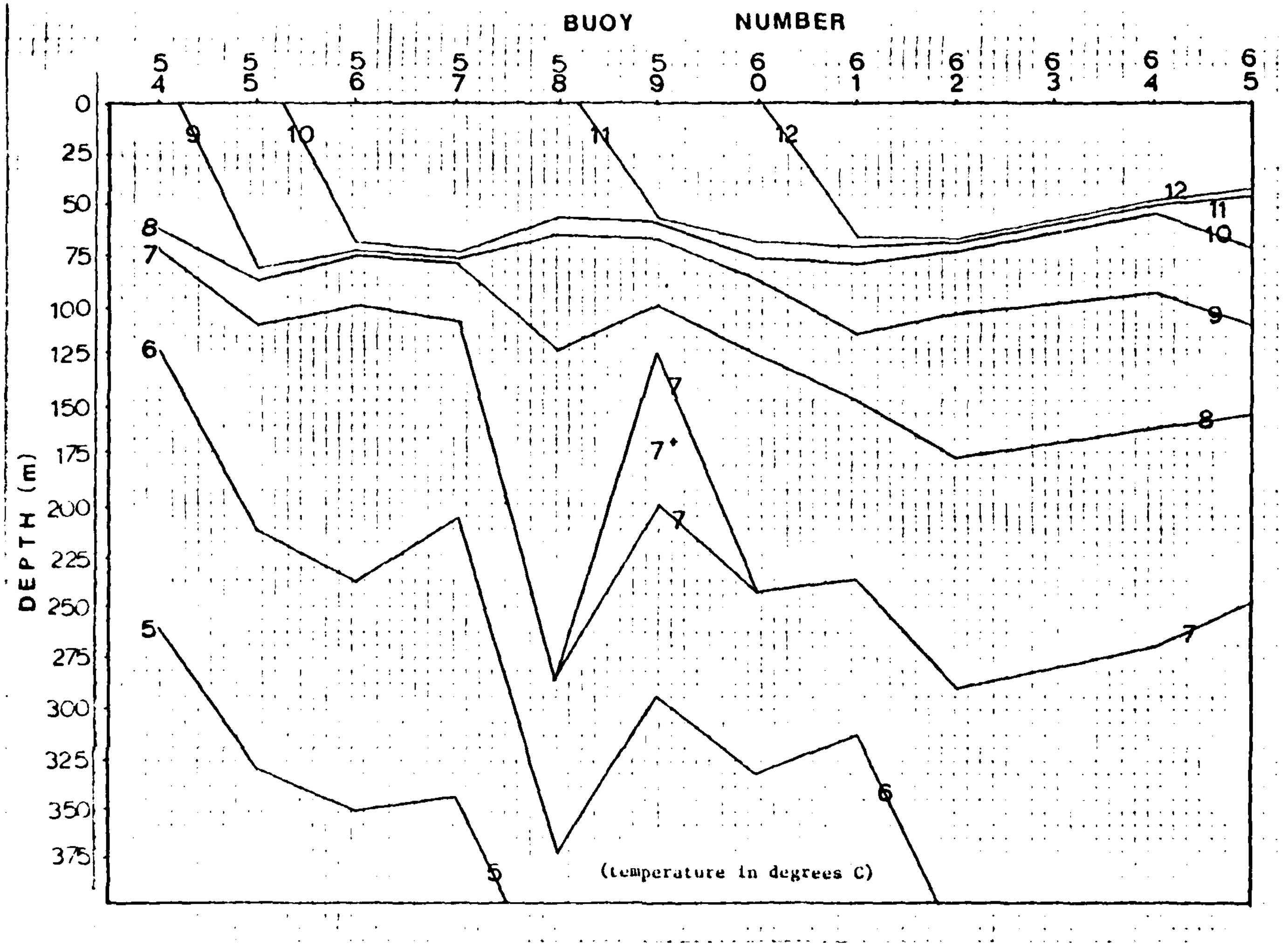

project, it is conceivable that flight crews, after observing a horizontal and vertical thermal analysis done on AXBT data and satellite images from a previous day(s) could view current satellite infrared images and through comparisons of surface temperatures (atmospherically corrected or not) could estimate the layer depth.

Further deployment of layer depth prediction techniques may be found in combining the works of James (1966), McAlister and McLeish (1970), and Mollo-Christensen and Mascarenhas (1979). James described a way of using heat budget calculations and wind-mixing parameters to predict the ocean thermal structure. McAlister and McLeish described an airborne system that was capable of measurement of the total heat flow from the sea. Mollo-Christiansen and Mascarenhas used LANDSAT data to calculate heat storage in the upper mixed layer of the ocean. The use of satellites to estimate wind speed and direction has been demonstrated. If the heat budget could be estimated using the principles described in the papers above, and the winds determined, then the procedures described by James may be applicable.

An example of how present satellites are inadequate to sense the vertical structure is the fact that only the AXBT traces located a region of a subsurface temperature maximum on the northern end of the buoy line. This region would help to define the lower extent of a subsurface sound channel. There was no surface manifestation of this feature, like the

warm meander, and hence the satellite completely missed it. This temperature maximum was relatively narrow (50 meters) and had an axis between 150 and 175 meters. On 17 November, the area affected by the temperature maximum was relatively large with the axis at the shallower depth. By 5 December, the area affected was reduced by half with the axis depth deepening in conjunction with the layer depth. The area of the subsurface temperature maximum can be seen in Figures 44, 45, 46, and 47.

V. CONCLUSIONS AND RECOMMENDATIONS FOR FURTHER STUDY

It was determined that geographical locations over open ocean areas could be located on satellite imagery to within 2 pixels or within 3 kilometers over 50% of the image (within 5 kilometers over 80%, worst case within 10.7 kilometers). Location of satellite features on geographical charts using a variation of the main program has similar accuracies.

Satellite observations can be a very effective tool if used in conjunction with available groundtruth data. The development of the NOAA-6 AVHRR allows a more accurate determination of sea surface temperatures than from previous satellites; however, the satellite mean values differ from groundtruth values by 2.9 degrees C. This bias is attributable directly to the effects of the atmosphere. By using a method of linear regression, it is possible to "field-calibrate" the satellite data so that the mean error between satellite and AXBT data is reduced to 0.3 degrees. This small bias held true whether 24 or 2 buoys were used to define the calibration constants for the linear regression equation for a single satellite pass. When these same constants were used to predict the sea surface temperature on satellite passes 4 days later and 15 days previous, the mean error increased slightly to between 0.4 and 0.5 degrees. This three-week prediction period saw the passage of numerous cold fronts and experienced long periods of turbulent mixing conditions so the

relatively small bias may make this procedure a possible prediction tool in calibrating satellite images without the need to use atmospheric attenuation models.

Relative temperature gradients were constant, as expected, between satellite and AXBT data values. The introduction into the project area of a warm-core meander in the final stages of becoming an eddy was apparent readily from both the AXBT data and the satellite imagery, although it was ignored by GOSSTCOMP. The detection of subsurface thermal structures by satellites is successful only if there is a surface manifestation of the feature such as the meander. A subsurface temperature maximum that is associated with a subsurface sound channel was not detected by the satellite, as no surface manifestations were present.

When GOSSTCOMP values were compared to AXBT values, an overall 0.3 degree bias was noted, although individual daily values ranged from 0.7 degrees colder to 1.2 degrees warmer than the corresponding AXBT data.

Over the project period, the sea surface temperature decreased on the average 1.8 degrees while the layer depth deepened on the average 13 meters. The cooling and deepening process was directly related to the number of frontal passages and the high wind speeds during the project period. It may be possible to use systems currently under development to sense remotely the existing thermal structure to 100 meters; or to use a combination of satellite instruments to determine the

heat budget and wind speeds and from this information to calculate the thermal structure.

Determining the exact location of thermal features on satellite imagery is only the beginning in tactically employing satellite data for naval missions. Further development of the relationship between the sea surface temperature and the vertical thermal structure is warranted. An excellent starting point would be along lines similar to those developed under the ASWEPS program. If a possible relationship could be derived, the use of environmental satellites by naval tacticians could advance far beyond its present stage.

Using methods developed by this thesis, it is possible to develop hypothetical scenarios that need to be tested operationally. Supposing that the 17 November satellite imagery and AXBT data, and the 1 December satellite imagery only were available, an antisubmarine aircraft flight crew assigned a surveillance mission on 1 December could have predicted within one half degree the sea surface temperature over a wide ocean area. Knowing both the vertical thermal structure from 17 November and the effects of cooler surfaces and sustained high winds on this structure, the flight crew could make a fairly accurate prediction of the 1 December oceanographic and acoustic conditions. Development of techniques that relate the surface temperature to the vertical structure would make this process that much easier.

In addition to predicting the vertical structure, some aspects of the horizontal structure are equally important,

especially to the fast-paced antisubmarine warfare efforts of the carrier-based S-3A aircraft. Submarines may be able to use sharply-delineated fronts and eddies to keep themselves acoustically hidden from aircraft carriers while remaining within weapons firing range. The persistence of these thermal features over a period of time is seen easily in satellite images and their exact geographical location can be determined using the methods derived in this thesis. A current satellite photo is far superior to other products now available in conveying this type of information. As an example, GOSSTCOMP missed totally the small (100 nm diameter) warm-core meander found in this project. GOSSTCOMP is also not a real-time product.

In conclusion, the following recommendations for further study are suggested:

(1) the development, where applicable, of an empirical relationship between the sea surface temperature and the vertical thermal structure;

(2) the development of thermal structure prediction techniques using both satellite data and the empirical relationship developed above;

(3) a study of the persistence of horizontal thermal features using satellite imagery;

(4) a study of how accurately satellite-observed surface thermal features reflect the subsurface structure;

(5) the development of a streamlined LOCATE program suitable for ship-board use so that surface thermal features from satellite imagery can be located more accurately;

(6) the further development and testing of the "field-calibration" technique of dealing with atmospheric attenuation; and,

(7) the investigation of including a current satellite image, with thermal features geographically located, in mission planning information.

APPENDIX A

COUNT-TO-TEMPERATURE CONVERSION TABLE

(from Kidwell, 1979)

COUNT	TEMPERATURE (degrees C)
95	16.33
96	15.91
97	15.48
98	15.06
99	14.63
100	14.20
101	13.77
102	13.34
103	12.90
104	12.03
105	11.59
106	11.59
107	11.15
108	10.70
109	10.26
110	9.81
111	9.36
112	8.91
113	8.46
114	8.00
115	7.54

116	7.08
117	6.62
118	6.16
119	5.69
120	5.23
121	4.76
122	4.28
123	3.81
124	3.33
125	2.85

```
C***********************************************************************SCA00010
C***********************************************************************SCA00020
C                                                                       SCA00030
C                                                                       SCA00040
C                      S C A N L I N E                                  SCA00050
C                                                                       SCA00060
C                                                                       SCA00070
C***********************************************************************SCA00080
C                                                                       SCA00090
C           SCANLINE IS A COMPUTER PROGRAM DESIGNED TO COUNT THE NUMBER SCA00100
C    OF RECORDED SCAN LINES FROM A NOAA-6 MAGNETIC TAPE.  THIS PROGRAM  SCA00110
C    ACTUALLY COUNTS THE NUMBER OF DATA BLOCKS ON THE MAGNETIC TAPE AND SCA00120
C    THE USER THEN DETERMINES THE NUMBER OF SCAN LINES FROM THE FORMULA: SCA00130
C                                                                       SCA00140
C            NO. OF SCAN LINES = (NUMBER OF BLOCKS - 1) / 3 .           SCA00150
C                                                                       SCA00160
C    THIS PROGRAM IS DESIGNED TO BE USED ON NOAA-NESS FIELD-STATION     SCA00170
C    FORMAT MAGNETIC TAPES.  A DISCUSSION OF THIS FORMAT CAN BE FOUND   SCA00180
C    IN THE ACCOMPANYING TEXT.  THERE ARE NO PROVISIONS FOR USER        SCA00190
C    MODIFICATIONS.                                                     SCA00200
C                                                                       SCA00210
C***********************************************************************SCA00220
C***********************************************************************SCA00230
C                                                                       SCA00240
C***** JOB CONTROL STATEMENTS *****                                     SCA00250
C*****  JOBNAME IS ANY NAME YOU WANT; EX: NOAATAPE                      SCA00260
C*****  NNNN IS COMPUTER CENTER USER NUMBER; EX: 1234                   SCA00270
C*****  MMMM IS COMPUTER CENTER-ASSIGNED PROJECT CODE; EX: 5678         SCA00280
C***** LASTNAME IS ANY NAME YOU WANT TO ENTER; EX: SMITH                SCA00290
C                                                                       SCA00300
//JOBNAME JOB (NNNN,MMMM),'LASTNAME',CLASS=D                            SCA00310
// EXEC FORTXCLG                                                        SCA00320
//SYSIN DD *                                                            SCA00330
C                                                                       SCA00340
300   FORMAT(1X,'EOF EXIT-NUMBER OF BLOCKS READ WAS',2X,I8)             SCA00350
301   FORMAT(1X,'I/O EXIT-NUMBER OF BLOCKS READ WAS',2X,I8)             SCA00360
```

```
      LOGICAL*1 DATA(2)                                                 SCA00370
      IBLOCK=0                                                          SCA00380
      IBYTES=2                                                          SCA00390
10    CALL TAPRD(DATA,IBYTES,&30,&35)                                   SCA00400
      IBLOCK=IBLOCK+1                                                   SCA00410
      GO TO 10                                                          SCA00420
30    WRITE(6,300)IBLOCK                                                SCA00430
      RETURN                                                            SCA00440
35    WRITE(6,301)IBLOCK                                                SCA00450
      RETURN                                                            SCA00460
      END                                                               SCA00470
C                                                                       SCA00480
C***** JOB CONTROL STATEMENTS *****                                     SCA00490
C***** TAPENAME IS THE NAME OF THE MAGNETIC TAPE ASSIGNED WHEN THE      SCA00500
C***** TAPE IS CHECKED INTO THE COMPUTER CENTER.                        SCA00510
C                                                                       SCA00520
//GO.METTAP DD UNIT=3400-3,VOL=SER=TAPENAME,DISP=OLD,LABEL=(1,BLP),     SCA00530
// DCB=(DEN=3)                                                          SCA00540
/*                                                                      SCA00550
```

```
C***********************************************************************
C***********************************************************************
C
C
C                         T A P E D U M P
C
C
C***********************************************************************
C
C          TAPEDUMP IS A COMPUTER PROGRAM DESIGNED TO READ, TRANSLATE,
C    AND DUMP TO A HIGH-SPEED PRINTER THE CONTENTS OF THE DATA RECORDS
C    THAT COMPRISE THE INFORMATION CONTAINED ON A NOAA-6 MAGNETIC TAPE.
C    THIS PROGRAM IS DESIGNED TO BE USED ON NOAA-NESS FIELD-STATION
C    MAGNETIC TAPES.  A DISCUSSION OF THE FIELD-STATION FORMAT CAN BE
C    FOUND IN THE ACCOMPANYING TEXT.  THE OUTPUT FOR THIS PROGRAM WILL
C    INCLUDE THE STATION IDENTIFIER, THE CHANNELS RECORDED, THE TIME OF
C    THE FIRST SCAN LINE, THE TOTAL DURATION IN MINUTES OF THE PASS, AND
C    THE ORBIT NUMBER OF THE PASS, ALL FROM THE HEADER RECORD.  FROM
C    THE INDIVIDUAL DATA RECORDS WILL COME THE SPECIFIC CHANNEL NUMBER
C    FOR THAT RECORD, THE JULIAN DATE, THE SPECIFIC SCAN LINE TIME,
C    TELEMETRY DATA, BACK SCAN DATA, SPACE VIEW DATA, SPACE DATA, AND
C    A LISTING OF THE INDIVIDUAL COUNT VALUES THAT REPRESENT THE
C    TEMPERATURE OF THE SURFACE SENSED BY THE RADIOMETER.
C
C***********************************************************************
C
C          THE PROCEDURE TO MODIFY THE PROGRAM SO THAT IT IS APPLICABLE
C    FOR THE USER'S PURPOSE IS AS FOLLOWS:
C
C         (1) TO DEFINE THE NUMBER OF DATA RECORDS TO BE DUMPED:
C             -CHANGE 'DO 20 J=1,NNNN' WHERE NNNN IS THE NUMBER OF
C              BLOCKS THAT THE USER WISHES TO BE DUMPED.  AS AN
C              EXAMPLE, TO DUMP THE FIRST 30 BLOCKS, NNNN = 30.
C
```

```
C        (2) TO BEGIN DUMPING DATA RECORDS FROM SOMEWHERE IN THE TAPE
C            OTHER THAN BEGINNING WITH RECORD NUMBER 1, THE FOLLOWING
C            STATEMENTS NEED TO BE ADDED TO THE PROGRAM AFTER THE
C            ARRAY INITIATION STATEMENTS:
C
C                 N=(NL*3)-NNNN     (NNNN = # OF SKIPPED RECORDS)
C                 DO 5 I=1,N
C                 CALL TAPRD(DATA,2,&30,&35)
C               5 CONTINUE
C
C***********************************************************************
C***********************************************************************
C
C
C***** JOB CONTROL CARDS *****
C***** JOBNAME IS ANY NAME YOU WANT; EX: NOAATAPE
C***** NNNN IS COMPUTER CENTER USER NUMBER; EX: 1234
C***** MMMM IS COMPUTER CENTER-ASSIGNED PROJECT NUMBER; EX: 5678
C***** LASTNAME IS ANYNAME YOU WANT TO ENTER; EX: SMITH
C
//JOBNAME JOB (NNNN,MMMM),'LASTNAME',CLASS=D
// EXEC FORTXCLG
//SYSIN DD *
C
C***** INPUT-OUTPUT FORMAT STATEMENTS *****
C
300   FORMAT(1X,'END OF FILE ENCOUNTERED')
301   FORMAT(1X,'INPUT-OUTPUT ERROR ENCOUNTERED')
400   FORMAT(1X,'STATION IDENTIFIER',2X,4A1)
401   FORMAT(1X,'BANDS RECORDED',2X,3(1X,I5))
402   FORMAT(1X,'TIME OF FIRST SCAN',2X,3(2X,2I5),2X,'ZULU')
403   FORMAT(1X,'DURATION OF PASS',2X,2(2X,2I5),2X,'MINUTES')
404   FORMAT(1X,'ORBIT NUMBER  N',4I5)
501   FORMAT(1X,'CHANNEL NUMBER',2X,I10)
502   FORMAT(1X,'JULIAN DATE',2X,3I1)
```

```
503   FORMAT(1X,'SCAN LINE TIME',2X,3(2X,2I1),2X,'ZULU')                       TAP00700
504   FORMAT(1X,'TELEMETRY DATA',2X,10I5)                                      TAP00710
505   FORMAT(1X,'BACK SCAN DATA',2X,6I5)                                       TAP00720
506   FORMAT(1X,'SPACE VIEW DATA',2X,10I5)                                     TAP00730
507   FORMAT(1X,'SPACE DATA')                                                  TAP00740
510   FORMAT(2(1X,10I5/))                                                      TAP00750
508   FORMAT(1X,'COUNT VALUES FOLLOW')                                         TAP00760
509   FORMAT(1X,5(1X,20I5/))                                                   TAP00770
C                                                                              TAP00780
C***** ARRAY INITIATION STATEMENTS *****                                       TAP00790
C                                                                              TAP00800
      EQUIVALENCE(ISCAN(1),SCAN(1))                                            TAP00810
      LOGICAL*1 DATA(2138),HEADER(40)                                          TAP00820
      LOGICAL*4 SCAN(2138)                                                     TAP00830
      INTEGER*4 ISCAN(2138)                                                    TAP00840
      INTEGER S/'S'/,F/'F'/,O/'O'/,BLANK/' '/                                  TAP00850
      DATA ISCAN/2138*0/                                                       TAP00860
C                                                                              TAP00870
C***** READ AND TRANSLATE THE HEADER RECORD INTO DECIMAL VALUES *****          TAP00880
C                                                                              TAP00890
      CALL TAPRD(HEADER,40,&30,&35)                                            TAP00900
      DO 10 I=1,40                                                             TAP00910
10    CALL SPRED(HEADER(I),SCAN(I))                                            TAP00920
      DO 11 I=6,18                                                             TAP00930
11    ISCAN(I)=ISCAN(I)-48                                                     TAP00940
      DO 12 I=20,23                                                            TAP00950
12    ISCAN(I)=ISCAN(I)-48                                                     TAP00960
      ISCAN(1)=S                                                               TAP00970
      ISCAN(2)=F                                                               TAP00980
      ISCAN(3)=O                                                               TAP00990
      ISCAN(4)=BLANK                                                           TAP01000
C                                                                              TAP01010
C***** OUTPUT THE HEADER RECORD TO THE PRINTER *****                           TAP01020
C                                                                              TAP01030
```

```
      WRITE(6,400)(ISCAN(I),I=1,4)                                      TAP01040
      WRITE(6,401)(ISCAN(I),I=6,8)                                      TAP01050
      WRITE(6,402)(ISCAN(I),I=9,14)                                     TAP01060
      WRITE(6,403)(ISCAN(I),I=15,18)                                    TAP01070
      WRITE(6,404)(ISCAN(I),I=20,23)                                    TAP01080
C                                                                       TAP01090
C***** READ AND TRANSLATE THE NEXT NNNN DATA RECORDS *****              TAP01100
C                                                                       TAP01110
      DO 20 J=1,NNNN                                                    TAP01120
      DATA ISCAN/2138*0/                                                TAP01130
      CALL TAPRD(DATA,2138,&30,&35)                                     TAP01140
      DO 31 I=1,2138                                                    TAP01150
31    CALL SPRED(DATA(I),SCAN(I))                                       TAP01160
      DO 41 I=6,14                                                      TAP01170
41    ISCAN(I)=ISCAN(I)-48                                              TAP01180
C                                                                       TAP01190
C***** OUTPUT THE DATA RECORDS TO THE PRINTER *****                     TAP01200
C                                                                       TAP01210
      WRITE(6,501)ISCAN(5)                                              TAP01220
      WRITE(6,502)(ISCAN(I),I=6,8)                                      TAP01230
      WRITE(6,503)(ISCAN(I),I=9,14)                                     TAP01240
      WRITE(6,504)(ISCAN(I),I=15,24)                                    TAP01250
      WRITE(6,505)(ISCAN(I),I=25,30)                                    TAP01260
      WRITE(6,506)(ISCAN(I),I=31,40)                                    TAP01270
      WRITE(6,507)                                                      TAP01280
      WRITE(6,510)(ISCAN(I),I=41,90)                                    TAP01290
      WRITE(6,508)                                                      TAP01300
      WRITE(6,509)(ISCAN(I),I=91,190)                                   TAP01310
20    CONTINUE                                                          TAP01320
      GO TO 40                                                          TAP01330
30    WRITE(6,300)                                                      TAP01340
35    WRITE(6,301)                                                      TAP01350
40    CONTINUE                                                          TAP01360
      STOP                                                              TAP01370
      END                                                               TAP01380
```

```
C
C***** SUBROUTINE SPRED FACILITATES THE TRANSLATION OF THE TAPE DATA
C***** INTO UNDERSTANDABLE DECIMAL VALUES *****
C
      SUBROUTINE SPRED(A,B)
      LOGICAL*1 A(1),B(4)
      B(4)=A(1)
      RETURN
      END
C
C***** JOB CONTROL CARDS *****
C*****  TAPENAME IS THE NAME OF THE MAGNETIC TAPE ASSIGNED WHEN THE
C*****  TAPE IS CHECKED INTO THE COMPUTER CENTER.
C
//GO.METTAP DD UNIT=3400-3,VOL=SER=TAPENAME,DISP=OLD,LABEL=(1,BLP),
// DCB=(DEN=3)
/*
```

```
C***********************************************************************
C***********************************************************************
C
C
C                          A R E A M A P
C
C
C***********************************************************************
C
C           AREAMAP IS A COMPUTER PROGRAM DESIGNED TO LOCATE A SPECIFIC
C    PIXEL, AS AN AXBT, SHIP, OR THERMAL FEATURE, ON A NOAA-6 SATELLITE
C    IMAGE.  THE MAGNETIC TAPE USED IN THIS PROGRAM MUST HAVE BEEN
C    RECORDED USING THE NOAA-NESS FIELD-STATION FORMAT.  A DISCUSSION
C    OF THIS FORMAT MAY BE FOUND IN THE ACCOMPANYING TEXT.  THE OUTPUT
C    OF THIS PROGRAM WILL BE AN AREA MAPPING OF THE COUNT VALUES FOR
C    PIXELS BEGINNING X SCAN LINES BEFORE AND ENDING Y SCAN LINES
C    AFTER THE SCAN LINE CONTAINING THE SPECIFIC PIXEL BEING LOCATED.
C    THIS MAPPING INCLUDES THOSE N PIXELS EITHER SIDE ON THE CENTER
C    PIXEL.  KEEP IN MIND THAT FOR ASCENDING PASSES NORTH WILL BE AT
C    THE BOTTOM OF THE ARRAY WHILE FOR DESCENDING PASSES NORTH WILL BE
C    AT THE TOP OF THE ARRAY.  ALSO INCLUDED IN THE OUTPUT IS THE TIME
C    OF THE SCAN LINE ALONG THE LEFT EDGE OF THE ARRAY.  THIS TIME IS
C    IN THE FORMAT HHMMSS (H=HOURS, M=MINUTES, S=SECONDS).
C
C***********************************************************************
C
C          THE PROCEDURE TO MODIFY THE PROGRAM SO THAT IT IS APPLICABLE
C    FOR THE USER'S PURPOSE IS AS FOLLOWS:
C
C         (1) TO DEFINE THE SPECIFIC AXBT, SHIP, ETC. PIXEL:
C             -CHANGE 'NL=NNNN' WHERE NNNN IS THE SCAN LINE NUMBER OF
C              THE PIXEL;
C             -CHANGE 'NS=NNNN' WHERE NNNN IS THE SAMPLE NUMBER OF THE
C              PIXEL.
C
```

```
C         (2) TO CHANGE THE NUMBER OF SCAN LINES IN THE AREA MAPPING:     ARE00360
C             -TO CHANGE THE NUMBER OF SCAN LINES PRECEEDING THE CENTER  ARE00370
C              PIXEL, CHANGE 'N=(NL*3)-NNNN' WHERE NNNN IS THREE TIMES   ARE00380
C              THE NUMBER OF SCAN LINES THAT YOU WISH TO PRINT BEFORE THEARE00390
C              CENTER PIXEL SCAN LINE.  THE REASON FOR THREE TIMES THE   ARE00400
C              NUMBER IS THAT THE FIELD-STATION FORMAT INTERLEAVES THE   ARE00410
C              THREE AVHRR CHANNELS RECORDED ON THE TAPE.  FOR EXAMPLE,  ARE00420
C              TO BEGIN PRINTING 20 LINES PRIOR TO THE CENTER PIXEL      ARE00430
C              SCAN LINE, NNNN = 60.                                     ARE00440
C             -TO CHANGE THE TOTAL NUMBER OF SCAN LINES PRINTED, CHANGE  ARE00450
C              'DO 20 J=1,NNNN' WHERE NNNN IS THE TOTAL NUMBER OF SCAN   ARE00460
C              LINES TO BE PRINTED INCLUDING THE NUMBER OF SCAN LINES    ARE00470
C              PRECEEDING THE CENTER PIXEL SCAN LINE.                    ARE00480
C         (3) TO CHANGE THE NUMBER OF PIXELS EITHER SIDE OF THE CENTER   ARE00490
C             PIXEL:                                                     ARE00500
C             -CHANGE 'FS=(NS-NNNN) + 90' WHERE NNNN IS THE NUMBER OF    ARE00510
C             PIXELS TO THE LEFT OF THE CENTER PIXEL AND CHANGE          ARE00520
C             'LS=(NS-NNNN) + 90' WHERE NNNN IS THE NUMBER OF PIXELS     ARE00530
C             TO THE RIGHT OF THE CENTER PIXEL.  KEEP IN MIND THE        ARE00540
C             LINE LENGTH LIMITS OF THE OUTPUT PRINTER.  SUGGESTED VALUESARE00550
C             FOR 'FS' IS 12 AND FOR 'LS' IS 11.  THIS WILL FILL A       ARE00560
C             120 COLUMN OUTPUT PAGE.                                    ARE00570
C                                                                        ARE00580
C***********************************************************************ARE00590
C***********************************************************************ARE00600
C                                                                        ARE00610
C                                                                        ARE00620
C***** JOB CONTROL STATEMENTS *****                                      ARE00630
C*****  JOBNAME IS ANY NAME THE USER WANTS; EX: NOAATAPE                 ARE00640
C*****  NNNN IS COMPUTER CENTER USER NUMBER; EX: 1234                    ARE00650
C*****  MMMM IS COMPUTER CENTER-ASSIGNED PROJECT NUMBER; EX: 5678        ARE00660
C*****  LASTNAME IS ANY NAME YOU WANT TO ENTER; EX: SMITH                ARE00670
C                                                                        ARE00680
//JOBNAME JOB (NNNN,MMMM),'LASTNAME',CLASS=D                             ARE00690
// EXEC FORTXCLG                                                         ARE00700
//SYSIN DD *                                                             ARE00710
C                                                                        ARE00720
```

```
C***** INFUT-OUTFUT FORMAT STATEMENTS *****                             ARE00730
C                                                                       ARE00740
100   FORMAT(1X,6I1,2X,24I5)                                            ARE00750
101   FORMAT(1X,I5)                                                     ARE00760
300   FORMAT(1X,'END OF FILE ENCOUNTERED')                              ARE00770
301   FORMAT(1X,'INFUT-OUTFUT ERROR ENCOUNTERED')                       ARE00780
C                                                                       ARE00790
C***** ARRAY INITIATION STATEMENTS *****                                ARE00800
C                                                                       ARE00810
      EQUIVALENCE (ISCAN(1),SCAN(1))                                    ARE00820
      INTEGER FS,LS                                                     ARE00830
      LOGICAL*1 DATA(2138)                                              ARE00840
      LOGICAL*4 SCAN(2138)                                              ARE00850
      INTEGER*4 ISCAN(2138)                                             ARE00860
      DATA SCAN/2138*0/                                                 ARE00870
C                                                                       ARE00880
C***** DEFINITION OF THE CENTER PIXEL AS PER INSTRUCTIONS ABOVE *****   ARE00890
C                                                                       ARE00900
      NL=NNNN                                                           ARE00910
      NS=NNNN                                                           ARE00920
C                                                                       ARE00930
C***** DETERMINE STARTING SCAN LINE AS PER INSTRUCTIONS ABOVE *****     ARE00940
C                                                                       ARE00950
      N=(NL*3)-NNNN                                                     ARE00960
C                                                                       ARE00970
C***** DETERMINE NO. OF PIXELS EITHER SIDE OF CENTER PIXEL *****        ARE00980
C                                                                       ARE00990
      FS=(NS-NNNN)+90                                                   ARE01000
      LS=(NS+NNNN)+90                                                   ARE01010
C                                                                       ARE01020
C***** INITIATE TAPE SEARCH FOR STARTING SCAN LINE *****                ARE01030
C                                                                       ARE01040
      IBLOCK=0                                                          ARE01050
      DO 10 I=1,N                                                       ARE01060
      CALL TAPRD(DATA,2,&30,&35)                                        ARE01070
10    IBLOCK=IBLOCK+1                                                   ARE01080
C                                                                       ARE01090
```

```
C***** LOCATE THE AREA MAPPING SET UP BY ABOVE STATEMENTS AND TRANSLATE
C***** THE BINARY COUNT VALUES TO DECIMAL COUNT VALUES FOR OUTPUT *****
C
      DO 20 J=1,NNNN
      CALL TAPRD(DATA,2138,&30,&35)
      DO 25 I=1,2138
25    CALL SPRED(DATA(I),SCAN(I))
      DO 27 I=9,14
27    ISCAN(I)=ISCAN(I)-48
      WRITE(6,100)(ISCAN(I),I=9,14),(ISCAN(I),I=FS,LS)
      IBLOCK=IBLOCK+1
      DO 26 L=1,2
      CALL TAPRD(DATA,2,&30,&35)
26    IBLOCK=IBLOCK+1
20    CONTINUE
      GO TO 50
30    WRITE(6,300)
35    WRITE(6,301)
50    CONTINUE
C
C***** OUTPUT THE AREA MAPPING TO THE PRINTER *****
C
      WRITE(6,101)IBLOCK
      STOP
      END
C
C***** SUBROUTINE SPRED FACILITATES THE TRANSLATION OF THE TAPE DATA
C***** INTO UNDERSTANDABLE DECIMAL VALUES *****
C
      SUBROUTINE SPRED(A,B)
      LOGICAL*1 A(1),B(4)
      B(4)=A(1)
      RETURN
      END
C
```

```
C***** JOB CONTROL STATEMENTS *****                                     ARE01450
C*****  TAPENAME IS THE NAME OF THE MAGNETIC TAPE ASSIGNED WHEN THE     ARE01460
C*****  TAPE IS CHECKED INTO THE COMPUTER CENTER.                       ARE01470
C                                                                       ARE01480
//GO.METTAP DD UNIT=3400-3,VOL=SER=TAPENAME,DISP=OLD,LABEL=(1,BLP),     ARE01490
// DCB=(DEN=3)                                                          ARE01500
/*                                                                      ARE01510
```

```
C***********************************************************************
C***********************************************************************
C
C
C                         L O C A T E
C
C
C***********************************************************************
C
C           LOCATE IS A COMPUTER PROGRAM DESIGNED TO LOCATE NOAA-6
C    SATELLITE IMAGE COORDINATES WHEN THE GEOGRAPHICAL COORDINATES OF
C    AN EARTH LOCATION ARE KNOWN.  THIS PROGRAM WAS SPECIFICALLY
C    DESIGNED TO BE USED WITH NOAA-NESS FIELD-STATION FORMAT MAGNETIC
C    TAPES.  A DISCUSSION OF THIS FORMAT MAY BE FOUND IN THE
C    ACCOMPANYING TEXT.  PROGRAM OUTPUT INCLUDES THE SCAN LINE
C    NUMBER AND THE SAMPLE NUMBER OF AN EARTH LOCATION AS A LANDMARK,
C    AXBT, OR SHIP.
C
C***********************************************************************
C
C     NOTE: THIS PROGRAM IS DESIGNED TO BE USED INTERACTIVELY
C     ON A TERMINAL. NO ATTEMPT HAS BEEN MADE TO PREVENT INPUT
C     ERRORS. THE SPECIFIED NUMBER OF DECIMAL PLACES MUST BE
C     ENTERED ESPECIALLY THE LEADING ZEROS.
C
C***********************************************************************
C
C                    REQUIRED PROGRAM INPUT
C
C     LANDMARK LOCATION CONSISTING OF:
C             LINE NUMBER (FROM IDIMS)
C             PIXEL NUMBER (FROM IDIMS)
C             LANDMARK LATITUDE (DECIMAL DEGREES)
C             LANDMARK LONGITUDE (DECIMAL DEGREES)
C             TIME THAT THE SATELLITE SCANNED THE LANDMARK
C
```

```
C     SATELLITE INFORMATION CONSISTING OF:
C             NUMBER OF SCAN LINES RECORDED
C             INCLINATION (IN DECIMAL DEGREES)
C             PERIOD (IN MINUTES)
C             KNOW WHETHER IT IS A DESCENDING OR ASCENDING PASS
C
C     SPECIAL PROVISIONS HAVE BEEN MADE TO HANDLE AN IDIMS' FLIPPED
C     AND MIRRORED PASS ONLY AS FAR AS THE ORBIT TIE-DOWN IS
C     CONCERNED.  THIS OPTION WILL NOT INTERFERE WITH NORMAL
C     PROCESSING.
C
C***********************************************************************
C***********************************************************************
C
C
C***** INPUT-OUTPUT FORMAT STATEMENTS *****
C
100   FORMAT(I4)
101   FORMAT(F6.3)
102   FORMAT(F7.3)
103   FORMAT(F14.10)
106   FORMAT(F10.6)
200   FORMAT(1X,'NL=',2X,I4,4X,'NS=',2X,I4/)
201   FORMAT(1X,'PHIGEE=',2X,F16.10/)
203   FORMAT(1X,'SSP LATITUDE IS   ',F6.3)
204   FORMAT(1X,'SSP LONGITUDE IS  ',F7.3)
205   FORMAT(1X,'ASC. NODE LONGITUDE IS',2X,F7.3)
207   FORMAT(1X,'TIME OF ASC. NODE IN SECONDS IS',F16.6)
701   FORMAT(I1)
702   FORMAT(1X,'HAS THIS ASC. PASS BEEN FLIPPED+MIRRORED?YES=1,NO=2')
703   FORMAT(1X,'ENTER SAMPLE (PIXEL) NUMBER (NS) AS NNNN')
704   FORMAT(1X,'ENTER TOTAL NUMBER OF LINES AS NNNN')
705   FORMAT(1X,'ENTER LINE NUMBER (NL) AS NNNN')
706   FORMAT(1X,'ENTER LANDMARK LATITUDE AS NN.NNN')
707   FORMAT(1X,'ENTER LANDMARK LONGITUDE AS NNN.NNN')
708   FORMAT(1X,'ENTER INCLINATION AS NNN.NNNNNNNNNN (10 DECIMAL PL.)')
```

```
709   FORMAT(1X,'ENTER PERIOD IN MINUTES AS NNN.NNNNNN (6 DEC. PL.)')
710   FORMAT(1X,'DO YOU WANT TO CHANGE THE INCLINATION?YES=1,NO=2')
712   FORMAT(1X,'IS THIS A DESCENDING PASS?YES=1,NO=2')
800   FORMAT(1X,'DO YOU WANT TO CONTINUE MAIN PROGRAM? YES=1, NO=2')
801   FORMAT(1X,'DO YOU WANT TO CALCULATE A SPECIFIC PIXEL? YES=1,NO=2')
601   FORMAT(1X,'ENTER LANDMARK TIME AS HHMMSS.SSS')
604   FORMAT(1X,'ENTER BUOY LATITUDE AS NN.NNN')
605   FORMAT(1X,'ENTER BUOY LONGITUDE AS NNN.NNN')
607   FORMAT('0','ENTER ARBITRARY STARTING SCAN LINE AS NNNN')
650   FORMAT(I2,I2,F6.3)
651   FORMAT('0','DO YOU WANT TO CALCULATE ANOTHER PIXEL? YES=1,NO=2')
C
C***** ARRAY INITIATION STATEMENTS *****
C
      DIMENSION FLATR(2048),FLONGR(2048),DIST(2048)
      REAL INCLIN,LO,LAMDAO,LAMDAS,LS,LAMANF,LAMDAN
      INTEGER TOTLIN,F1,F2
      ICOUNT=1
C
C***** INITIATE THE INPUT DATA STATEMENTS *****
C
4     WRITE(6,705)
      READ(5,100)ILINE
      K=0
      WRITE(6,703)
      READ(5,100)IPIXEL
      WRITE(6,704)
      READ(5,100)TOTLIN
      WRITE(6,706)
      READ(5,101)LO
      WRITE(6,707)
      READ(5,102)LAMDAO
      WRITE(6,601)
      READ(5,650)IHOURS,IMINS,SECS
C
```

```
C***** CONVERSION OF TAPE TIME TO SECONDS *****
C
      TSECS=(IHOURS*3600.)+(IMINS*60.)+SECS
C
C***** IN THE FOLLOWING, ICOUNT WILL BE GREATER THAN 1 ONLY IF THIS IS
C***** THE SECOND OR MORE TIMES THROUGH THE PROGRAM, IE. YOU ARE
C***** PREDICTING MORE THAN ONE AXBT OR LANDMARK, ETC. *****
C
      IF(ICOUNT.EQ.1)GO TO 5
      WRITE(6,710)
      READ(5,701)K
      IF(K.EQ.2)GO TO 7
5     WRITE(6,708)
      READ(5,103)INCLIN
6     WRITE(6,709)
      READ(5,106)PERIOD
7     CONTINUE
C
C***** IN THE FOLLOWING, IF A DESCENDING PASS IS BEING PROCESSED, THEN
C***** J IS EQUAL TO 1; IF AN ASCENDING PASS, J IS EQUAL TO 2.  THIS
C***** ASSIGNMENT OF VALUES FOR J HOLDS TRUE THROUGHOUT THE PROGRAM.****
C
      WRITE(6,712)
      READ(5,701)J
      IF(J.EQ.1)GO TO 44
      WRITE(6,702)
C
C***** IN THE FOLLOWING, IF AN IDIM'S FLIPPED AND MIRRORED PASS IS
C***** BEING PROCESSED, THAN II IS ASSIGNED A VALUE OF 1.  THIS
C***** ASSIGNMENT HOLDS TRUE THROUGHOUT THE PROGRAM. *****
C
      READ(5,701)II
      IF(II.EQ.1)GO TO 9
C
```

```
C***** IN THE FOLLOWING, IF THIS PASS IS NOT A FLIPPED AND MIRRORED PASS
C***** THEN THE SAMPLE NUMBER SEQUENCE IS REVERSED. A DESCENDING PASS
C***** IS NOT ALTERED.
C
      IF(II.EQ.2)IPIXEL=2049-IPIXEL
      IF(II.EQ.2)ILINE=TOTLIN-ILINE+1
      GO TO 9
44    II=1
C
C***** SET UP PI CONVERSIONS *****
C
9     PIO4=ATAN(1.0)
      PI=4.*PIO4
      TWOPI=8.*PIO4
      PIO2=2.*PIO4
C
C***** CONVERT DEGREES TO RADIANS;CONVERT TO RETROGRADE INCLINATION
C
      LO=(LO*PIO4)/45.
      LAMDAO=(LAMDAO*PIO4)/45.
      IF(K.EQ.2)GO TO 91
      INCLIN=((180.-INCLIN)*PIO4)/45.
C
C***** CALCULATE EARTH RADIUS AT VP *****
C
91    TEMP7=(COS(LO))**2
      TEMP8=(SIN(LO))**2
      TEMP7A=TEMP7/(3443.925**2)
      TEMP8A=TEMP8/(3432.381**2)
      TEMP9=TEMP7A+TEMP8A
      TEMP9A=SQRT(TEMP9)
      ERAD=1./TEMP9A
      RADORB=3887.248747
C
```

```
C*CALCULATE THE GCD BETWEEN THE VP AND THE SSP USING LANDMARK PIXEL NO.
C
      CLICK=110.8/2048
      IF(IPIXEL.GT.1024)GO TO 10
      IF(IPIXEL.LT.1024)GO TO 11
      IF(IPIXEL.EQ.1024)GO TO 12
10    THETAS=(IPIXEL-1024)*CLICK
      GO TO 13
11    THETAS=(1025-IPIXEL)*CLICK
      GO TO 13
12    THETAS=CLICK
13    THETAS=(THETAS*PI04)/45.
      THETAP=ARSIN((RADORB*SIN(THETAS))/ERAD)
      THETAG=THETAP-THETAS
      PHIGEE=ERAD*THETAG
      PHIGEE=((PHIGEE/60.)*PI04)/45.
C
C**********TERMINATION OF THE PHIGEE CALCULATIONS******************
C*****
C*****
C*****NEXT STATEMENT ASKS IF THIS IS A DESCENDING PASS INDICATED BY
C*****J EQUALLING 1, AND IF SO, SKIPS DOWN THE PROGRAM TO THE
C*****DESCENDING PASS CALCULATIONS.
C*****
C***** IF J EQUALLED 2, THE FOLLOWING ASCENDING PASS CALCULATIONS
C***** ARE DONE BEGINNING WITH THOSE (NL,NS) THAT HAVE ALREADY BEEN
C***** FLIPPED AND MIRRORED ON THE IDIMS SYSTEM FOLLOWED BY THOSE
C***** (NL,NS) THAT STILL NEED TO BE FLIPPED AND MIRRORED.
C*****
C*****
      IF(J.EQ.1)GO TO 40
C
```

```
C***** CASE 1 CALCULATIONS *****                                        LOC02080
C                                                                       LOC02090
      IF(IPIXEL.LT.1024)GO TO 20                                        LOC02100
      PSI=ATAN(SIN(INCLIN)/((SIN(LO)/SIN(PHIGEE))-COS(INCLIN)))         LOC02110
      PHINOT=ARSIN((SIN(PHIGEE)/SIN(PSI)))                              LOC02120
      PHITEE=ARCOS((TAN(PHIGEE)/(SIN(PSI)*TAN(PHINOT))))                LOC02130
      LS=ARSIN((SIN(INCLIN)*SIN(PHITEE)))                               LOC02140
      DLMANF=ARCOS((TAN(LS)/(SIN(INCLIN)*TAN(PHITEE))))                 LOC02150
      ALPHA=ARSIN((SIN(DLMANF)/SIN(PHITEE)))                            LOC02160
      DLAMDA=ARSIN(((COS(ALPHA)*SIN(PHIGEE))/COS(LO)))                  LOC02170
      LAMDAS=LAMDAO+DLAMDA                                              LOC02180
      LAMANF=LAMDAS-DLMANF                                              LOC02190
      GO TO 30                                                          LOC02200
C                                                                       LOC02210
C***** CASE 2 CALCULATIONS *****                                        LOC02220
C                                                                       LOC02230
20    PSI=ATAN(SIN(INCLIN)/((SIN(PHIGEE)/SIN(LO))+COS(INCLIN)))         LOC02240
      PHINOT=ARSIN(SIN(LO)/SIN(PSI))                                    LOC02250
      PHITEE=ARCOS(COS(PHINOT)/COS(PHIGEE))                             LOC02260
      LS=ARSIN(SIN(INCLIN)*SIN(PHITEE))                                 LOC02270
      DLMANF=ARCOS(COS(PHINOT)/COS(LO))                                 LOC02280
      DLAMDA=ARCOS(COS(PHITEE)/COS(LS))                                 LOC02290
      LAMDAS=LAMDAO-(DLMANF-DLAMDA)                                     LOC02300
      LAMANF=LAMDAO-DLMANF                                              LOC02310
30    CONTINUE                                                          LOC02320
```

```
C
C***** ASCENDING NODE CALCULATIONS *****
C
      DTIME=(PHITEE/TWOPI)*PERIOD
      DSECS=DTIME*60.
      DLMROT=(TWOPI/24.)*1.002738*(DTIME/60.)
      LAMDAN=LAMANF-DLMROT
      GO TO 60
40    IF(IPIXEL.GT.1024)GO TO 50
C
C***** CASE 4 CALCULATIONS *****
C
      PSI=ATAN(SIN(INCLIN)/((SIN(LO)/SIN(PHIGEE))-COS(INCLIN)))
      PHINOT=ARSIN(SIN(PHIGEE)/SIN(PSI))
      PHITEE=ARCOS(COS(PHINOT)/COS(PHIGEE))
      LS=ARSIN(SIN(PHITEE)*SIN(INCLIN))
      DLAMDA=ARCOS(COS(PHITEE)/COS(LS))
      DLMANF=ARCOS(COS(PHINOT)/COS(LO))
      LAMDAS=LAMDAO-(DLAMDA-DLMANF)
      LAMANF=LAMDAO+DLMANF
      GO TO 55
C
C***** CASE 3 CALCULATIONS *****
C
50    PSI=ATAN(SIN(INCLIN)/((SIN(PHIGEE)/SIN(LO))+COS(INCLIN)))
      PHINOT=ARSIN(SIN(LO)/SIN(PSI))
      PHITEE=ARCOS(COS(PHINOT)/COS(PHIGEE))
      LS=ARSIN(SIN(INCLIN)*SIN(PHITEE))
      DLMANF=ARCOS(COS(PHINOT)/COS(LO))
      DLAMDA=ARCOS(COS(PHITEE)/COS(LS))
      LAMDAS=LAMDAO+(DLMANF-DLAMDA)
      LAMANF=LAMDAO+DLMANF
C
```

```
C***** DESCENDING NODE CALCULATIONS *****
C
55     DTIME=(PHITEE/TWOPI)*PERIOD
       DSECS=DTIME*60.
       DLMROT=(TWOPI/24.)*1.002738*(DTIME/60.)
       LAMDAN=LAMANF+DLMROT
60     CONTINUE
C
C***** RADIAN-TO-DEGREE CONVERSION FOR OUTPUT *****
C
       LS=(45./PI04)*LS
       LAMDAS=(45./PI04)*LAMDAS
       PHIGEE=(45./PI04)*PHIGEE*60.
       LAMDAN=(45./PI04)*LAMDAN
C
C***** IN THE FOLLOWING, A NON-FLIPPED AND MIRRORED PASS IS CONVERTED
C***** BACK TO ITS ORIGIONAL COORDINATE SYSTEM FOR OUTPUT *****
C
       IF(II.EQ.2)ILINE=TOTLIN-ILINE+1
       IF(II.EQ.2)IPIXEL=2049-IPIXEL
C
C***** OUTPUT STATEMENTS FOR THE FIRST HALF OF THE PROGRAM. *****
C
       WRITE(6,200)ILINE,IPIXEL
       WRITE(6,201)PHIGEE
       WRITE(6,203)LS
       WRITE(6,204)LAMDAS
C
C***** NODAL TIME CALCULATION *****
C
       TIMEAN=ISECS-DSECS
C
C***** REMAINDER OF INITIAL OUTPUT STATEMENTS *****
C
       WRITE(6,207)TIMEAN
       WRITE(6,205)LAMDAN
       ICOUNT=ICOUNT+1
```

```
C
C***** THE FIRST HALF OF THE PROGRAM IS NOW CONCLUDED.  AT THIS POINT
C***** IF THE USER WANTS TO CALCULATE THE IMAGE COORDINATES OF A
C***** LOCATION, THEN A YES ANSWER TO THE QUESTION ON CONTINUING
C***** WILL INITIATE THE LAST HALF OF THE PROGRAM.  A NO ANSWER
C***** WILL THEN ASK THE USER IF HE/SHE WOULD LIKE TO CALCULATE
C***** ANOTHER ORBIT.  A YES ANSWER WILL START THE FIRST HALF
C***** CALCUALTIONS AGAIN WHILE A NO ANSWER WILL EXIT THE PROGRAM.*****
C
      WRITE(6,801)
      READ(5,701)I
      IF(I.EQ.2)GO TO 65
      PSECS=PERIOD*60.
      LAMDAN=(LAMDAN*PI04)/45.
C
C***** INITIATE REQUIRED INPUTS FOR SECOND HALF OF PROGRAM *****
C
64    WRITE(6,604)
      READ(5,101)BLAT
      WRITE(6,605)
      READ(5,102)BLONG
C
C***** IN THE FOLLOWING, JLINE IS THE ARBITRARILY-CHOSEN SCAN LINE
C***** THAT IS MENTIONED IN THE BODY OF THE THESIS.  THIS SCAN LINE
C***** CAN BE ANY NUMBER. *****
C
      WRITE(6,607)
      READ(5,100)JLINE
      WRITE(6,4001)
4001  FORMAT('0','BUOY LATITUDE',1X,'BUOY LONGITUDE',1X,'LINE NUMBER',3X
     1,'PIXEL NUMBER')
C
```

```
C***** SUBROUTINE SUBSAT CONTAINS THE ENTIRE PROCESSING FOR THE          LOC03350
C***** SECOND HALF OF THE LOCATE PROGRAM. *****                          LOC03360
C                                                                        LOC03370
      CALL SUBSAT(ILINE,JLINE,PIO4,TIMEAN,TSECS,PSECS,LAMDAN,INCLIN,CLICLOC03380
     1K,ERAD,RADORB,BLAT,BLONG,II,J)                                     LOC03390
C                                                                        LOC03400
C***** PROGRAM EXIT STATEMENTS *****                                     LOC03410
C                                                                        LOC03420
      WRITE(6,651)                                                       LOC03430
      READ(5,701)I                                                       LOC03440
      IF(I.EQ.1) GO TO 64                                                LOC03450
65    WRITE(6,800)                                                       LOC03460
      READ(5,701)I                                                       LOC03470
      IF(I.EQ.1)GO TO 4                                                  LOC03480
      STOP                                                               LOC03490
      END                                                                LOC03500
C                                                                        LOC03510
C***** SUBROUTINE SUBSAT CONTAINS THE PROCESSING FOR THE SECOND          LOC03520
C***** HALF OF THE LOCATE PROGRAM. *****                                 LOC03530
C                                                                        LOC03540
      SUBROUTINE SUBSAT(ILINE,JLINE,PIO4,TIMEAN,TSECS,PSECS,LAMDAN,INCLILOC03550
     1N,CLICK,ERAD,RADORB,BLAT,BLONG,II,J)                               LOC03560
      DIMENSION FLATR(2048),FLONGR(2048),DIST(2048)                      LOC03570
      REAL LAMDAN,INCLIN                                                 LOC03580
      INTEGER P1,P2                                                      LOC03590
C                                                                        LOC03600
C***** DETERMINATION OF THE DIFFERENCE IN SCAN LINES BETWEEN THE         LOC03610
C***** LANDMARK SCAN LINE AND THE ARBITRARILY-CHOSEN SCAN LINE. *****    LOC03620
C                                                                        LOC03630
      LLINE=JLINE-ILINE                                                  LOC03640
C                                                                        LOC03650
C***** CALCULATION OF HOW MANY SECONDS IT WOULD TAKE THE SATELLITE TO    LOC03660
C***** FLY THIS DISTANCE IN SCAN LINES *****                             LOC03670
C                                                                        LOC03680
      DS=LLINE/6.                                                        LOC03690
C                                                                        LOC03700
```

```
C***** CALCULATION OF TOTAL FLIGHT TIME BETWEEN THE ASCENDING OR
C***** DESCENDING NODE AND THE ARBITRARY SCAN LINE *****
C
      IF(J.EQ.1)TTIME=TSECS-DS
      IF(J.EQ.2)TTIME=TSECS+DS
C
C***** CONVERSION OF DECIMAL DEGREES TO RADIANS FOR AXBT POSITIONS *****
C
      BLATR=(BLAT*PI04)/45.
      BLONGR=(BLONG*PI04)/45.
C
C***** INITIATION OF A SERIES OF SUBROUTINES THAT CALCULATES THE
C***** SUBSATELLITE POINT OF THE ARBITRARY SCAN LINE, THE GREAT CIRCLE
C***** DISTANCES BETWEEN THE AXBT POSITION AND SELECTED PIXELS ALONG
C***** THE ARBITRARY SCAN LINE, AND SELECTS THE SMALLEST OF THESE
C***** DIFFERENCES. *****
C
92    CALL POINT(JLINE,PI04,TTIME,TIMEAN,LAMDAN,INCLIN,PSECS,TLAT,TLONG,
     1J)
      CALL PIXEL(PI04,BLATR,BLONGR,CLICK,ERAD,RADORB,INCLIN,TLAT,TLONG,P
     1LATR,PLONGR,DIST,1,2048,89,J)
      CALL SMALL(DIST,1,2048,89,K)
      CALL MED(DIST,1,2048,89,K,KK)
      CALL LARGE(DIST,1,2048,89,K,KK,KKK)
C
C***** THE FOLLOWING SEQUENCE SELECTS A 89 PIXEL BRACKET AROUND THE
C***** PIXEL WITH THE SMALLEST GREAT CIRCLE DISTANCE *****
C
      IF(K.GT.KK.AND.K.GT.KKK)GO TO 77
      IF(K.LT.KK.AND.K.LT.KKK)GO TO 73
      IF(KK.LT.KKK)GO TO 78
      IF(KKK.LT.KK)GO TO 79
78    P1=KK
      P2=KKK
      GO TO 80
```

```
79    P1=KKK
      P2=KK
      GO TO 80
77    IF(KK.LT.KKK)GO TO 76
      IF(KKK.LT.KK)GO TO 74
76    P1=KK
      P2=K
      GO TO 80
74    P1=KKK
      P2=K
      GO TO 80
73    IF(KK.LT.KKK)GO TO 72
      IF(KKK.LT.KK)GO TO 71
72    P1=K-89
      P2=K+89
      GO TO 80
71    P1=K
      P2=KKK
      GO TO 80
C
C***** TH  OLLOWING TWO SUBROUTINES AGAIN CALCULATE THE GREAT CIRCLE
C***** DISTANCES ALONG THE ARBITRARY SCAN LINE BUT FOR EVERY ONE OF
C***** THE    PIXELS IN THE BRACKET CREATED ABOVE.  THE SMALLEST GREAT
C***** CI     DISTANCE IS SELECTED AS AN OUTPUT *****
C
80    CALL PIXEL(PIO4,BLATR,BLONGR,CLICK,ERAD,RADORB,INCLIN,TLAT,TLONG,P
     1LATR,PLONGR,DIST,P1,P2,1,J)
      CALL SMALL(DIST,P1,P2,1,K)
C
C***** A BRACKET 5 PIXELS WIDE EITHER SIDE OF THE PIXEL WITH THE
C***** SMALLEST GREAT CIRCLE DISTANCE IS CREATED *****
C
      N1=K-5
      N2=K+5
C
```

```
C***** THE FOLLOWING TWO STATEMENTS DECIDE IF THE ARBITRARY SCAN LINE   LOC04410
C***** IS WITHIN 5 SCAN LINES OF THE TRUE AXBT SCAN LINE BY CHECKING TO LOC04420
C***** SEE WHAT THE LATITUDES ARE OF THE LEFT AND RIGHT PIXELS IN THE   LOC04430
C***** 10 PIXEL BOX THAT SURROUNDS THE PIXEL WITH THE SMALLEST GREAT    LOC04440
C***** CIRCLE DISTANCE. *****                                           LOC04450
C                                                                       LOC04460
      IF((BLATR-PLATR(N1)).GT.O..AND.(BLATR-PLATR(N2)).GT.O.)GO TO 93   LOC04470
      IF((BLATR-PLATR(N1)).LT.O..AND.(BLATR-PLATR(N2)).LT.O.)GO TO 94   LOC04480
C                                                                       LOC04490
C***** THE FINAL 10 BY 10 PIXEL BOX IS SET UP *****                     LOC04500
C                                                                       LOC04510
96    L1=JLINE-5                                                        LOC04520
      L2=JLINE+5                                                        LOC04530
      L5=L1-ILINE                                                       LOC04540
      L6=L2-ILINE                                                       LOC04550
      CS1=L5/6.                                                         LOC04560
      CS2=L6/6.                                                         LOC04570
      TTIM1=TSECS+CS1                                                   LOC04580
      TTIM2=TSECS+CS2                                                   LOC04590
C                                                                       LOC04600
C***** THE FOLLOWING SEQUENCE CALCULATES THE SUBSATELLITE POINTS AND    LOC04610
C***** THE GEOGRAPHICAL COORDINATES OF THE CORNERS OF THE FINAL BOX ****LOC04620
C                                                                       LOC04630
      CALL POINT(L1,PIO4,TTIM1,TIMEAN,LAMDAN,INCLIN,PSECS,TLAT,TLONG,J) LOC04640
      CALL PIXEL(PIO4,BLATR,BLONGR,CLICK,ERAD,RADORB,INCLIN,TLAT,TLONG,PLOC04650
     1LATR,PLONGR,DIST,N1,N2,1,J)                                       LOC04660
      PLAT1=PLATR(N1)                                                   LOC04670
      PLONG1=PLONGR(N1)                                                 LOC04680
      PLAT2=PLATR(N2)                                                   LOC04690
      PLONG2=PLONGR(N2)                                                 LOC04700
      CALL POINT(L2,PIO4,TTIM2,TIMEAN,LAMDAN,INCLIN,PSECS,TLAT,TLONG,J) LOC04710
      CALL PIXEL(PIO4,BLATR,BLONGR,CLICK,ERAD,RADORB,INCLIN,TLAT,TLONG,PLOC04720
     1LATR,PLONGR,DIST,N1,N2,1,J)                                       LOC04730
      PLAT3=PLATR(N1)                                                   LOC04740
      PLONG3=PLONGR(N1)                                                 LOC04750
      PLAT4=PLATR(N2)                                                   LOC04760
      PLONG4=PLONGR(N2)                                                 LOC04770
      GO TO 97                                                          LOC04780
```

```
C
C***** THE FOLLOWING CALCULATIONS DEFINE THE SIZE OF THE JUMP IN SCAN
C***** LINES THAT THE PROGRAM WILL MAKE AND THEN ROUTES THE PROCESS TO
C***** THE BEGINNING SO THE ABOVE CALCULATIONS ARE DONE ON THE NEW
C***** SCAN LINE THAT REPLACED THE INTIAL ARBITRARY SCAN LINE. *****
C
93    DSCAN=1.30005202*DIST(K)
      GO TO 95
9     DSCAN=-1.30005202*DIST(K)
95    DSCAN=(45./PID4)*DSCAN*60.
      ISCAN=DSCAN
      IF(ISCAN.LE.5)GO TO 96
      JLINE=JLINE+ISCAN
      MLINE=JLINE-ILINE
      BS=MLINE/6.
      TTIME=TSECS+BS
      GO TO 92
97    CONTINUE
C
C***** SUBROUTINE FINAL OUTPUTS THE SATELLITE IMAGE COORDINATES *****
C
      CALL FINAL(BLATR,BLONGR,PLAT1,PLAT2,PLAT3,PLAT4,PLONG1,PLONG2,PLON
     1G3,PLONG4,L1,N1,II,ILINE)
      RETURN
      END
C
```

```
C***** SUBROUTINE POINT CALCUALATES THE SUBSATELLITE POINT OF A SCAN    LOC05050
C***** LINE *****                                                       LOC05060
C                                                                       LOC05070
      SUBROUTINE POINT(JLINE,PIO4,TTIME,TIMEAN,LAMDAN,INCLIN,PSECS,TLAT,LOC05080
     1TLONG,J)                                                          LOC05090
      REAL LAMDAN,INCLIN                                                LOC05100
      PHIS=(8*PIO4*(TTIME-TIMEAN))/PSECS                                LOC05110
      TLAT=ARSIN(SIN(INCLIN)*SIN(PHIS))                                 LOC05120
      F=ARCOS(COS(PHIS)/COS(TLAT))                                      LOC05130
      R=0.00007291*(TTIME-TIMEAN)                                       LOC05140
      IF(J.EQ.1)TLONG=LAMDAN-F-R                                        LOC05150
      IF(J.EQ.2)TLONG=LAMDAN+F+R                                        LOC05160
      RETURN                                                            LOC05170
      END                                                               LOC05180
C                                                                       LOC05190
C***** SUBROUTINE PIXEL CALCULATES THE LATITUDE AND LONGITUDE OF        LOC05200
C***** A SELECTED PIXEL AND ALSO CALCULATES THE GREAT CIRCLE DISTANCE   LOC05210
C***** BETWEEN THE AXBT AND THE PIXEL. *****                            LOC05220
C                                                                       LOC05230
      SUBROUTINE PIXEL(PIO4,BLATR,BLONGR,CLICK,ERAD,RADORB,INCLIN,TLAT,TLOC05240
     1LONG,PLATR,PLONGR,DIST,I1,I2,I3,J)                                LOC05250
      DIMENSION PLATR(2048),PLONGR(2048),DIST(2048)                     LOC05260
      REAL INCLIN                                                       LOC05270
      DO 81 I=I1,I2,I3                                                  LOC05280
      IF(I.GT.1024)TSD=(I-1024)*CLICK                                   LOC05290
      IF(I.LE.1024)TSD=(1025-I)*CLICK                                   LOC05300
      TSR=(TSD*PIO4)/45.                                                LOC05310
      TPR=ARSIN((RADORB*SIN(TSR))/ERAD)                                 LOC05320
      TGR=TPR-TSR                                                       LOC05330
      PGNM=ERAD*TGR                                                     LOC05340
      PGR=((PGNM/60.)*PIO4)/45.                                         LOC05350
      EPR=ARCOS(COS(INCLIN)/COS(TLAT))                                  LOC05360
      SIR=ARCOS(SIN(EPR)*COS(TLAT))                                     LOC05370
      PHISR=ARSIN(SIN(TLAT)/SIN(SIR))                                   LOC05380
      IF(I.LE.1024)GO TO 811                                            LOC05390
      IF(J.EQ.2)GO TO 810                                               LOC05400
```

```
C
C***** CASE 3 CALCULATIONS *****
C
      FLATR(I)=ARSIN(SIN(SIR)*SIN(PHISR-PGR))
      GAMMA=ARSIN(COS(SIR)/COS(PLATR(I)))
      DLPR=ARSIN((SIN(GAMMA)*SIN(PGR))/COS(TLAT))
      FLONGR(I)=TLONG-DLPR
      GO TO 813
C
C***** CASE 1 CALCULATIONS *****
C
810   FLATR(I)=ARSIN(SIN(SIR)*SIN(PHISR+PGR))
      DLPR=ARSIN((SIN(EPR)*SIN(PGR))/COS(PLATR(I)))
      FLONGR(I)=TLONG-DLPR
      GO TO 813
811   IF(J.EQ.2)GO TO 812
C
C***** CASE 4 CALCULATIONS *****
C
      FLATR(I)=ARSIN(SIN(SIR)*SIN(PHISR+PGR))
      DLPR=ARSIN((SIN(EPR)*SIN(PGR))/COS(PLATR(I)))
      FLONGR(I)=TLONG+DLPR
      GO TO 813
C
C***** CASE 2 CALCULATIONS *****
C
812   FLATR(I)=ARSIN(SIN(SIR)*SIN(PHISR-PGR))
      GAMMA=ARSIN(COS(SIR)/COS(PLATR(I)))
      DLPR=ARSIN((SIN(GAMMA)*SIN(PGR))/COS(TLAT))
      FLONGR(I)=TLONG+DLPR
C
C***** GREAT CIRCLE DISTANCE *****
C
813   DIST(I)=ARCOS((SIN(BLATR)*SIN(FLATR(I)))+(COS(BLATR)*COS(PLATR(I))
     1*COS(FLONGR(I)-BLONGR)))
81    CONTINUE
      RETURN
      END
```

```
C
C***** SUBROUTINE SMALL FINDS THE PIXEL WITH THE SMALLEST G.C.D. *****
C
      SUBROUTINE SMALL(DIST,I1,I2,I3,K)
      DIMENSION DIST(2048)
      DO 84 I=I1,I2,I3
      J=I+I3
      IF(J.EQ.2048)GO TO 85
      IF(DIST(I).GT.DIST(J))GO TO 84
      K=I
      RETURN
85    K=1959
      RETURN
84    CONTINUE
      RETURN
      END
C
C***** SUBROUTINE MED FINDS THE PIXEL WITH THE 2ND SMALLEST G.C.D. *****
C
      SUBROUTINE MED(DIST,I1,I2,I3,K,KK)
      DIMENSION DIST(2048)
      DO 86 I=I1,I2,I3
      IF(K.EQ.2048)GO TO 87
      J=I+89
      IF(J.EQ.2048) GO TO 87
      IF(J.EQ.K)J=J+89
      IF(J.EQ.2048) GO TO 87
      IF(I.EQ.K)GO TO 86
      IF(DIST(I).GT.DIST(J))GO TO 86
      KK=I
      RETURN
87    KK=K-89
      RETURN
86    CONTINUE
      RETURN
      END
```

```
C
C***** SUBROUTINE LARGE FINDS THE PIXEL WITH THE 3RD SMALLEST G.C.D. ***
C
      SUBROUTINE LARGE(DIST,I1,I2,I3,K,KK,KKK)
      DIMENSION DIST(2048)
      DO 89 I=I1,I2,I3
      IF(K.EQ.2048)GO TO 98
      J=I+89
      IF(J.EQ.2048)GO TO 90
      IF(J.EQ.K)J=J+89
      IF(J.EQ.KK)J=J+89
      IF(J.EQ.K)J=J+89
      IF(J.EQ.2048)GO TO 90
      IF(I.EQ.K) GO TO 89
      IF(I.EQ.KK)GO TO 89
      IF(DIST(I).GT.DIST(J))GO TO 89
      KKK=I
      RETURN
90    KKK=K+89
      RETURN
98    KKK=K-178
      RETURN
89    CONTINUE
      RETURN
      END
C
```

```
C***** SUBROUTINE FINAL CALCUALTES THE SCAN LINE NUMBER AND THE
C***** SAMPLE NUMBER OF THE AXBT, SHIP, OR LANDMARK. *****
C
      SUBROUTINE FINAL(BLATR,BLONGR,PLAT1,PLAT2,PLAT3,PLAT4,PLONG1,PLONG
     12,PLONG3,PLONG4,L1,N1,II,ILINE)
      DLATDL=((PLAT3-PLAT1)+(PLAT4-PLAT2))/20.
      DLATDP=((PLAT2-PLAT1)+(PLAT4-PLAT3))/20.
      DLONDL=((PLONG3-PLONG1)+(PLONG4-PLONG2))/20.
      DLONDP=((PLONG2-PLONG1)+(PLONG4-PLONG3))/20.
      AZERO=(BLONGR-PLONG1)+(DLONDP*N1)+(DLONDL*L1)
      BZERO=(BLATR-PLAT1)+(DLATDP*N1)+(DLATDL*L1)
      RLINE=((AZERO/DLONDP)-(BZERO/DLATDP))/((DLONDL/DLONDP)-(DLATDL/DLA
     1TDP))
      PIXNUM=(AZERO/DLONDP)-((DLONDL/DLONDP)*RLINE)
      PIO4=ATAN(1.0)
      BLATD=(45./PIO4)*BLATR
      BLONGD=(45./PIO4)*BLONGR
      IF(II.EQ.2)PIXNUM=2049.000-PIXNUM
      SLINE=ILINE
      IF(II.EQ.1)RLINE=(SLINE-RLINE)+SLINE
      WRITE(6,4002)BLATD,BLONGD,RLINE,PIXNUM
4002  FORMAT(1X,F9.3,5X,F9.3,7X,F9.3,5X,F9.3)
      RETURN
      END
```

LIST OF REFERENCES

Barnett, T.P., Patzert, W.C., Webb, S.C., and Bean, B.R., "Climatological Usefulness of Satellite Determined Sea-Surface Temperatures in the Tropical Pacific," Bulletin of the American Meteorological Society, v. 60(3), pp. 197-205, March 1979.

Bernstein, R. and Ferneyhough, D.G., "Digital Image Processing," Photogrammetric Engineering and Remote Sensing, v. 31(12), pp. 1465-1476, December 1975.

Bernstein, R.L., Breaker, L., and Whirtner, R., "California Current Eddy Formation: Ship, Air, and Satellite Results," Science, v. 195, pp. 353-359, 28 January 1977.

Breaker, L., Ephemeris Data Package, Environmental Acoustic Research Group Internal Document, Naval Postgraduate School, Monterey, CA., November, 1980.

Brouwer, D., "Solution of the Problem of Artificial Satellite Theory without Drag," Astronautical Journal, v. 64(1274), pp. 378-397, 1959.

Brower, R.L., Pichel, W.G., Walton, C.C., and Signore, T.L., Current Status and Quality of Global Operational Sea Surface Temperatures from Satellite Infrared Data, paper presented at the Proceedings of the Tenth International Symposium on Remote Sensing of the Environment, Environmental Research Institute of Michigan, Ann Arbor, Michigan, 6-10 October, 1975.

Brower, R.L., Gohrband, H.S., Pichel, W.G., Signore, T.L., and Walton, C.C., U.S. Department of Commerce, NOAA Technical Memorandum NESS 78, Satellite Dervied Sea-Surface Temperatures from NOAA Spacecraft, pp. 1-74, June 1976.

Chahine, M.T., Limits of the Accuracy of Satellite Derived Sea Surface Temperature, seminar given to the Department of Oceanography, Naval Postgraduate School, Monterey, California, 3 October 1980.

Cogan, J.L. and Willand, J.H., "Measurement of Sea Surface Temperature by the NOAA-2 Satellite," Journal of Applied Meteorology, v. 15, pp. 173-180, February 1976.

Conlon, E.F., U.S. Department of Commerce, NOAA Technical Memorandum NESS 52, Operational Products from ITOS Scanning Radiometer Data, pp. 1-57, 1973.

Corliss, W.R., National Aeronautics and Space Administration Report SP-133, Scientific Satellites, pp. 31-71, 1967.

Deschamps, P.Y. and Phulpin, T., "Atmospheric Correction of Infrared Measurements of Sea Surface Temperature using Channels at 3, 7, 11, and 12 μm," Boundary-Layer Meteorology, v. 18(2), pp. 131-143, March 1980.

ESL, Incorporated, IDIMS Functional Guide, Vol. II, Technical Manual ESL-TM705, Revision A, 1 October 1978.

Fett, R.W. and Mitchell, W.F., Navy Environmental Prediction Research Facility Applications Report 77-03, Navy Tactical Applications Guide, Volume I. Techniques and Applications of Image Analysis, p. 1c-3, January 1977.

Hussey, J.W., U.S. Department of Commerce, NOAA-NESS, The TIROS-N/NOAA Operational Satellite System, pp. 1-35, May 1979.

ITT Aerospace, Advanced Very High Resolution Radiometer for the TIROS-N Spacecraft Alignment and Calibration Data Book, NASA Contract NAS5-22497, undated.

James, R.W., U.S. Naval Oceanographic Office Report SP-105, ASWEPS Manual Volume 5: Ocean Thermal Structure Forecasting, pp. 74-138, 1966.

Katsaros, K.B., "The Aqueous Thermal Boundary Layer," Boundary-Layer Meteorology, v. 18(1), pp. 107-127, February 1980.

Kibblewhite, A.C., Bedfore, N.L., and Mitchell, S.K., "Regional Dependence of Low-Frequency Attenuation in the North Pacific Ocean," Journal of the Acoustical Society of America, v. 61(5), pp. 1169-1177, May 1977.

Kidwell, K.B., U.S. Department of Commerce, NOAA-Satellite Data Services Division, NOAA Polar Orbiter Data (TIROS-N and NOAA-6), preliminary copy, December 1979.

Kilonsky, B., ASTREX Data Package, Environmental Acoustic Research Group Internal Document, Naval Postgraduate School, Monterey, CA., June 1981.

King-Hele, D., "The Effect of the Earth's Oblateness on the Orbit of a Near Satellite," Proceedings of the Royal Society of London, v. 247A, pp. 49-72, 21 October 1958.

Klein, F.C., An Evaluation of the GOSSTCOMP Model in Determining Ocean Thermal Features with a Literature Summary of Remote Sensing of the Oceans (Northeast Pacific Ocean, August 1977), Master's Thesis, Naval Postgraduate School, Monterey, California, June 1979.

Knauss, J.A., Introduction to Physical Oceanography, pp. 150-151, Prentice-Hall, Inc., Englewood Cliffs, New Jersey, 1978.

Lauritson, L., Nelson, G.J., and Porto, F.W., U.S. Department of Commerce, NOAA Technical Memorandum NESS 107, Data Extraction and Calibration of TIROS-N/NOAA Radiometers, pp. 1-58, November 1979.

LaViolette, P.E. and Chabot, P.L., "NIMBUS-II Satellite Sea Surface Temperatures versus Historical Data in a Selected Region: A Comparative Study," Deep-Sea Research, v. 15(5), pp. 617-622, October 1968.

LaViolette, P.E., "A Satellite-Aircraft Study of the Upwelled Waters off Spanish Sahara," Journal of Physical Oceanography, v. 4(4), pp. 676-684, October 1974.

Legeckis, R. and Pritchard, J., U.S. Department of Commerce, NOAA Technical Memorandum NESS 77, Algorithm for Correcting the VHRR Imagery for Geometric Distortions due to the Earth Curvature, Earth Rotation, and Spacecraft Roll Attitude Errors, pp. 1-13, April 1976.

Legeckis, R., "A Survey of Worldwide Sea Surface Temperature Fronts Detected by Environmental Satellites," Journal of Geophysical Research, v. 83(9), pp. 4501-4522, 20 September 1978.

Leonard, D.A., Caputo, B., and Hoge, F.E., "Remote Sensing of Subsurface Water Temperature by Raman Scattering," Applied Optics, v. 18(11), pp. 1732-1745, 1 June 1979.

Maul, G.A. and Sidran, M., "Atmospheric Effect on Ocean Surface Temperature Sensing from the NOAA Satellite Scanning Radiometer," Journal of Geophysical Research, v. 78(12), pp. 1909-1916, 20 April 1973.

McAlister, E.D. and McLeish, W., "A Radiometric System for Airborne Measurement of the Total Heat Flow from the Sea," Applied Optics, v. 9(12), pp. 2697-2705, December 1970.

McMillin, L.M., "Estimation of Sea Surface Temperatures from Two Infrared Window Measurements with Different Absorption," Journal of Geophysical Research, v. 80(36), pp. 5113-5117, 20 December 1975.

Miyake, M., Institute of Ocean Sciences, Sideney, B.C., Oceanographic Observations at Station P during STREX Experiment, November 1 to December 13, 1980, preliminary report, undated.

Mollo-Christensen, E. and Mascarenhas, A., "Heat Storage in the Oceanic Upper Mixed Layer Inferred from LANDSAT Data," Science, v. 203, pp. 653-654, 16 February 1979.

Morton, W.T. and Lowrie, A., U.S. Naval Oceanographic Office Reference Publication RP-16, Regional Geological Maps of the Northeast Pacific, plate 4, 1978.

Mueller, J., Naval Postgraduate School Course OC-3660 classnotes, 1981.

Murphy, W.F. and Bernstein, H.J., "Raman Spectra and an Assignment of the Vibrational Stretching Region of Water," Journal of Physical Chemistry, v. 76(8), pp. 1147-1152, 13 April 1972.

National Weather Service, STREX Weather Plotting Charts, Naval Postgraduate School Environmental Acoustic Research Group internal documents, 1980a.

National Weather Service, Surface and 1000-500 MB Weather Depiction Charts 12 November to 8 December 1980, 1980b.

Ponte, L., "What's New Under the Sun?" Reader's Digest, v. 118(710), pp. 82-86, June 1981.

Rao, P.K., Smith, W.L., and Koffler, P., "Global Sea-Surface Temperature Distribution Determined from an Environmental Satellite," Monthly Weather Review, v. 100(1), pp. 10-14, January 1972.

Reed, R.J. and Mullen, S.L., U.S. Department of Commerce, Pacific Marine Environmental Laboratory, Storm Transfer and Response Experiment: Meteorological Atlas, unpaged, 30 June 1981.

Renner, J.A., U.S. Department of Commerce, National Marine Fisheries Service, Fishing Information, v. 11, p. 6, November 1980.

Roberts, S.E., Selby, J.E.A., and Biberman, L.M., "Infrared Continuum Absorption by Atmospheric Water Vapor in the 8-12 μm Windown," Applied Optics, v. 15(9), pp. 2085-2090, September 1976.

Robinson, M.N., U.S. Naval Oceanographic Office Reference Publication 2, Atlas of North Pacific Ocean Monthly Mean Temperatures and Mean Salinities of the Surface Layer, figures 122-144, 1976.

Roden, G.I., "On North Pacific Temperature, Salinity, Sound Velocity, and Density Fronts and their Relation to the Wind and Energy Flux Fields," Journal of Physical Oceanography, v. 4(4), pp. 557-571, October 1975.

Schwalb, A., U.S. Department of Commerce, NOAA Technical Memorandum NESS 95, The TIROS-N/NOAA A-G Satellite Series, pp. 1-75, March 1978.

Sessions, M.H. and Wilson, W.S., "The Airborne Expendable Bathythermograph," Deep-Sea Research, v. 23(8), pp. 779-782, August 1976.

Smith, W.L., Rao, P.K., Koffler, R., and Curtis, W.R., "The Determination of Sea-Surface Temperature from Satellite High Resolution Infrared Window Radiation Measurements," Monthly Weather Review, v. 98(8), pp. 604-611, August 1970.

Sparton Electronics, Sparton Sonobuoys, pp. 19-20, 5 October 1976.

Stewart, R.H., Notes on Satellite Oceanography, preliminary copy, pp. 254-268, Scripps Institution of Oceanography, La Jolla, Ca., 1979.

Stumpf, H.G. and Rao, P.K., "Evolution of Gulf Stream Eddies as seen in Satellite Infrared Imagery," Journal of Physical Oceanography, v. 5(2), pp. 388-393, April 1975.

Tabata, S., "Temporal Changes of Salinity, Temperature, and Dissolved Oxygen Content of the Water at Station "P" in the Northeast Pacific Ocean, and Some of their Determining Factors," Journal of the Fisheries Research Board of Canada, v. 18(6), pp. 1073-1124, December 1961.

Tabata, S., "Variability of Oceanographic Conditions at Ocean Station "P" in the Northeast Pacific Ocean," Transactions of the Royal Society of Canada, v. 3(4), pp. 367-418, June 1965.

Tabata, S., "Comparisons of Observations of Sea Surface Temperature at Ocean Station "P" and NOAA Buoy Stations and Those Made by Merchant Ships Traveling in their Vicinities, in the Northeast Pacific Ocean," Journal of Applied Meteorology, v. 17, pp. 374-385, March 1978.

Tabata, S. and Giovando, L.F., Fisheries Research Board of Canada Manuscript Series No. 132, Prediction of Transient Temperature Structure in the Surface Layers of the Ocean, pp. 1-11, 8 June 1962.

Tabata, S. and Gower, J.F.R., "A Comparison of Ship and Satellite Measurements of Sea Surface Temperatures off the Pacific Coast of Canada," Journal of Geophysical Research, v. 85(C11), pp. 6636-6648, 20 November 1980.

Tully, J.P., Fisheries Research Board of Canada Manuscript Series No. 103, Assessment of Temperature Structure in the Eastern Subarctic Pacific Ocean, pp. 1-22, 16 November 1961.

Tully, J.P., "Oceanographic Regions and Assessment of Temperature Structure in the Seasonal Zone of the North Pacific Ocean," Journal of the Fisheries Research Board of Canada, v. 21(5), pp. 941-970, September 1964.

Vukovich, F.M., "Estimation of the Effect of Partial Cloud Cover on the Radiation Received by the NIMBUS HRIR," Monthly Weather Review, v. 99(11), pp. 807-811, November 1971.

Weinreb, M.P. and Hill, M.L., U.S. Department of Commerce, NOAA Technical Report NESS 80, Calculation of Atmospheric Radiances and Brightness Temperatures in Infrared Window Channels of Satellite Radiometers, pp. 1-40, March 1980.

INITIAL DISTRIBUTION LIST

		No. Copies
1.	Defense Technical Information Center Cameron Station Alexandria, VA 22314	2
2.	Superintendent Attn: Library, Code 0142 Naval Postgraduate School Monterey, CA 93940	2
3.	Superintendent Attn: Code 68Jg Naval Postgraduate School Monterey, CA 93940	2
4.	Superintendent Attn: Code 68Du Naval Postgraduate School Monterey, CA 93940	6
5.	Superintendent Attn: Code 68Mu Naval Postgraduate School Monterey, CA 93940	1
6.	Superintendent Attn: Code 68Bf Naval Postgraduate School Monterey, CA 93940	1
7.	Commander Naval Electronic Systems Command Attn: PME-124-60 Naval Electronic Systems Command Headquarters Washington, D.C. 20360	1
8.	Commander Oceanographic System, Pacific Box 1390 Pearl Harbor, HI 96860	1
9.	Commander Attn: Code 531 Naval Ocean Systems Center San Diego, CA 92152	1

10. Chief of Naval Operations 1
Attn: OP951F
Navy Department
Washington, D.C. 20350

11. LT Glenn W. Lundell, USN 1
56 Montana Drive
Holden, MA 01520

12. Commanding Officer 1
Attn: Code 5101
Naval Research Laboratory
Washington, D.C. 20375

13. Commanding Officer 3
Attn: Seas Program Officer, Code 520
Naval Ocean Research and Development Activity
NSTL Station
Bay St. Louis, MS 39522

14. Commanding Officer 1
Attn: Mr. William Jobst, Code 7300
Naval Oceanographic Office
NSTL Station
Bay St. Louis, MS 39522

15. Director of Astronautics 1
Attn: Mr. Robert Wrigley, Code SEA
National Aeronautics and Space Administration
Ames Research Center
Airborne Missions and Applications Division
Technology Applications Branch
Moffett Field, CA 94035

16. Mr. Larry Breaker 1
Satellite Field Services Station
National ENvironmental Satellite Service
National Oceanic and Atmospheric Administration
660 Prince Avenue
Redwood City, CA 94063

17. Library 1
Attn: Dr. Robert Bernstein, Code A-030
Scripps Institution of Oceanography
University of California, San Diego
La Jolla, CA 92037

18. Commanding Officer 1
Attn: Mr. Walter Brown, Code 7331
Naval Oceanographic Office
NSTL Station
Bay St. Louis, MS 39522

END

DATE
FILMED

3-82

DTIC